Department of Engineering Design and Production

Development of Material Models and Acquisition of Model Parameters for Metal Cutting Simulations

Sampsa Vili Antero Laakso

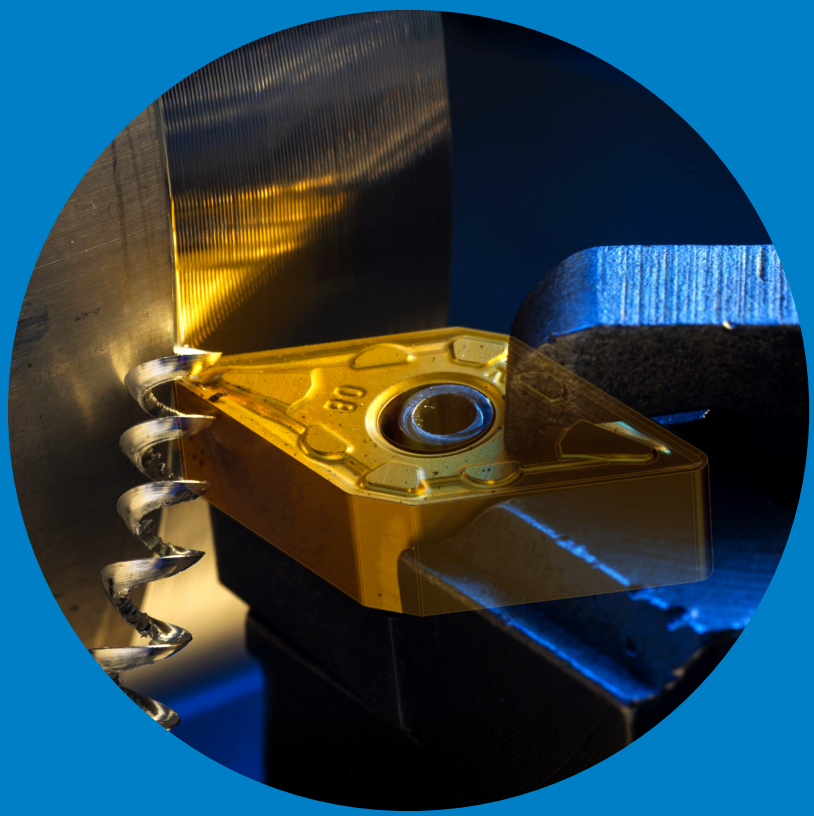

Aalto University

DOCTORAL DISSERTATIONS

Sampsa Vili Antero Laakso

Development of Material Models and Acquisition of Model Parameters for Metal Cutting Simulations

Aalto University

2015

Aalto University publication series
DOCTORAL DISSERTATIONS 190/2015

Development of Material Models and Acquisition of Model Parameters for Metal Cutting Simulations

Sampsa Vili Antero Laakso

A doctoral dissertation completed for the degree of Doctor of Science (Technology) to be defended, with the permission of the Aalto University School of Engineering, at a public examination held at the building K1 and lecture hall K215 of the school on 18.12.2015 at 12:15.

Aalto University
School of Engineering
Engineering Design and Production
Production Engineering

Supervising professor
Professor Esko Niemi, Aalto University, Finland

Preliminary examiners
Professor Kai Cheng, Brunel, UK
Professor Jan-Eric Ståhl, Lund University, Sweden

Opponent
Professor Jari Larkiola, University of Oulu, Finland

Aalto University publication series
DOCTORAL DISSERTATIONS 190/2015

ISBN 978-952-60-6523-6 (printed)
ISBN 978-952-60-6524-3 (pdf)
ISSN-L 1799-4934
ISSN 1799-4934 (printed)
ISSN 1799-4942 (pdf)
http://urn.fi/URN:ISBN:978-952-60-6524-3

Images: Cover Image ©Arto Rusanen

Unigrafia Oy
Helsinki 2015

Finland

Publication orders (printed book):
sampsa.laakso@aalto.fi

441 697
Printed matter

Aalto University

Abstract

Aalto University, P.O. Box 11000, FI-00076 Aalto www.aalto.fi

Author
Sampsa Laakso

Name of the doctoral dissertation
Development of Material Models and Acquisition of Model Parameters for Metal Cutting Simulations

Publisher School of Engineering

Unit Engineering Design and Production

Series Aalto University publication series DOCTORAL DISSERTATIONS 190/2015

Field of research Production Engineering

Manuscript submitted 28 August 2015 **Date of the defence** 18 December 2015

Permission to publish granted (date) 29 October 2015 **Language** English

☐ **Monograph** ☒ **Article dissertation (summary + original articles)**

Abstract

Metal cutting is a complex physical problem with many interdependent operational parameters. To illustrate this, a graph analysis is performed for the network of relationships between the parameters. In order to systematically develop metal cutting operations, a tool such as finite element simulations, capable of simultaneously calculating the combined effect of the parameters, is required. Metal cutting simulations are a useful tool for optimizing machining parameters and tool design with respect to quality and costs. Wide range of different cutting parameters or tool geometries can be simulated to find conditions to minimize tool wear or residuals stresses on the workpiece and finding appropriate level of cutting temperature, cutting forces, chip geometry or the thermal and mechanical loading of the tool. Simulations are faster and cheaper to perform than cutting experiments especially since simulations do not disrupt the production. Especially with recent interest in digital manufacturing, expert systems and design tools, finite element modeling of cutting is in research focus. The use of the finite element method for metal cutting simulations has been researched for several decades and the method is progressively reaching maturity. The first machining simulations date back to 1970's observed from Mackerle's bibliography from 1998. There are a few commercial software packages available for cutting simulations and the industry has slowly started to take advantage of the method. The major difficulty is that even though the software includes extensive work material libraries, many engineering materials are not included in them. When the material is not included in the library, the process of testing and characterizing the new material for the simulations is expensive, time consuming and requires a high level of expertise. In this dissertation, the state-of-the-art method of traditional materials testing for determining the material model parameters is investigated through practical implementation. A method for using cutting experiments for material characterization instead of tensile testing or other traditional methods is investigated. The approach is to use an analytical cutting model to map the measurable outputs of cutting experiments to material deformation characteristics. The method is validated with simulations. Additionally, a new material model is investigated for modeling work material thermal softening damping behavior that was observed during the state-of-the-art method. The research is done with cutting experiments, analytical modeling, materials testing, and simulations. The results show that using the cutting experiments as a materials testing method has practical potential. It is also observed that the testing conditions in traditional methods of tensile testing and SHPB testing are not completely compatible with metal cutting conditions.

Keywords Finite Element Method, Metal Cutting, Johnson-Cook Model, Inverse Analysis, Graph Analysis, SHPB, Turning, Cutting Force, Oxley's Model, Parallel Sided Shear Zone Model

ISBN (printed) 978-952-60-6523-6 **ISBN (pdf)** 978-952-60-6524-3

ISSN-L 1799-4934 **ISSN (printed)** 1799-4934 **ISSN (pdf)** 1799-4942

Location of publisher Helsinki **Location of printing** Helsinki **Year** 2015

Pages 103 **urn** http://urn.fi/URN:ISBN:978-952-60-6524-3

Aalto-yliopisto

Tiivistelmä

Aalto-yliopisto, PL 11000, 00076 Aalto www.aalto.fi

Tekijä
Sampsa Laakso

Väitöskirjan nimi
Materiaalimallien kehitys ja materiaaliparametrien määrittäminen lastuavan työstön simulointia varten

Julkaisija Insinööritieteiden korkeakoulu

Yksikkö Koneenrakennustekniikan laitos

Sarja Aalto University publication series DOCTORAL DISSERTATIONS 190/2015

Tutkimusala Tuotantotekniikka

Käsikirjoituksen pvm 28.08.2015 **Väitöspäivä** 18.12.2015

Julkaisuluvan myöntämispäivä 29.10.2015 **Kieli** Englanti

☐ **Monografia** ☒ **Yhdistelmäväitöskirja (yhteenveto-osa + erillisartikkelit)**

Tiivistelmä

Lastuava työstö on kompleksinen fysikaalinen prosessi jossa prosessiparametrien vaikutukset ovat kytköksissä toisiinsa. Tämän havainnollistamiseksi on tehty graafi-analyysi, jossa kunkin prosessiparametrin kytkökset toisiinsa on esitetty vuorovaikutusverkkona. Lastuavan työstön systemaattisen kehittämäisen avuksi on olemassa työkaluja, kuten elementtimenetelmä, jolla pystyy laskemaan usean prosessiparametrin vaikutukset yhtäaikaisesti. Lastuavan työstön simuloinnilla voidaan saavuttaa merkittävää hyötyä optimoimalla kustannuksia ja laatua. Erityisesti viimeaikainen kiinnostus teollisuudessa digitaaliseen valmistukseen, suunnittelu-automaatteihin, älykkäisiin järjestelmiin ja teolliseen internetiin on tuonut lastuavan työstön mallintamisen tutkimuksen ajankohtaiseksi. Lastuavan työstön elementtimallintamista on tutkittu muutama vuosikymmen, ja menetelmä alkaa olla riittävän kehittynyt, jotta sitä voidaan soveltaa teollisuudessa. Muutamia kaupallisia mallinnusohjelmistoja on jo markkinoilla ja jotkut, erityisesti sota ja ilmailuteollisuuden yritykset ovat alkaneet soveltaa menetelmää. Menetelmän haasteena ovat materiaalimallit. Vaikka ohjelmistoissa on laajat materiaali-kirjastot, ne eivät sisällä läheskään kaikkia teollisuudessa käytettyjä materiaaleja. Kun materiaalia ei löydy kirjastosta, materiaalimallin laatiminen vaatii aikaa, erikoisosaamista ja kustannukset ovat korkeat. Tässä väitöskirjassa tutkitaan perinteisen materiaalimallinnuksen haasteita ja haetaan vaihtoehtoista tapaa materiaalikarakterisoinnille. Vaihtoehtoiseksi tavaksi esitetään lastuamiskokeiden käyttämistä materiaaliparametrien määrittämiseksi. Tätä varten käytetään analyyttistä lastuamismallia, jonka avulla lastuamiskokeista mitattavat suureet voidaan kytkeä materiaalimallissa esiintyvien suureiden kanssa. Menetelmällä saadut malliparametrit todennetaan simulaatioilla ja lastuamiskokeilla. Tämän lisäksi esitetään uutta materiaalimallia, joka pystyy mallintamaan lämpöpehmenemisen vaimentumisen. Lämpöpehmenemisen vaimentuminen huomattiin koearvoista, joita käytettiin perinteisen menetelmän arviointiin. Tutkimusmenetelmät tässä väitöskirjassa ovat lastuamiskokeet, materiaalikokeet, analyyttinen mallinnus ja simulaatiot. Tulokset osoittavat että lastuamiskokeiden käyttäminen materiaalimallinnukseen on mahdollista ja menetelmässä on käytännön kannalta potentiaalia. Lisähuomiona työssä todetaan materiaalikokeiden koeympäristön poikkeavan lastuamisen ympäristöstä siinä määrin, että pelkkien materiaalikokeiden arvojen käyttäminen lastuamisen mallintamiseen johtaa merkittävään virheeseen.

Avainsanat Elementtimenetelmä, Lastuava työstö, Johnson-Cook malli, Inversio-analyysi, Graafi-analyysi, Suuren muodonmuutosnopeuden materiaalikokeet, Sorvaaminen, Lastuamisvoima, Oxleyn malli, Tasasivuisen muodonmuutosvyöhykkeen malli

ISBN (painettu) 978-952-60-6523-6 **ISBN (pdf)** 978-952-60-6524-3

ISSN-L 1799-4934 **ISSN (painettu)** 1799-4934 **ISSN (pdf)** 1799-4942

Julkaisupaikka Helsinki **Painopaikka** Helsinki **Vuosi** 2015

Sivumäärä 103 **urn** http://urn.fi/URN:ISBN:978-952-60-6524-3

Foreword

I will begin the fo**r**ew**o**rd with one of my favorite quotes that sums u**p** the primary requirement for individual**s** doing a doctoral degree:

> "It requires a very unusual mind to undertake the analysis of the obvious."
> -Alfred North Whitehead

The concept of the obvious is in the eye of the beholder. To some people the ideas of gravity, forces or mass are trivial and mundane, though in science, those concepts are probably the most intriguing, and the research community is willing to and has already spent millions of hours and euros on the analysis. Even though the analysis does not always directly contribute to technology or business, the cumulative effects are undisputable. The quote could be rephrased thus: "It requires a very unusual imagination to see the future benefits of analyzing the obvious", though I don't think that was the original author's intent. I think that the message is closer to another quote:

> "The best scientist is open to experience and begins with romance – the idea that anything is possible."
> -Ray Bradbury

The love of knowledge and experimenting must be the driving force behind science. A career in science nowadays is not an attractive choice if one is seeking good job security, salary, status, or fame. It is an underpaid and unappreciated calling, but a calling nevertheless. I didn't realize I had this calling until I was half way through my master's degree. This endeavor of pursuing my degree has been time of self-doubt, difficulties and hardship, but also an inspiring journey into the realm of science. In writing this foreword, I can't help but feel a sense of unreal triumph. The feeling that comes from completing something that took me years of hard work and determination. I would like to thank my professor, Dr. Esko Niemi, for guiding and encouraging me through the process, my colleagues and the staff in the production engineering laboratory for their peer support and technical expertise, and all the co-authors. Thanks to my friends and peers in the Aalto University Doctoral Student Association (keep up the fight) and the industry partners and foundations for their trust and support. Finally, I would like to thank my friends and family for tolerating me during these years and letting me pursue my true love. Now it is time for another...[a]

-In Espoo, 29th of October 2015, Sampsa Laakso

[a] Foreword in: Laakso S., Finite element modeling of cutting, Master's Thesis, 2009

Contents

Abbreviations and Definitions

A	Johnson-Cook Parameter For Yield Stress
α	Rake Angle
B	Johnson-Cook Parameter For Strain Hardening
C	Johnson-Cook Parameter For Rate Hardening
C_O	Oxley's Models Strain Rate Modifier
$c_i, i \in [0,5]$	Thermal Softening Parameters For Marusich Model
C_Y	Power-Law Model Yield Stress Parameter
ΔL	Tensile Specimen Elongation
Δs_2	Shear Band Thickness
ε	Plastic Strain
$\dot{\varepsilon}$	Strain Rate
ε_{AB}	Strain In Shear Zone
$\dot{\varepsilon}_{AB}$	Strain Rate In Shear Zone
ε_{cut}	Cutoff Strain
$\dot{\varepsilon}_{ref}$	Reference Strain Rate
$\dot{\varepsilon}_t$	High Strain Rate Limit
$\dot{\varepsilon}_x$	Rate Of Strain To Direction Of X-Axis
$\dot{\varepsilon}_y$	Rate Of Strain To Direction Of Y-Axis
$\dot{\varepsilon}_z$	Rate Of Strain To Direction Of Z-Axis
FEM	Finite Element Method
f	Cutting Feed
F_c	Cutting Force
F_e, R	Resultant Force
F_f	Feed Force
F_p	Perpendicular Force
F_x	Piezoelectric Sensor's x-axis Force Component
F_y	Piezoelectric Sensor's y-axis Force Component
F_z	Piezoelectric Sensor's z-axis Force Component
k	Shear Stress In Slipline
k_{AB}	Specific Cutting Force
l	Shear Zone Length
L_0	Original Length Of Tensile Specimen
m	Thermal Softening Exponent
m_1	Rate Hardening Exponent 1 For Marusich Model
m_2	Rate Hardening Exponent 2 For Marusich Model

n	Strain Hardening Exponent
n_1	Strain Hardening Exponent For Marusich Model
n_{eq}	Oxley's Models Strain Hardening Modifier
n_Y	Power Law Strain Hardening Exponent
p	Mean Compressive Stress In Slipline
r_β	Cutting Edge Radius (Edge Preparation)
ϕ	Shear Zone Angle
ψ	Angle Of Maximum Shear Stress And Shear Strain Rate
rpm	Revolutions Per Minute
SHPB	Split Hopkinson Pressure Bar
s_1	Distance Along Slipline I
s_2	Distance Along Slipline II
σ_H	Hydrostatic Stress
σ_i	Deviatoric Stress
σ_{AB}	Stress In Shear Zone
σ_{flow}	Flow Stress
σ_x	Deviatoric Stress To Direction Of X-Axis
σ'_x	Stress To Direction Of X-Axis
σ_y	Deviatoric Stress To Direction Of X-Axis
σ'_y	Stress To Direction Of Y-Axis
σ_{yield}	Yield Stress
σ_z	Deviatoric Stress To Direction Of X-Axis
σ'_z	Stress To Direction Of Z-Axis
t_1	Uncut Chip Thickness
T_{cut}	Cutoff Temperature For Marusich Model
θ	Angle Between Resultant Force And Shear Zone
T_{melt}	Melting Temperature
T_{ref}	Reference Temperature
τ_{xy}	Shear Stress In XY-Plane
U	Cutting Speed
u	Velocity Along Slipline I
v	Velocity Along Slipline II
v_c	Cutting Speed
V_S	Shear Speed
w	Width Of Cut

List of Publications

This doctoral dissertation consists of a summary and the following publications, which are referred to in the text by their numerals.

1. Laakso, Sampsa, V.A.; Peltokorpi, Jaakko; Ratava, Juho; Lohtander, Mika; Varis, Juha. 2013. Graph-based Analysis of Metal Cutting Parameters. In: Azevedo A (ed.) Advances in sustainable and competitive manufacturing systems: 23rd International Conference on Flexible Automation & Intelligent Manufacturing. Porto, Portugal, 2628 June, 2013. Springer. Lecture Notes in Mechanical Engineering, Pages 627–636. ISBN 9783319005560.

2. Laakso, Sampsa. V.A., Hokka, Mikko; Niemi, Esko; Kuokkala, Veli-Tapani. 2013. Investigation of the effect of different cutting parameters on chip formation of low-lead brass with experiments and simulations. Sage Journals. Proceedings of the Institution of Mechanical Engineers, Part B: Journal of Engineering Manufacture, vol. 227 no. 11 pages 16201634. DOI: 0954405413492732.

3. Laakso, Sampsa V.A.; Niemi, Esko. 2015. Determination of material model parameters from orthogonal cutting experiments. Sage Journals. Proceedings of the Institution of Mechanical Engineers, Part B: Journal of Engineering Manufacture, January 8, 2015, DOI: 0954405414560620.

4. Laakso, Sampsa, V.A.; Niemi, Esko. 2015. Using FEM Simulations of Cutting for Evaluating the Performance of Different Johnson-Cook Parameter Sets Acquired with Inverse Methods. In: Chike F. Oduoza. Proceedings of the 25th International Conference on Flexible Automation and Intelligent Manufacturing, Designing for Advanced, High Value Manufacturing and Intelligent Systems for the 21st Century, Wolverhampton, United Kingdom, June 23-26, 2015. The Choir Press. Volume 2, Pages 172-180. ISBN: 9781910864012.

5. Laakso, Sampsa V.A.; Niemi, Esko. 2015. Modified Johnson-Cook Flow Stress Model with Thermal Softening Damping for Finite Element Modeling of Cutting. Sage Journals. Proceedings of the Institution of Mechanical Engineers, Part B: Journal of Engineering Manufacture, ACCEPTED FOR PUBLICATION

Author's Contribution

Publication 1: Graph-based Analysis of Metal Cutting Parameters.

The author developed the graph-based method, performed the analysis and wrote most of the article, with the exception of some parts of the introduction.

Publication 2: Investigation of the effect of different cutting parameters on chip formation of low-lead brass with experiments and simulations.

The author performed all the experimental work, with the exception of the tensile testing and SHPB experiments. All the simulations and analysis of the results of simulations and experiments were performed by the author. The article was written by the author with the exception of the parts of the results chapter related to compression tests.

Publication 3: Determination of material model parameters from orthogonal cutting experiments.

All of the work in this article was carried out by the author.

Publication 4: Using FEM Simulations of Cutting for Evaluating the Performance of Different Johnson-Cook Parameter Sets Acquired with Inverse Methods.

All of the work in this article was performed by the author.

Publication 5: Modified Johnson-Cook Flow Stress Model with Thermal Softening Damping for Finite Element Modeling of Cutting.

All of the work in this article was performed by the author.

1 Introduction

Metal cutting is one of the most common processes in industry, and annual sales of machine tools have been growing since the 1980s. In the last few years sales have been worth roughly 60 billion euros according to Gardner's World Machine-Tool Output & Consumption Survey [1]. The metal cutting process is of interest to researchers because of the high costs and case-specific process control parameters. As a result, the research results are valuable for increasing the efficiency of industrial production. Additionally, metal cutting involves unique material deformation characteristics. Therefore, the theoretical foundation in metal cutting mechanics and materials technology is scientifically interesting. Even though machining and the process of chip formation in metal cutting have been researched since the beginning of the 20th century, most notably by Taylor in 1907 [2], there are still many unanswered questions and researchers have not been able to develop a general theory that explains every phenomenon occurring during the cutting process. A quote from a research paper by Usui et al. in 1984 is still a good guideline for modern metal cutting research [3]:

> "It should be recalled that the goal of metal cutting research is to establish the theory or analytical model which enables the cutting tool wear and other necessary parameters such as chip formation, cutting force, cutting temperature and surface finish to be predicted quantitatively without any cutting experiment."

Over the last few decades, metal cutting research has been focusing more on Finite Element Modeling (FEM), and it seems that this direction could lead to the model that Usui et al. wrote about. Mackerle composed a bibliography of research papers where FEM is applied to the cutting process from years 1976-2002 [4,5]. A review article by Arrazola et al. from 2013 investigates the advancements made in metal machining processes. In summary, it suggests that despite the advancements in predictive modeling, using these methods in industry is not yet practical due to the high skill requirements and case-specific conditions. The research should be more collaborative and practical applications should be emphasized. [6] The major difficulty in FE modeling of cutting is obtaining the parameters describing the material behavior characteristics in a similar environment to metal cutting, which are required to numerically solve the governing partial differential equations behind the physics of the cutting process. This dissertation aims to address that by investigating the state-of-the art process of material characterization and the difficulties involved, estimating the complexity of the cutting process with graph analysis, and comparing different methods for material parameter acquisition from cutting experiments.

1.1 Background and Research Gap

Material models used in FE simulations of cutting are generally phenomenological descriptions of the stress-strain relation of the work materials. The material models are called flow stress models or yield surfaces. [7] The stress-strain behavior is considered to be dependent on strain, strain rate and temperature. [8] The output of the model is flow stress, which is the equivalent of yield stress after which the deformation of the material leads to chip formation. There are three main procedures to obtaining the parameters for the flow stress models: materials testing [8], inverse modeling with simulations, [9] and inverse modeling with analytical models [10]. Inverse modeling with cutting experiments and analytical models were suggested as subjects for investigation in the dissertation by Sartkulvanich in 2007, [11] which was used as the starting point of the research plan in this dissertation after identifying it as the research gap.

The main difficulty in materials testing, namely tensile or compression testing and Split Hopkinson Pressure Bar (SHPB) testing, is that the experimental conditions are not close enough to cutting conditions. The most difficult condition to achieve is the level of strain, that is around 1-2.0 in cutting, but in materials testing, depending on the work material, 0.5 is already difficult to test. Second, the strain rate in cutting is around 50,000 1/s and even up to 10^6 1/s, but with SHPB testing the highest measurable strain rates are of the magnitude of 10000 1/s. [8,12] The testing is even more difficult to conduct in cutting temperatures that reach almost up to the work materials' melting point in some cases. Different solutions for preheated material specimens or special ovens for material testing have been found, but exact temperature control is difficult.

Inverse modeling with simulations is a good way to directly tune the material model to produce results that are close to cutting experiments, but this method is time consuming due to the number of simulations required. This method requires two or three different values for each material model parameter to be simulated, and the multiplicative effect of the complexity of the material model, i.e. the number of parameters in the model, is exponential. This method is best used in fine tuning the model, especially when damage models are used in addition to flow stress models. Damage models track the loading history of the work material and adjust the flow stress or yield stress accordingly. Damage models are important in simulating chip breakage and saw-toothed chip formation. [13,14]

Inverse modeling with an analytical model is faster than with simulations, but the use of analytical model adds another layer of uncertainty between the experiments and simulations. The typical approach is to use a parallel-sided shear zone model for inverse analysis, like in Sartkulvanich et al. in 2004. [10] Another interesting method was proposed by Agmell et al. in 2013 and 2014 [15,16], which is to use a Kalman filter for the inverse determination of Johnson-Cook parameters from cutting experiment data; the results show good agreement with the experiments.

Overall, the best results can be achieved by using all the three methods together, but the expertise, time, and cost demands are high. Materials testing is not overly expensive or time consuming when identifying the stress-strain behavior at room temperature and a moderate strain rate. That data can be used as a starting point for inverse analysis with analytical models to reduce the number of simulations required in full factorial analysis. The most difficult part is to calculate the strain, strain rate and

temperature with analytical models, and the method also requires a wide set of cutting conditions for good results. Plastic strain in particular is subject to some debate in the cutting research community; Astakhov and Shvets criticize the method of defining plastic strain in cutting based on the geometry, and state that the magnitude of strain is much higher than the theoretical maximum. They propose to use the chip compression ratio as the measurement of strain. [17] In 2009 Davim and Maranhão reported totally opposite results in their research, where they compared plastic strain and strain rate calculated using the single shear plane theory [18,19] to simulate results, and the correlation was excellent. [20] This dissertation aims to add to the research in inverse modeling and material parameter acquisition by investigating all the methods in parallel fashion.

1.2 Objectives, Scope and Research Questions

The research in this dissertation addresses the problems in obtaining the material model parameters and fitting the model parameters to material data. Each of the articles presented in the thesis have their independent objectives that are discussed only in the papers; in addition, the objectives discussed in this chapter focus on the larger scale objectives in the framework of this dissertation. Figure 1 presents the dissertation framework regarding the original articles (marked in blue) and how the individual articles are related to the wider context. The red parts in the figure are out of scope for this thesis, but are significant elements of the preliminary work that led to this dissertation.

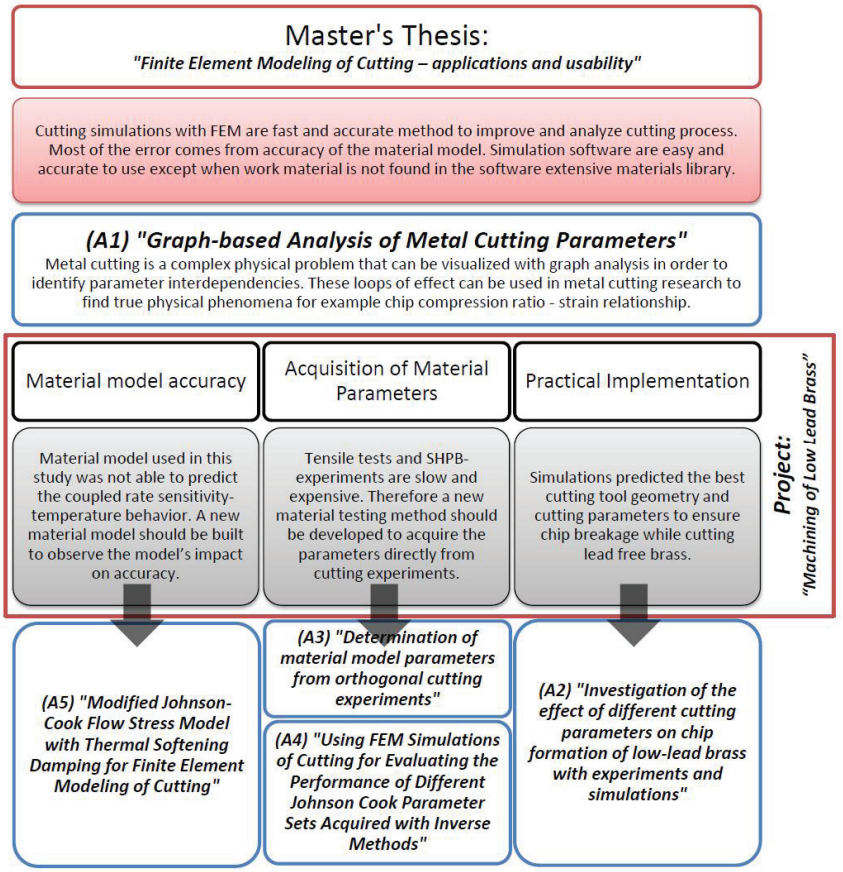

Figure 1. The framework of the dissertation from the original articles. Red parts are out of scope of the dissertation

The first conference article (A1) focuses on the complexity of the cutting process and the interdependencies of different cutting parameters, and on identifying the major parameters that affect the measurable variables in cutting. On a larger scale, the research answers the question of whether it is possible to differentiate between the effect of strain, strain rate and temperature on flow stress by means of adjusting cutting parameters like cutting speed, feed, or tool geometry. This paper outlined the qualitative relations between parameters found in the literature. The second paper (A2) investigates the effect of different cutting parameters on chip breakage of low-lead brass. It is a state-of-the-art review of the process of initially performing material testing to obtain the material model parameters and then evaluating and adjusting the simulation model to cutting experiments. The research objectives were to identify the shortcomings of the standard procedure of material modeling. A new research question was identified from the results regarding the material model incapability of modeling thermal behavior. The third article (A3) investigates an inverse method of obtaining the model parameters using an analytical model and cutting experiments. The experimental data on cutting force, chip thickness, and cutting temperature is used as an input instead of relying on analytical solutions regarding those variables. This investigation is outlined in non-brittle materials, namely AISI-1045 steel. The proposed method performed well, but the capability of identifying complex thermal behavior

was questioned. The paper also investigates the definition of plastic strain in cutting, which has been the subject of some debate in the research community. The outcome in this paper is that when using Oxley's parallel-sided shear zone theory, the definition proposed by Oxley should also be used. The fourth paper (A4) is a conference article which expands the results of the third article in practice and compares the simulation results with parameters obtained from the inverse method for cutting experiments. The fifth paper (A5) revisits the material data of low-lead brass and investigates the issues related to thermal softening dampening: The effect of thermal softening diminishes with increasing strain rate in the material testing results. A new material model was developed to address this phenomenon and simulations with the model were compared to cutting experiments to determine the significance of this dampening effect on cutting. This article also responds to a question that arose from the results of articles 2 and 3 regarding the thermal behavior.

1.3 Research Methods and Dissertation Structure

This dissertation approaches the research questions with a strong emphasis on quantitative experimental methods and simulations. All hypotheses are scrutinized by comparing them to literature results. The experimental methods used are cutting force measurements, material testing and chip morphology measurements. Simulations are performed using the finite element method and analytical models. Materials testing includes tensile and compression test and SHPB measurements. This dissertation first presents the theoretical foundation behind metal cutting, the parallel-sided shear zone model, materials testing, the finite element method and cutting experiments. The second part presents the primary findings in the research articles and closes with a discussion on the practical and theoretical implications of the results. The articles are included in the appendices.

2 Theoretical Foundation

The theories and methods used in this dissertation and in the articles are presented in the following chapters. The theoretical foundation in this dissertation is based on the mechanical behavior of materials under metal cutting conditions. Definitions and theories of metal cutting are presented first in order to form a picture of the conditions which the work materials are exposed to. Presenting the standard definitions is critical for establishing general terminology to avoid vagueness and misconceptions. The theory of metal cutting and the parallel-sided shear zone model play a key role in articles 3 and 4, and are therefore presented in more detail. Following this, the materials testing methods are presented to understand how the material behavior is experimentally determined. The finite element method is introduced to explain how the material data is used in the models. Cutting experiments are presented regarding cutting force, temperature and chip morphology measurements. Finally, since friction is an important factor in metal cutting, the theory and difficulties in friction modeling are presented to explain the unique contact conditions in the tool-chip interface, though friction is not within the scope of this work.

2.1 Metal Cutting

Metal cutting is a material removal process where relative movement between the tool and the work produces the energy required for material removal. There are two main categories of metal cutting: Cutting with arbitrarily-shaped abrasive tools, and cutting with determined-shaped, single-point tools. Processes with arbitrarily-shaped abrasive tools include grinding, lapping, and polishing, whereas turning, milling, drilling, and boring are cutting processes with determined-shaped, single-point tools. This dissertation focuses on cutting with determined-shaped, single-point tools – turning, to be exact. Process variation caused by the changes in microgeometry of the tool due to manufacturing tolerances and tool wear are minimized in this work by using new tool in each experiment or the tool is sharpened after each experiment. The microgeometry such as the rake face surface roughness or cutting edge preparation, i.e. the cutting edge roundness r_β are not measured except in macro level.

If cutting can be reduced to a single plane, i.e., the chip flow is on the same plane as the cutting motion, it is called orthogonal cutting, as presented in Figure 2 b). [21] In that case, the cutting motion is perpendicular to the tool cutting edge. If the direction of the flow deviates from the direction of the cutting motion, the cutting is oblique, as in Figure 2 a). There are not many cases where the cutting is completely orthogonal, but often it can be used as a good approximation: Turning with a cutting edge angle of 90 degrees, for example, can be considered orthogonal if the diameter of the work is much larger than the cutting depth, and the nose radius of the tool is left out of consideration, or groove turning of flanges with a radial feed, especially with larger work

diameters, can be considered as orthogonal cutting. Fully orthogonal cases are found in broaching or planing processes. [22]

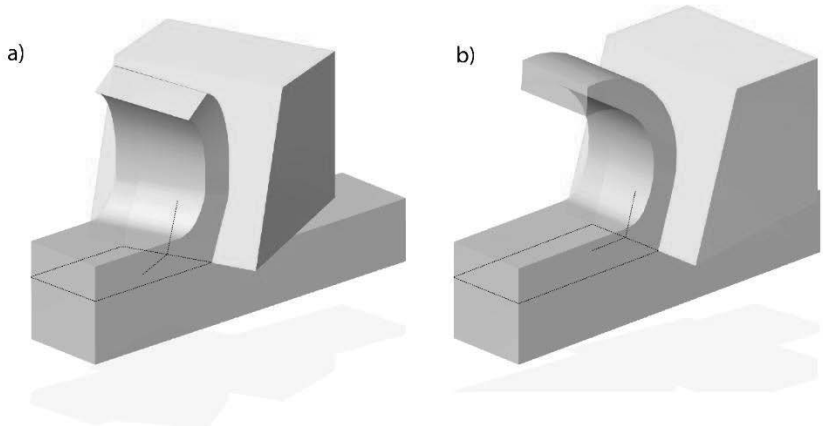

Figure 2. a) Oblique and b) orthogonal cutting

Turning is a process where the cutting movement is produced by the rotating spindle where the work is fixed. Figure 3 presents the cutting parameters and cutting forces. The cutting speed is given either as rotation speed (rpm) or surface speed (mm/min), denoted by U or v_c. The work in this dissertation is always a round cylinder, but the turning of a rectangular or other arbitrarily-shaped work is also possible. Feed (mm/r) denoted by f is the movement of the tool at a speed that is synchronous with the rotational speed, therefore keeping the undeformed chip thickness constant. The feed direction is either radial or axial to the work. The width of cut is either the radial depth of the tool or the width of the tool in the case of radial feed. Cutting forces are denoted by F_c, F_p and F_f. Cutting force F_C is the primary force that is tangential to the work. Perpendicular force F_e is parallel to the tool holder in turning and perpendicular to the other two force components. Feed force F_f is parallel to the feed direction but in groove turning the force is equal to the perpendicular force F_e. [22]

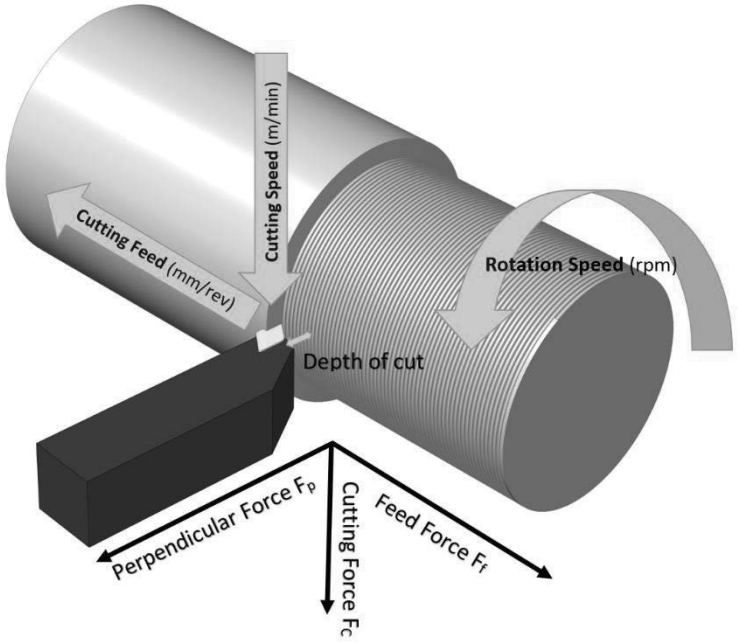

Figure 3. Cutting Forces and Primary Cutting Parameters

The tool geometry is defined by the rake angle, release angle, cutting edge angle, inclination angle, nose radius and cutting edge preparation. The most relevant tool geometry is presented in Figure 4. [23]

A) Rake Face and G) Rake Angle
B) Cutting Edge Preparation
C) Flank / Clearance Angle I) Flank Face
D) Tool Nose Radius
E) Cutting Edge
F) Cutting Edge Angle
H) Inclination Angle

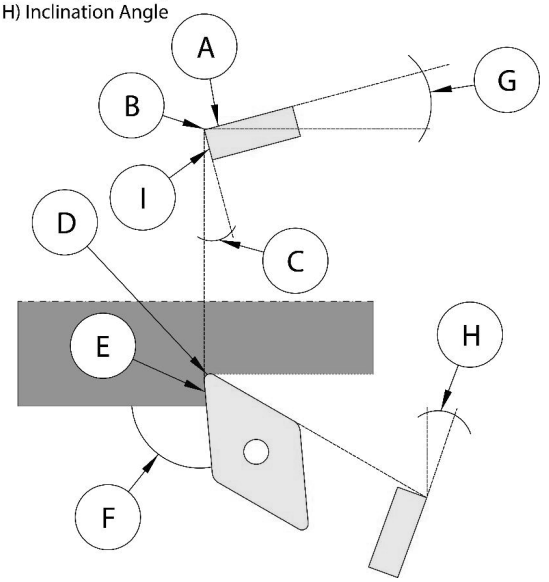

Figure 4. Turning Tool Geometry

2.1.1 Oxley's Parallel-Sided Shear Zone Model

Oxley's shear zone model (Oxley, 1989) builds on the assumption of plane strain conditions, i.e., in orthogonal cutting all deformations take place in the x-y plane, as in Figure 5. Elastic strain is considered negligible, and Lévy-Mises equations (1-3) are used to describe the strain behavior in different directions for isotropic materials. Deformation takes place in the direction of the load, as presented in equation 1, which leads to the deviatoric stress component in the direction of the Z-axis, which is equal to zero in plane strain conditions. Stress in the direction of the Z-axis can be calculated from the definition in equation 2 that leads to the Lévy-Mises equations for plane strain conditions presented in equation 3. The von Mises yield criteria is used to calculate the combined effect of the stresses, which is used as an equivalent stress on a yield surface. For plane strain conditions, the von Mises yield criteria is reduced to the form presented in equation 4. The sum of all forces must be zero and body forces are assumed to be negligible. Volume is assumed to be constant.

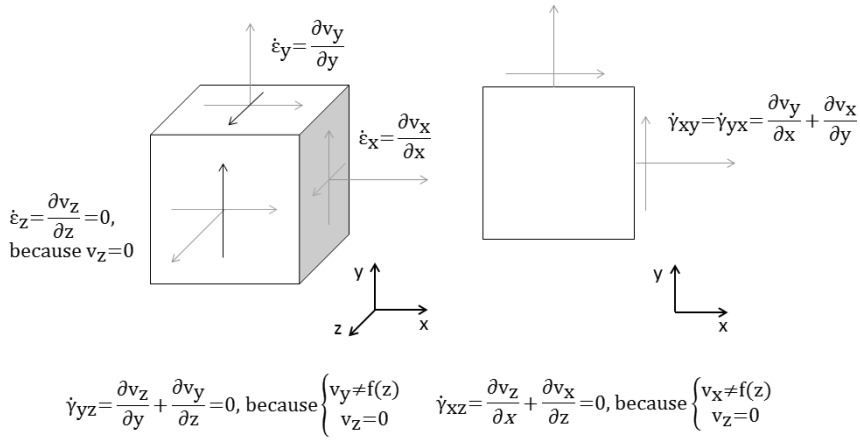

Figure 5. Plane strain conditions, rate of deformation is zero in the z-direction

Lévy-Mises equations	$\frac{\dot{\varepsilon}_x}{\sigma'_x} = \frac{\dot{\varepsilon}_y}{\sigma'_y} = \frac{\dot{\varepsilon}_z}{\sigma'_z}$	1
Stresses divided into hydrostatic and deviatoric components	$\sigma'_i = \sigma_i - \sigma_H$ $\sigma_H = \frac{1}{3}(\sigma_x + \sigma_y + \sigma_z)$	2
Lévy-Mises equations for plane strain	$\sigma_z = \frac{1}{2}(\sigma_x + \sigma_y)$	3
Von Mises yield criteria	$1/4\,(\sigma_x - \sigma_y)^2 + (\tau_{xy})^2 \geq 1/3\,\sigma_{yield}^2$	4

Slip lines are formed in the directions of the maximum shear in each point of the deforming work, as presented in Figure 6, where k represents the shear stress and p is the mean compressive stress. The sliplines can be presented as functions (equations 5-6) derived from equilibrium equations and stress transformations. Geiringer equations (7-8) are the velocity transformations along lines I and II that fundamentally state that the deformation speed is highest in the direction of the lines. The deformation zone is where the largest strains form a field of slip lines. Oxley's model assumes that the deformation zone can be approximated with the parallel-sided shear

zone, where the deformations takes place in the rectangular area in front of the tool-chip contact surface.

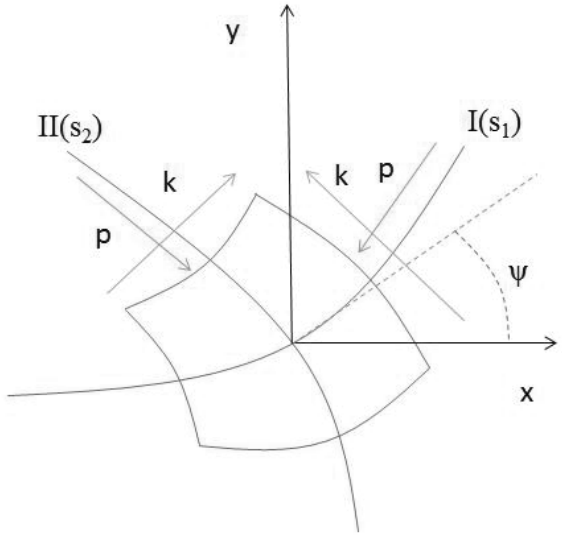

Figure 6. Slipline I presents the positive shear stresses and II presents negative shear stresses

Slipline equation along line I	$\frac{\partial p}{\partial s_1} + 2k\frac{\partial \psi}{\partial s_1} - \frac{\partial k}{\partial s_2} = 0$	5
Slipline equation along line II	$\frac{\partial p}{\partial s_2} - 2k\frac{\partial \psi}{\partial s_2} - \frac{\partial k}{\partial s_1} = 0$	6
Geiringer equation along line I	$du - vd\psi = 0$	7
Geiringer equation along line II	$dv + ud\psi = 0$	8

Figure 7 presents the geometrical definition of the model. In the figure, lines FE and DC represent the boundaries of the parallel-sided shear zone. The height of the zone, shear band thickness, is denoted as Δs_2. The geometry is defined by the shear zone angle ϕ, rake angle α and uncut chip thickness t_1. The shear strain takes place in plane AB.

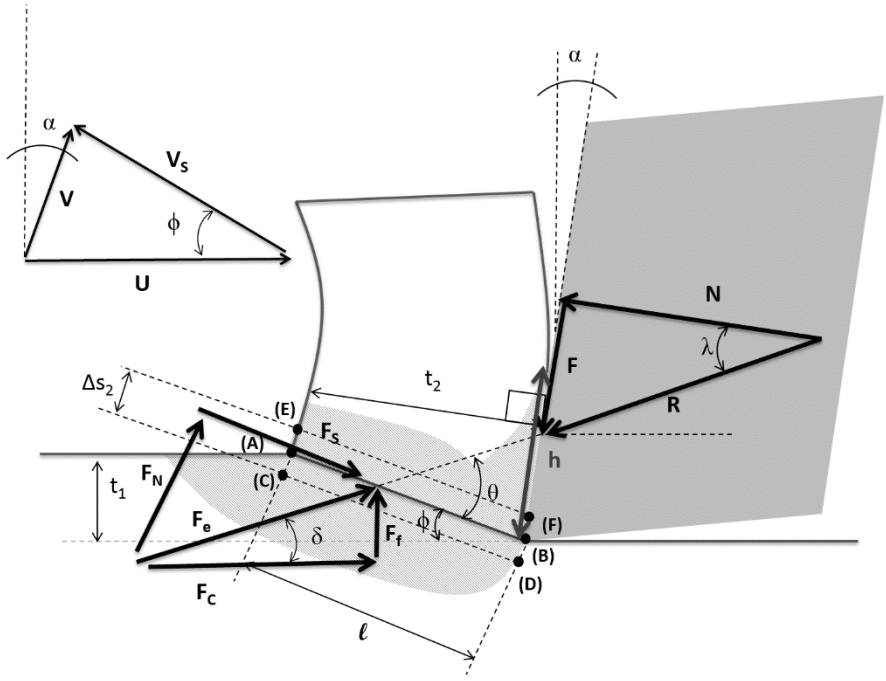

Figure 7. Oxley's shear zone model and velocity diagram modified from Oxley [24]

The shear stress is calculated from cutting forces as defined in equation 9. The shear stress required for chip formation is named "specific cutting force k_{AB}", which is equivalent to yield stress using the von Mises yield criteria as defined in equation 10. Equation 11 provides the relationship between resultant force angle and shear plane angle, which is referred to as Oxley's model. The model has been derived from the slipline equations by substituting k, p, s_1, s_2 and Ψ with observed conditions from cutting experiments. Yield stress at different temperatures and strain rates is modeled with flow stress models. Flow stress models give the corresponding stress for the strain, strain rate, and temperature in the shear zone during cutting. The flow stress model used in the original work of Oxley is the power law, presented in equation 12. [24] The coefficient C_Y is the equivalent of initial yield stress and n_Y is the strain hardening exponent. In addition, Johnson-Cook model is presented in equation 13. [25] This model has an important role in this dissertation since it is used in articles 3-5 for inverse modeling and as a basis for modeling thermal damping. The Johnson-Cook model is discussed in more detail in section 2.3.1. C_o and n_{eq} are parameters that take into account the effect of strain hardening, temperature and strain rate. Both are dependent on which flow stress model is used. The values are calculated from equations 14 and 15. Equations 16-18 present the modifiers for the power law and the Johnson-Cook model. Equation 16 was introduced by Lalwani et al. in 2009 to implement the Johnson-Cook model to Oxley's parallel-sided shear zone theory [26]. Strain and strain rate are calculated from the geometry using equations 19 and 20. The shear speed required for calculating strain rate can be calculated from the velocity diagram in equation 21. Temperature can be calculated using the model proposed by Boothroyd et al. in 1989, but the model is not used in this dissertation since the temperature is measured from experiments. [27]

Resultant force	$R = F_e = \sqrt{{F_C}^2 + {F_f}^2} = \frac{k_{AB} t_1 w}{\sin\phi \cos\theta}$	9
Specific cutting force	$k_{AB} = \frac{1}{\sqrt{3}} \sigma_{yield} = \sigma_{flow}(\varepsilon, \dot{\varepsilon}, T)$	10
Oxley's model	$\tan\theta = 1 + 2(\frac{\pi}{4} - \phi) - C_0 n_{eq}$	11
Power law model	$\sigma = C_Y \varepsilon^{n_Y}$	12
Johnson-Cook model	$\sigma = (A + B\varepsilon^n)\left[1 + C \ln\left(\frac{\dot{\varepsilon}}{\dot{\varepsilon}_{ref}}\right)\right]\left[1 - \left(\frac{T - T_{ref}}{T_{melt} - T_{ref}}\right)^m\right]$	13
Strain rate modifier	$C_0 = 1 + 2\left(\frac{\pi}{4} - \phi\right) - \frac{\tan\theta}{n_{eq}}$	14
Strain hardening modifier	$n_{eq} = \left(\frac{d\sigma_{AB}}{d\varepsilon_{AB}}\right)\left(\frac{\varepsilon_{AB}}{\sigma_{AB}}\right)$	15
Strain hardening modifier for power law	$n_{eq} = \left(\frac{d(C_Y \varepsilon^{n_Y})}{d\varepsilon}\right)\left(\frac{\varepsilon}{C_Y \varepsilon^{n_Y}}\right) = n_Y$	16
Strain hardening modifier for Johnson-Cook	$n_{eq} = \left[\left(\frac{\partial\sigma}{\partial\varepsilon}\frac{d\varepsilon}{d\varepsilon}\right) + \left(\frac{\partial\sigma}{\partial\varepsilon}\frac{d\dot{\varepsilon}}{d\varepsilon}\right) + \left(\frac{\partial\sigma}{\partial T}\frac{dT}{d\varepsilon}\right)\right]\left(\frac{\varepsilon_{AB}}{\sigma_{AB}}\right)$	17
Simplified strain hardening modifier for Johnson-Cook	$n_{eq} \approx \frac{nB\varepsilon^n}{A + B\varepsilon^n}$	18
Strain	$\varepsilon = \frac{1}{2\sqrt{3}} \frac{\cos\alpha}{\sin\phi \cos(\phi - \alpha)}$	19
Strain rate	$\dot{\varepsilon}_{AB} = C_0 \frac{V_S}{l\sqrt{3}}$	20
Shear speed in respect to cutting speed	$V_S = \frac{U \cos\alpha}{\cos(\phi - \alpha)}$	21

2.2 Material Testing

The material testing methods in this dissertation are tensile testing, compression testing and SHPB testing. Tensile testing subjects the material specimen to tensile load. The tensile loading force is measured in respect to the elongation of the specimen. The data can be presented as an engineering stress-strain curve or a true stress-strain curve. Engineering stress is calculated by dividing the load by the area of the specimen's cross-section. An engineering strain is calculated as a ratio of elongation and the original specimen length. Since the cross-section area of the specimen decreases with increasing elongation, true stress is calculated by dividing the prevailing force with the actual cross-section of the specimen at each time step. True strain is an incremental change in length divided by the original length, integrated over time. This leads to equation 22 [28, pg. 4-12]. All the material testing data in this dissertation is presented as true stress-strain curves.

True stress	$\varepsilon = \ln \Delta L / L_0$	22

SHPB testing can be used to test a material's response to high speed deformation. Tensile and compression tests can be performed at up to 10^4 1/s strain rate. The device consists of testing a specimen placed between an incident bar and a transmission bar. A high speed stress wave is generated at the front end of the incident bar with an external impact device such as a hammer or a bullet. The stress wave travels through the incident bar, the specimen and the transmission bar, and then travels back through. The wave is measured traveling in both directions with strain gauges. The response of the test specimen can be then calculated from the difference between

the propagating and reflected waves. The specimen can be preheated for testing at a high temperature. Conducting the experiments at a static strain rate and temperature is difficult and the exact data often requires inverse methods with FEM. [29, pp. 1-11]

2.3 Finite Element Method

The finite element method is used for solving differential equations describing the physics behind a problem, using numerical methods. In metal cutting simulations, the non-linear coupled governing equations require special attention in the solving routines. First of all, the simulation requires that the tool and work geometry are discretized, i.e., they are presented as a mesh of triangular or quadrilateral elements. This is done because an analytical solution to the equations for the complex geometry cannot be found. The solution is calculated for the nodal points of the elements in the mesh and the point vice values are interpolated along the element sides. Interpolation can be performed with linear or higher degree functions. Different formulations for kinetics, kinematics and mesh are Eulerian, Lagrangian, and a combination of both. The fundamental difference is that the mesh in the Lagrangian formulation changes shape with the solution, while the mesh in the Eulerian formulation is static. An arbitrary Lagrangian Eulerian formulation utilizes the benefits of both methods so that the boundary elements deform with the solution but the internal elements retain their shape to minimize the element distortion, which is a major drawback of the Lagrangian method, especially with problems that include large deformations. Eulerian formulation can be used also in situations where the mesh retains the shape, for example in the machined surface that the tool has already passed. A model by Miguélez et al. [30] presents a method to minimize the iteration required to guess the initial shape of the chip with Eulerian mesh on the entrance of the workpiece and on the chip. To further avoid the mesh distortion, especially in cutting simulations, the meshing is done again when the element distortion reaches a certain limit. This is called remeshing. This way the use of a chip separation criteria can be also avoided, which has a significant effect on accuracy. The chip separation criteria deletes the elements in which the strain reaches a certain limit and thus allows for chip formation. This method causes volume loss in the workpiece and thus the accuracy of the model is decreased [31]. The uniqueness of the chip separation criteria was criticized in Zhang, 1999 where it is concluded that none of the chip separation criteria produce reliable results and the criteria are cutting parameter dependent [32]. This method was used in early works of cutting simulations, but with remeshing the use of it has reduced. Time integration is done either implicitly or explicitly. [33] In this dissertation, the finite element software used is Third Wave Systems' AdvantEdge, which was first presented in a paper by Marusich and Ortiz in 1995 [34]. The software is based on a dynamic explicit Lagrangian finite element model, which employs adaptive remeshing to avoid element distortions. The model is based on equations of motion and a thermomechanically coupled material model.

2.3.1 Flow Stress Models

Flow stress models or yield surfaces are functions that determine the corresponding stress for a given strain, strain rate and temperature. In AdvantEdge FEM, the yield stress is calculated as von Mises equivalent stress with equivalent plastic strain, strain

rate and temperature. One of the most common models is the Johnson-Cook model [25], presented in equation 13, where each variable has its own independent multiplicative effect on yield stress. Strain hardening causes the yield stress to increase with increasing plastic strain. Rate sensitivity increases the yield stress when strain rate increases. Thermal softening decreases the yield stress with an increase in the temperature. Similar model is implemented in AdvantEdge (equation 23) as a built-in custom material model. Johnson Cook model is presented in Figure 8, Figure 9 and Figure 10 using AISI 1045 and AISI 316L steel values to compare to Marusich model that is presented using values for EN CW511L brass. These figures present a typical behavior for most engineering materials. The values for AISI 316L are from Tounsi et al. 2002 [35] and AISI 1045 from author's 3rd publication. The values for AISI 316L were later validated in Umbrello et al. 2007 [36], where they compared 5 different sets of Johnson-Cook parameters for AISI 316L and the set by Tounsi et al. produced the best results compared to cutting experiments. The values for EN CW511L brass are modified after author's publications 1 and 5 for compatibility with Marusich model. The models have a few differences: First, the most significant difference is that the strain hardening (equation 24) is limited by cut-off strain, after which the stress does not increase with increasing strain, as presented in Figure 8. Also, the rate sensitivity function (equation 25) is a piecewise defined exponential function as presented in Figure 9, instead of the logarithmic function in Johnson-Cook model. The rate sensitivity function has different exponents for different strain rate intervals, one for strain rates less and another for strain rates greater than the transitional strain rate. Finally, the form of the thermal softening function (equation 26) is a user-defined polynomial of up to 5th order, presented in Figure 10 instead of the exponential function.

Extended power law (Marusich model)

$$\sigma = \sigma_{yield} g(\varepsilon) \Gamma(\dot{\varepsilon}) \Theta(T) \tag{23}$$

Strain hardening with hardening cut-off

$$g(\varepsilon) = \begin{cases} \left(1 + \dfrac{\varepsilon}{\varepsilon_{ref}}\right)^{\frac{1}{n_1}} & when\ \varepsilon < \varepsilon_{cut} \\ \left(1 + \dfrac{\varepsilon_{cut}}{\varepsilon_{ref}}\right)^{\frac{1}{n_1}} & when\ \varepsilon \geq \varepsilon_{cut} \end{cases} \tag{24}$$

Rate sensitivity

$$\Gamma(\dot{\varepsilon}) = \begin{cases} \left(1 + \dfrac{\dot{\varepsilon}}{\dot{\varepsilon}_{ref}}\right)^{\frac{1}{m_1}} & when\ \dot{\varepsilon} \leq \dot{\varepsilon}_t \\ \left(1 + \dfrac{\dot{\varepsilon}}{\dot{\varepsilon}_{ref}}\right)^{\frac{1}{m_1}} \left(1 + \dfrac{\dot{\varepsilon}_t}{\dot{\varepsilon}_{ref}}\right)^{\frac{1}{m_1} - \frac{1}{m_2}} & when\ \dot{\varepsilon} > \dot{\varepsilon}_t \end{cases} \tag{25}$$

Thermal softening

$$\Theta(T) = \begin{cases} \displaystyle\sum_{i=0}^{k} c_i T^i & when\ T < T_{cut} \\ \left(\displaystyle\sum_{i=0}^{k} c_i {T_{cut}}^i\right)\left[1 - \dfrac{T - T_{cut}}{T_{melt} - T_{cut}}\right] & when\ T \geq T_{cut} \end{cases} \tag{26}$$

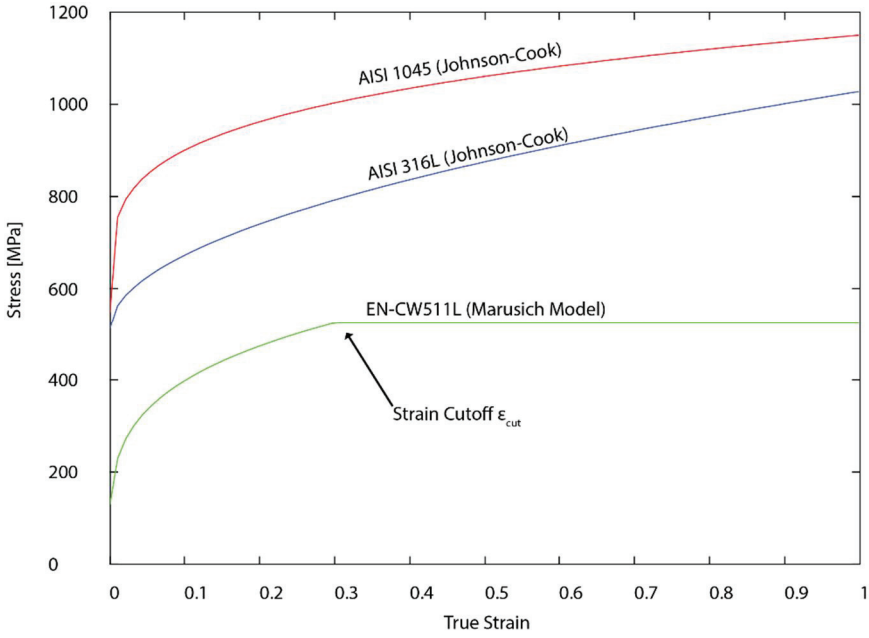

Figure 8. Strain hardening multiplier

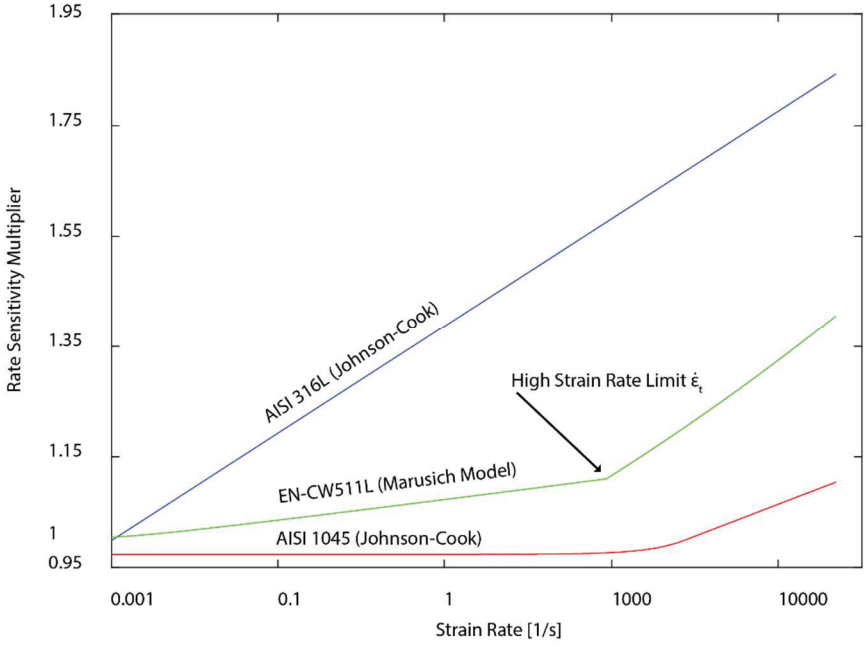

Figure 9. Rate sensitivity multiplier

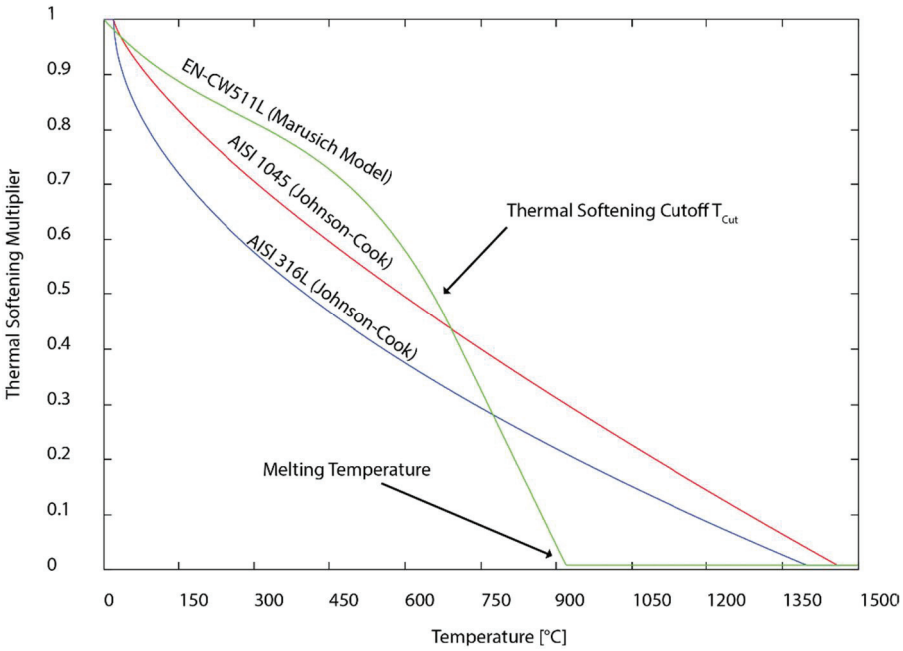

Figure 10. Thermal softening multiplier

2.3.2 Friction

Friction is an important factor in cutting, but no single ubiquitous friction model has been developed that explains the contact phenomena at the tool-chip interface. Analytical models and FE simulations of cutting are often required to use friction coefficients that are significantly greater than those measured from experiments in tribology. Friction does not have a particularly important role in this dissertation, since the material model performance is unrelated to the friction model. The final results are affected by the friction model but it is proportional to the cutting force so the different material models can be evaluated against each other. The friction model used in the accompanying papers is Coulomb friction model. The friction model has been shown to have a significant effect on simulated results of chip geometry, forces, stresses on the tool, and the temperature at the tool-chip contact interface. The simulations are in best agreement with experiments regarding the above mentioned values when a variable friction model is used. [37] A variable friction model was proposed by Childs in 2006, where the friction coefficient is a function of plastic strain. [38] A recent study by Puls et al. in 2014 shows that the friction coefficient is temperature-dependent so that as the temperature increases, the friction coefficient decreases. The article proposes a friction model that is similar to the Johnson-Cook thermal softening term. Simulations with the model are in good agreement with experiments. [39]

2.4 Cutting Experiments

Cutting experiments have been the primary research method in metal cutting research since the beginning of the 20th century. Cutting forces, cutting temperature and chip morphology have been established as the primary variables of measurement from the

experiments. Recent developments in high speed imaging and digital image correlation have resulted in attempts to perform direct measuring of strain and strain rate, as in Mahadevan, 2005 [40], or by Mäenpää et al. 2003 [41]. Thermal imaging can also be used to determine the shear zone characteristics as in Artozoul et al. in 2014 [47]. Other important but more practical variables for cutting experiments are tool wear, surface quality, and residual stresses.

2.4.1 Cutting Forces

Cutting forces are measured directly with piezoelectric force sensors and indirectly using spindle power with accelerometers or with strain gauges placed in the tool holder. Piezoelectric sensors have high dynamic response (natural frequency >3.5 kHz) and better accuracy compared to indirect measuring [42]. The instruction manual [43] of a similar Kistler sensor as used in the experiments in this dissertation states that the natural frequency of the sensor should be about 3 times the signal frequency to avoid significant error in the measurement. Chip formation is cyclic in nature and for example, the frequency (number of chip teeth formed in unit time) of the chip formation for AISI 1045 steel is between 0.1-4.5 kHz with cutting speeds of 12-180 m/min after Astakhov, 2006 [49, pages 53-57]. A signal processing theory, the Nyquist-Shannon theorem states that the measuring frequency higher than or equal to twice the frequency of the measured signal is enough for sampling the signal [44]. Therefore, the sampling rate in the case of AISI 1045 should be around 10 kHz, and if the chip formation cycle is required to be measured, cutting speed up to 120 m/min can be used for sensor with natural frequency of 3.5 kHz. Figure 11 presents the structure of a 3-axis dynamometer. The orientation of the sensor on the lathe affects the designation of force component in relation to the sensor co-ordinate system: Cutting force Fc is always to the F_Z direction but F_X and F_Y can either represent feed force F_f or perpendicular force F_p. Figure 11 presents the structure of a 3-axis dynamometer. Piezoelectric sensors in metal cutting applications have the following sources of error: Triboelectric effect can disturb charge signals when the charge is small, e.g., small forces, and the effect can be generated if the cables are shifting. Charge amplifiers have electrical drift that stabilizes approximately 30 min. after powering up the amplifier. The amplifier drift is ±0,03 pC/s that equals at maximum about ±0.2%/s depending on the measured force, according to a presentation by Blattner, 2013 [45]. The insulation and connectors of the cables causes signal drift, especially if the connectors are polluted. Thermal drift of the sensor is caused by thermal expansion of the preloading bolt during use. The mounting of the dynamometer on the machine table is essential, and the more connection points there are, the better. The added mass on the dynamometer, such as a tool holder, for example, should be as light as possible since the added mass decreases the frequency response and higher mass causes higher inertial forces thus the signal peaks are overestimated.

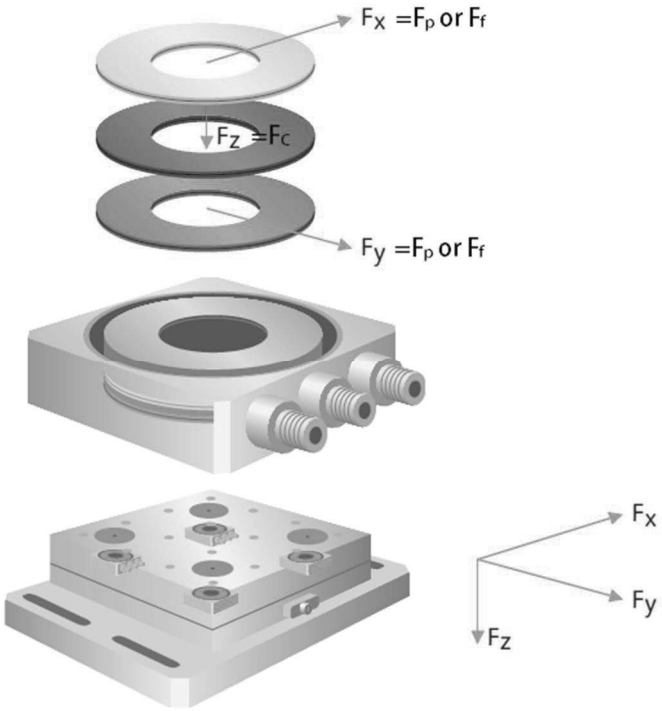

Figure 11. Structure of a 3-axis piezoelectric force sensor, modified after [45]

2.4.2 Cutting Temperature

Cutting temperature can be measured with a thermocouple composed of the cutting tool and work. This gives the mean temperature difference between the two. This method provides good dynamic response but it is not clear what exact temperature is measured. Another use of a thermocouple is to embed it inside the tool, but this method has a slow response to temperature changes and errors can be high because the air between the thermocouple and the tool acts as an insulator. Single wire thermocouples have been used for measuring the temperature inside the work during milling. Infrared pyrometers are optical temperature sensors that have a fast response time and they do not require contact with the measured object. As with all infrared measuring methods, the object's emissivity must be taken into account. This can be done by calibrating the sensor. Infrared cameras or thermal cameras are viable methods for measuring the temperature. With the correct emissivity value, the measurements are accurate. The object should be painted black to minimize the error resulting from the emissivity. The difficulty is the sample rate and thus resolution that is too low for high speed machining experiments. Other more exotic methods have been used, but often their wider use is not practical. [46] One successfully applied IR method is presented by Artozoul et al. in 2014, where an infrared camera and a force measuring system were used to calculate not only the temperature fields, but also friction, tool-chip contact length, specific cutting energy, and shear angle. [47]

2.4.3 Chip Morphology

Chip morphology is measured from the formed chip, quick stop experiment samples, or from the cutting process with a high speed camera. The most important measures in chip morphology are the chip thickness, the shear band thickness and chip segmentation. Sometimes the chip curvature and chip length are measured but that is more of an application-specific requirement. The measurement is performed with an optical microscope in case of chip thickness. In this work, the chip thickness and chip compression ratio calculated from it are the most important measures since they can be used for evaluating the plastic strain in shear zone. Shear band thickness can also be measured with an optical microscope, but metallography or scanning electron microscopy (SEM) should be used for better results. [48] Figure 12 presents SEM images of different chip morphologies of AISI 1045. Chip compression ratio is considered an important factor in cutting by some researchers. [17] Chip compression ratio is the ratio between undeformed chip thickness and actual chip thickness. This can be measured by measuring the chip thickness directly or by calculating the thickness based on known chip length, density and mass. [49]

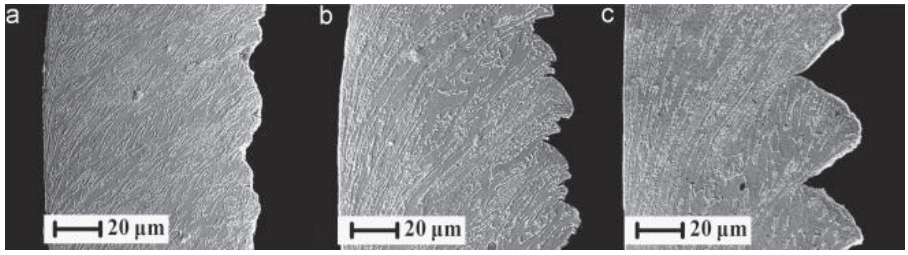

Figure 12. SEM Images of AISI 1045 chips [48]

3 Results

The main aspects and the primary findings of the articles included in this dissertation are presented in this chapter. The descriptions of the articles focus on the details that are essential to this dissertation framework, but some other interesting findings are also pointed out.

3.1 Article 1: Graph-based Analysis of Metal Cutting Parameters.

The first article compiles an interdependency matrix of the most critical parameters in metal cutting. Based on the matrix, a graphic presentation with graph analysis is performed to identify the most important factors among the parameters. The analysis was done with Gephi – an open source network and graph analysis software package. [50] The level of importance is determined with eigenvector centrality that determines a value of a node based on how many other nodes it is connected to and what the value of the connected nodes is. [51] The parameters are categorized to machine parameters and design parameters based on modularity analysis. [52] The most important machine parameters are cutting temperature, cutting tool, cutting feed, cutting speed, cutting force, tool wear and cutting depth. The most important design parameters are surface quality, tolerances, and residual stresses.

These results are of interest in this dissertation framework, since by controlling these parameters, the variation can be minimized in the cutting experiments in articles 2 and 5. The effect of cutting tool wear is circumvented by using an unworn tool for each experiment. Cutting forces are measured and included in the analysis. Cutting speed, feed and depth are process parameters that can be varied, and their effect on other parameters is analyzed. Cutting temperature is measured, but in this dissertation, temperature is either simulated or the temperature data is found in the literature.

3.2 Article 2: Investigation of the Effect of Different Cutting Parameters on Chip Formation of Low-lead Brass with Experiments and Simulations.

In this article, the state-of-the-art procedure of modeling material behavior for cutting simulations is performed. Low-lead brass was characterized with tensile testing, SHPB experiments and cutting experiments. Tensile testing was done with 0.1 1/s and 0.001 1/s strain rates and at 25 °C, 200 °C and 450 °C. SHPB experiments were conducted at the same temperature but with strain rates from 1250 1/s to 3200 1/s. The material model was fitted to the stress-strain data, and cutting experiments were used to determine the cut-off strain in the material model. Relatively good correlation was achieved between cutting experiments and simulations, but the material model was realized to be inadequate to take thermal softening behavior into account on all strain

rates. The material experiments for material characterization were found to be expensive and time consuming. The practical implications in the research showed that high cutting speed, small feed, and low cutting temperature improved chip breakage, and the same behavior was also identified in the cutting experiments.

3.3 Article 3: Determination of material model parameters from orthogonal cutting experiments.

This article applies an extended Oxley's parallel-sided shear zone model to an inverse analysis of cutting experiment data to identify Johnson-Cook flow stress model parameters. The extended Oxley's model replaces the power law material model originally implemented by Oxley with Johnson-Cook material model. AISI-1045 steel was used as a pilot material since there are many literature sources including cutting experiment data and material testing data for the material. The parameters identified with the proposed method are compared to parameter values from the literature and the performance of the parameters is evaluated. Based on the results, the extended Oxley model has the best fit to the cutting experiment data with the parameters from the proposed method. Another important result is that the optimization routine leads to different solutions depending on the boundary conditions, i.e., how many static material model parameters are used during the optimization. This leads to the conclusion that the problem has multiple local minima and thus it is advisable to keep the parameters that are directly measurable from material properties as static variables to ensure that the model yields realistic parameter sets.

3.4 Article 4: Using FEM Simulations of Cutting for Evaluating the Performance of Different Johnson-Cook Parameter Sets Acquired with Inverse Methods.

This article is an extension to article 3. Here the Johnson-Cook parameters acquired through the inverse analysis with extended Oxley's model are evaluated with FEM simulations. The same simulation set-up was also used with parameters from literature sources. The results are close to those of the analytical model and the proposed inverse method also produces the best parameters for the simulations. The simulation results underlined the conclusion made in article 3 regarding the multiple local minima: The simulations that used the parameters acquired with optimization runs with few static parameters yields to unrealistic results.

3.5 Article 5: Modified Johnson-Cook Flow Stress Model with Thermal Softening Damping for Finite Element Modeling of Cutting.

This article investigates the thermal behavior identified in article 2. A new material model was developed to take into account the coupled behavior of thermal softening and rate sensitivity. The Johnson-Cook model was modified with a thermal damping function and the model was fitted to the material data acquired for low-lead brass. The model fit was excellent and thus the model was implemented in FEM software. Orthogonal cutting experiments were conducted for reference. The model performance was better than the unmodified Johnson-Cook model, but further investigation identified the reason to be strain hardening cut-off rather than thermal damping. It was

left unproved as to why the damping behavior is present in material testing but not in cutting experiments. In the wider context of this dissertation, the lack of presence of the damping behavior is beneficial, since the inverse analysis for material model parameter acquisition would have been a more complex optimization problem for a material model with the thermal damping effect.

4 Discussion and Conclusions

The complex coupled nature of metal cutting makes it difficult to identify the effect of an individual parameter. The graph analysis in article 1 addressed this difficulty and showed that it is possible to identify loops of interconnected parameters. The analysis was done only with qualitative relationships but nevertheless the outcome was sensible. The analysis identified the most important machine parameters to be cutting temperature, cutting tool, cutting feed, cutting speed, cutting force, tool wear and cutting depth. Additionally, the parameters were grouped with modularity analysis to two distinct categories: Design parameters and machine parameters. The analysis showed potential and in future an analysis with a quantitative connection between the parameters could be investigated. The same methodology was applied to a manual assembly environment and similarly the method proved sensible [53,54]. The work has also been applied for sustainability estimation of machining in Bhanot et al. 2014. [55]

In the second article, cutting simulations and cutting experiments for low-lead brass were performed in order to investigate the effect of cutting parameters on the cutting process. The results suggested the use of high cutting speed and low cutting feed to ensure good chip breakage. The larger scale implications in this article are related to the inadequacy of the material model regarding the thermal effects, and the heavy process of acquiring the material model parameters with material testing. The material model was optimized to the data so that the best fit is around 200 °C. It was decided to investigate this later in the research.

To develop the material model parameters acquisition, an inverse routine was developed based on parallel-sided shear zone theory and cutting experiments. The method is presented and evaluated in article 3. The method was compared to other parameter sets for AISI 1045 found in literature. In the test group, the proposed model gave the best results for the analytic prediction of cutting forces. The method was further validated in article 4, where the parameter set was used for FEM simulations. The proposed model also gave the best results with the simulations. Both articles also point out that the optimization routine has multiple local minima and the model parameters should be kept static regarding those parameters that are directly linked to measurable material properties like yield stress or melting temperature. The results so far are encouraging, but the method must be validated for multiple materials. The parallel-sided shear zone model has difficulties when considering materials with a strong tendency of forming saw-toothed chips, built-up edge or discontinuous chips. There are some extensions to Oxley's model like that proposed by Fang et al. in 2001, where a slipline model for restricted tool-chip contact was developed [56], or the slipline model by Uysal and Altan in 2015 for rounded-edge cutting tools [57], but it is not obvious if the extensions to the slipline theory are practical or universal enough to be used in inverse analysis.

Finally, in article 5, the issue identified in article 2 regarding the material model inadequacy for thermal behavior is investigated. The material testing data is unambiguous and the thermal damping at high strain rates is an existing behavior. A new material model was developed based on the Johnson-Cook model. The model has excellent fit to the data and thus it was an unexpected result to find that the simulations with the model were not in good agreement with cutting experiments. The effect of variables other than the new modification in the model was ruled out by making yet another modified version of the Johnson-Cook model with strain hardening cut-off. This model had a simple thermal softening behavior but the strain hardening was limited by cut-off strain. This model produced significantly better results compared to the cutting experiments, and it was concluded that the thermal damping effect does not affect the cutting process. The physical explanation behind this should be investigated to better understand material behavior under cutting conditions.

5 Summary

This dissertation investigates the material model parameter acquisition for finite element simulations of cutting. The model parameters are traditionally determined from tensile testing and SHPB testing, but the shortcoming of this method is that the testing conditions are not the same as in the cutting process. The theory of metal cutting, materials testing, the finite element method and cutting experiments are introduced as the theoretical foundation to this dissertation. Using cutting experiments as a materials testing method is proposed in order to test the material properties in cutting conditions. This requires an analytical model for determining the relationship between cutting experiment outputs, cutting force, temperature and chip morphology to material model inputs that are strain, strain rate and temperature.

The first article investigates the interdependencies of the cutting parameters with graph analysis and qualitative data found in literature. A binary matrix of relationships was compiled and used as an input in Gephi network analysis software. Modularity analysis was done that show that the parameters can be divided in machine parameters and design parameters, as shown with red and turquoise in the Figure 13. The results also shows that cutting temperature, cutting tool, cutting feed, cutting speed, cutting force, tool wear and cutting depth are the most critical machine parameters in cutting. Most important design parameters are surface quality, tolerances and residual stresses.

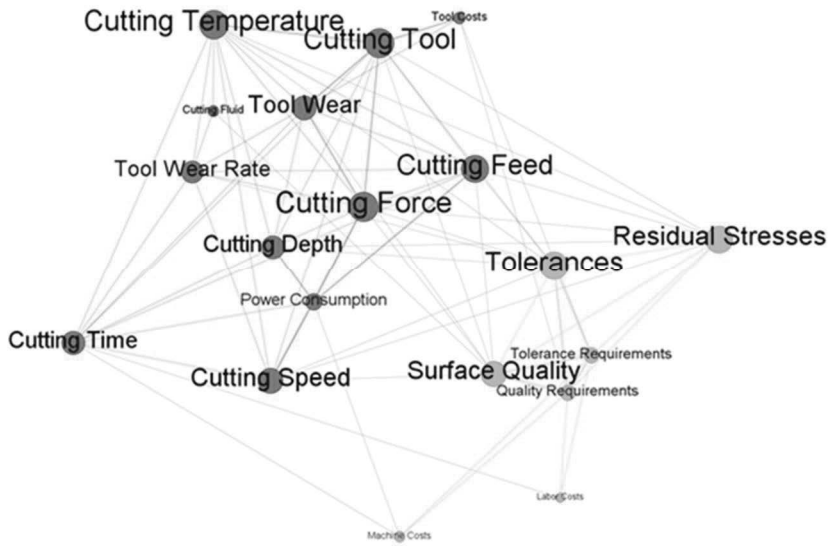

Figure 13 Cutting Parameter Relationship Graph [Publication 1]

The second paper investigates the state-of-the-art method of acquiring the material model parameters with material testing methods. Low-lead brass is characterized with tensile testing and SHPB tests. The material model is used in FEM simulations and the results are compared to cutting experiments. This investigation resulted in two conclusions: Materials testing is expensive and time consuming, and the material model used is not able to take into account thermal behavior in all strain rates. This results are discussed in depth in publication 5. The practical implications of the work are that the chip breakage of the low lead brass can be achieved when the cutting temperature can be kept moderate. This is managed by minimizing plastic strain in the chip formation zone. The simulations show that plastic strain and temperature are minimized with positive rake angle, high cutting speed and small feed. This conclusion was also observed in the cutting experiments. The experimented chip lengths are shown in Figure 14.

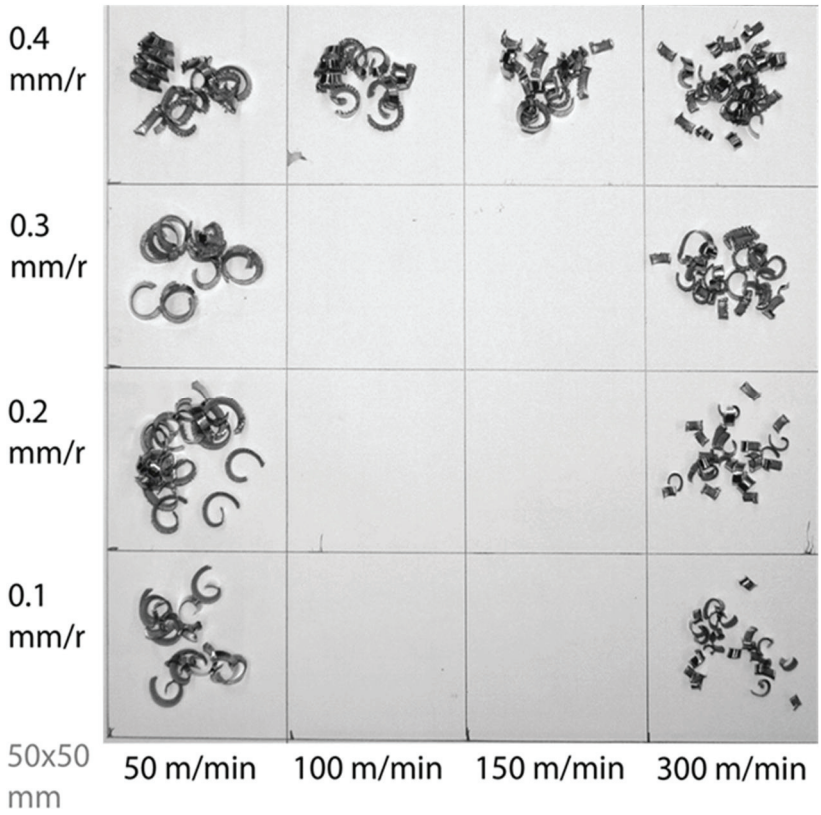

Figure 14 Chip Length as Observed from Cutting Experiments [Publication 2]

The analytical model used in this dissertation is an extension of Oxley's parallel-sided shear zone theory, where the original stress-strain relation is replaced with the Johnson-Cook material model. This method is presented in publication 3. Strain is calculated from cutting experiment data with Oxley's model, strain rate is calculated with the extension of Oxley's model, and the temperature is used as measured. These values are used as inputs to the Johnson-Cook model and the output, i.e., flow stress, is used in Oxley's model to calculate the resultant force. The resultant force is compared to the experiments and Johnson-Cook parameters are iterated to achieve the

minimum mean square of errors. Cutting experiment data from AISI 1045 is used as the testing data for the method. The method gives the best fit to the data compared to Johnson-Cook parameters found in literature as shown in Table 1. The iterative fitting process gives 3 sets of parameters depending on what limits are used for the parameters. It was concluded that there are many local optimal solutions for flow stress model parameters and it is advisable to use compression test values for setting the reference frame for the model parameters.

Table 1 Johnson-Cook Parameters and Accompanying Error in Resultant Cutting Force from Oxley's Model Compared to Experiments [Publication 3]

nr.	Laakso 1	Laakso 2	Laakso 3	Jaspers et al. 4	Klocke et al. 5
A	550	391	290	553	546
B	600	217	283	601	487
n	0.234	0.340	0.249	0.234	0.250
C	0.025	0.003	0.004	0.013	0.027
m	0.741	3.283	3.365	1.000	0.631
T_{melt}	1460	1460	1460	1460	1460
T_{ref}	20	20	20	20	20
$(d\varepsilon/dt)_{ref}$	7500	7500	0.001	7500	0.001
avg. error	**5.3 %**	**5.0 %**	**5.0 %**	**20.4 %**	**13.4 %**
max. error	**12.6 %**	**9.9 %**	**9.9 %**	**34.9 %**	**28.4 %**
min. error	**0.0 %**	**1.1 %**	**1.1 %**	**7.5 %**	**0.8 %**

The inverse analysis routine is further examined in publication 4 using the acquired Johnson-Cook parameters in FEM simulations, to compare if the simulated results are in agreement with analytical model and cutting experiments. The parameter sets 1-3 by Laakso and parameter sets 4 and 5 for reference were simulated with AdvantEdge 2D. The results show that parameter set 1 gives the best fit to experimented data as seen in Table 2. Also, the issue that was raised in the publication 3 regarding the multiple local solutions for the fitting of the model was confirmed. The parameters sets that were less restricted regarding the yield stress and strain hardening give unrealistic results from simulations that can be observed in Figure 15, where the chip formation is unrealistic regarding parameter sets 2 and 3.

Table 2 FEM Simulation Error Compared to Experiments [Publication 4]

	Laakso 1 Avg. Error	Laakso 2 Avg. Error	Laakso 3 Avg. Error	Jaspers et al. 4 Avg. Error	Klocke et al. 5 Avg. Error
FC	7 %	39 %	42 %	28 %	30 %
FT	17 %	39 %	41 %	28 %	35 %
R	9 %	39 %	41 %	27 %	31 %
T	10 %	14 %	16 %	15 %	26 %

Figure 15 Simulation Results from FEM Analysis, the Parameters Sets from Left to Right are in Numerical Order 1-5 [Publication 4]

The last article revisits the material testing data of lead free brass to develop a new material model that is able to model the thermal behavior in all strain rates. The behavior is named thermal damping. The damping effect is illustrated in Figure 16. Johnson-Cook model was modified to include the damping function. The modified Johnson-Cook model has significantly better fit to the material testing data than unmodified model. The modified model is plotted in Figure 17. Based on simulations, cutting experiments and the materials testing data, it is concluded that the behavior does not occur in cutting conditions even though it does occur in material testing conditions.

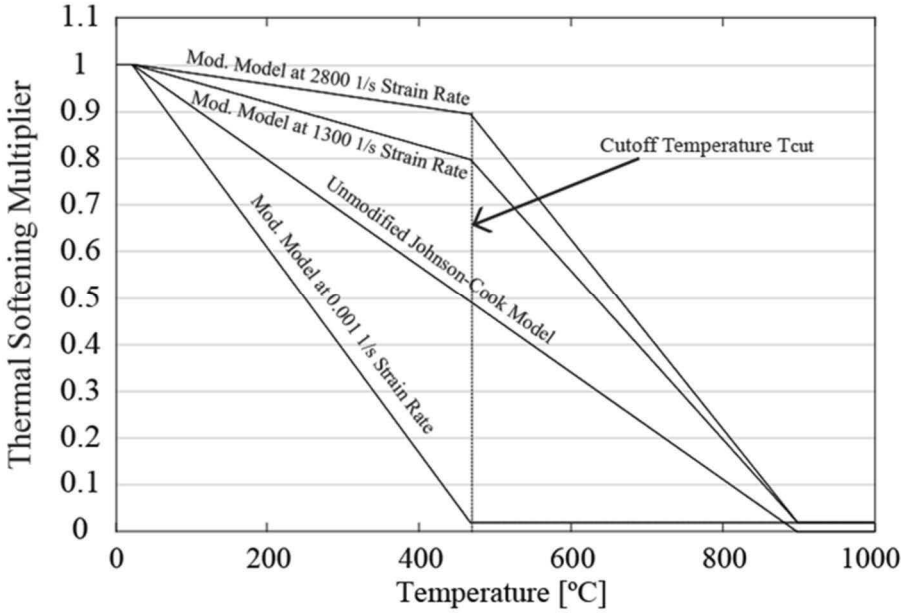

Figure 16 Thermal Softening Curves with Damping Function and Unmodified Johnson-Cook Thermal Softening [Publication 5]

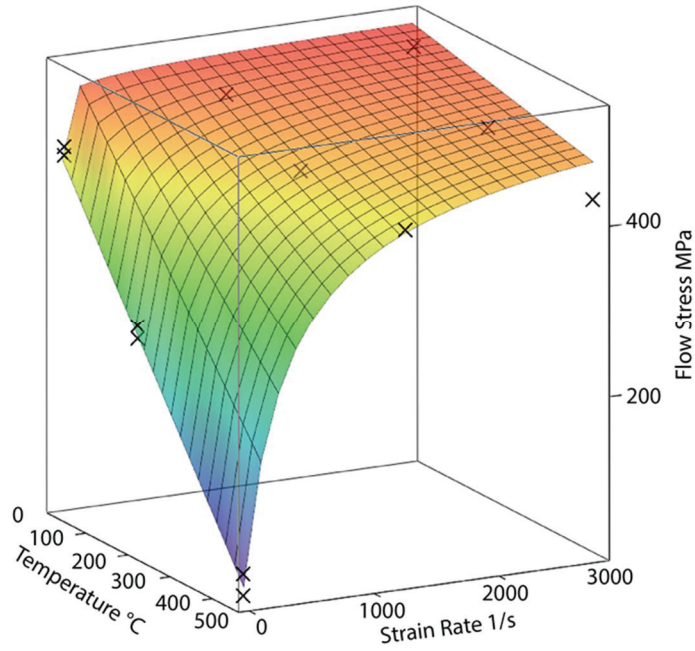

Figure 17 Modified Johnson-Cook Model Plot with Material Testing Data Points (Small X's) [Publication 5]

To conclude, the work done in this dissertation shows that cutting experiments have potential as materials testing method and the difference in testing conditions of materials testing and cutting experiments can lead to great errors in simulations. Further development should be done regarding more complex material behavior like yield delay and chip formation models for built up edge, saw toothed chip and discontinuous chip.

References

[1] Gardner Research, 2015 World Machine-Tool Output & Consumption Survey, http://www.gardnerweb.com/cdn/cms/GR-2015-WMTS.pdf, Cited 20.7.2015

[2] Taylor, F.W., On the art of cutting metals, Transactions of ASME, 1907, vol. 28, pp. 30-58

[3] Usui, E., Shirakashi, T., & Kitagawa, T. Analytical prediction of cutting tool wear. Wear, 1984, 100(1), 129-151.

[4] Mackerle J. Finite element analysis and simulation of machining: a bibliography (1976–1996). J Mater Process Tech 1998; 86(1): 17–44.

[5] Mackerle J. Finite element analysis and simulation of machining: an addendum: a bibliography (1996–2002). Int J Mach Tool Manu 2003; 43(1): 103–114.

[6] Arrazola, P. J., Özel, T., Umbrello, D., Davies, M., & Jawahir, I. S. (2013). Recent advances in modelling of metal machining processes. CIRP Annals-Manufacturing Technology, 62(2), 695-718.

[7] Iqbal SA, Mativenga PT and Sheikh MA. Characterization of machining of AISI 1045 steel over a wide range of cutting speeds. Part 2: evaluation of flow stress models and interface friction distribution schemes. Proc IMechE, Part B: J Engineering Manufacture 2007; 221(5): 917–926.

[8] Jaspers SPFC and Dautzenberg JH. Material behaviour in conditions similar to metal cutting: flow stress in the primary shear zone. J Mater Process Tech 2002; 122(2–3): 322–330.

[9] Klocke F, Lung D and Buchkremer S. Inverse identification of the constitutive equation of Inconel 718 and AISI 1045 from FE machining simulations. Proced CIRP 2013; 8: 212–217.

[10] Sartkulvanich P, Koppka F and Altan T. Determination of flow stress for metal cutting simulation—a progress report. J Mater Process Tech 2004; 146(1): 61–71.

[11] Sartkulvanich, P. (2007). Determination of material properties for use in FEM simulations of machining and roller burnishing (Doctoral dissertation, Ohio State University).

[12] Denkena, B., Ben Amor, R., De Leon-Garcia, L., & Dege, J. (2007). Material specific definition of the high speed cutting range. International Journal of Machining and Machinability of Materials, 2(2), 176-185.

[13] O. Pantalé, J.-L. Bacaria, O. Dalverny, R. Rakotomalala, S. Caperaa, 2D and 3D numerical models of metal cutting with damage effects, Computer Methods in Applied Mechanics and Engineering, Volume 193, Issues 39–41, 1 October 2004, 4383-4399, ISSN 0045-7825

[14] Y.B. Guo, David W. Yen, A FEM study on mechanisms of discontinuous chip formation in hard machining, Journal of Materials Processing Technology, Volumes 155–156, 30 November 2004, 1350-1356, ISSN 0924-0136

[15] Agmell, M., Ahadi, A., & Ståhl, J. E. (2013). The link between plasticity parameters and process parameters in orthogonal cutting. Procedia CIRP, 8, 224-229.

[16] Agmell, M., Ahadi, A., & Ståhl, J. E. (2014). Identification of plasticity constants from orthogonal cutting and inverse analysis. Mechanics of Materials, 77, 43-51.
[17] Astakhov VP and Shvets S. The assessment of plastic deformation in metal cutting. J Mater Process Tech 2004; 146(2): 193–202.
[18] Eugene Merchant M. Mechanics of the metal cutting process. I. Orthogonal cutting and a type 2 chip. J Appl Phys 1945; 16: 267–275, http://dx.doi.org/10.1063/1.1707586
[19] Piispanen V. Theory of formation of metal chips. J Appl Phys 1948; 19: 876–881, http://dx.doi.org/10.1063/ 1.1697893
[20] J.P. Davim, C. Maranhão, A study of plastic strain and plastic strain rate in machining of steel AISI 1045 using FEM analysis, Materials & Design, Volume 30, Issue 1, January 2009, Pages 160-165, ISSN 0261-3069
[21] Shaw, M. C. (2005). Metal cutting principles (Vol. 2). New York: Oxford university press., pg. 13
[22] Childs, T. (2000). Metal machining: theory and applications. Butterworth-Heinemann. Chapter 2.2: pg. 37-41
[23] Astakhov, V. P. (2010). Geometry of single-point turning tools and drills: fundamentals and practical applications. Springer Science & Business Media. Appendix A.2: pg. 444-450
[24] Oxley PLB. The mechanics of machining: an analytical approach to assessing machinability (Ellis Horwood series in mechanical engineering). West Sussex, UK: Market Cross House, 1989.
[25] Johnson GR and Cook WH. A constitutive model and data for metals subjected to large strains, high strain rates and high temperatures. In: Proceedings of the 7th international symposium on ballistics, The Hague, 19–21 April 1983, vol. 21, pp.541–547. Hague, Netherlands: International Symposium on Ballistics, American Defense Preparedness Association, and Koninklijk Instituut van Ingenieurs.
[26] D.I. Lalwani, N.K. Mehta, P.K. Jain, Extension of Oxley's predictive machining theory for Johnson and Cook flow stress model, Journal of Materials Processing Technology, Volume 209, Issues 12–13, 1 July 2009, Pages 5305-5312, ISSN 0924-0136
[27] Boothroyd G. Knight, WA. Fundamentals Of Machining and Machine Tools, 2nd edition, Marcel Dekker Inc. 1989, ISBN: 0-8247-7852-9
[28] Han, Patricia (ed.). Tensile testing. ASM International (OH), 1992., ISBN: 9780871704405
[29] Chen, Weinong W., and Bo Song. Split Hopkinson (Kolsky) bar: design, testing and applications. Springer Science & Business Media, 2010, ISBN: 978-1-4419-7981-0
[30] Miguélez, María H. et al. An efficient implementation of boundary conditions in an ALE model for orthogonal cutting. Journal of Theoretical and Applied Mechanics, [S.l.], v. 47, n. 3, p. 599-616, Jan. 2009. ISSN 1429-2955
[31] Klocke, Fritz, Kuchle, Aaron, Manufacturing Processes 1, RWTH edition, Book Section: Finite Element Method (FEM), Springer Berlin Heidelberg, 2011, pages 207-209, ISBN: 978-3-642-11978-1
[32] Liangchi Zhang, On the separation criteria in the simulation of orthogonal metal cutting using the finite element method, Journal of Materials Processing Technology, Volumes 89–90, 19 May 1999, Pages 273-278, ISSN 0924-0136
[33] Priyadarshini, A., Pal, S.,K., Samantaray, A.,K., Finite Element Modeling of Chip Formation in Orthogonal Machining, In: (Editor) Davim, J.Paulo, Statistical and Computational Techniques in Manufacturing, 2012, pp. 101-144, Springer, ISBN: 978-3-642-25858-9
[34] Marusich, T.D., Ortiz, M., Modeling and Simulation of High Speed Machining, International Journal for Numerical Methods in Engineering, Volume 38, Issue 21, 1995, 3675 3694

[35] N. Tounsi, J. Vincenti, A. Otho, M.A. Elbestawi, From the basic mechanics of orthogonal metal cutting toward the identification of the constitutive equation, International Journal of Machine Tools and Manufacture, Volume 42, Issue 12, September 2002, Pages 1373-1383, ISSN 0890-6955

[36] D. Umbrello, R. M'Saoubi, J.C. Outeiro, The influence of Johnson–Cook material constants on finite element simulation of machining of AISI 316L steel, International Journal of Machine Tools and Manufacture, Volume 47, Issues 3–4, March 2007, Pages 462-470, ISSN 0890-6955

[37] Özel, T. (2006). The influence of friction models on finite element simulations of machining. International Journal of Machine Tools and Manufacture, 46(5), 518-530.

[38] T.H.C. Childs, Friction modelling in metal cutting, Wear, Volume 260, Issue 3, 10 February 2006, 310-318, ISSN 0043-1648

[39] H. Puls, F. Klocke, D. Lung, Experimental investigation on friction under metal cutting conditions, Wear, Volume 310, Issues 1–2, 15 February 2014, 63-71, ISSN 0043-1648

[40] Mahadevan D. Experimental determination of velocity and strain rate fields in metal cutting of OFHC copper. Master's Thesis, Wichita State University, 2007, http://soar.-wichita.edu/handle/10057/1522 (accessed 23 September 2015).

[41] Mäenpää, M., Alahautala, T., Lassila, E., Andersson, P. H., & Hernberg, R. (2003, June). Experimental set-up for study of chip formation in turning. In XVII IMEKO World Congress, Dubrovnik, Croatia (pp. 22-27).

[42] Kulianic, E., Sortino, M., Recent Developement and Trends in Tool Condition Monitoring, Book Section: AMST'02 Advanced Manufacturing Systems and Technology, Volume 437 of the series International Centre for Mechanical Sci-ences, pages 15-35, 2002, 978-3-7091-2557-1

[43] Kistler, Instruction Manual, Quartz 3-Component Dynamometer Type 9257B, 9257B_002-054e-03.15, Kistler Group, Eulachstrasse 22, 8408 Winterthur, Switzerland, (http://www.kistler.com/fi/en/applications/sensor-technology/cutting-force-measurement/milling/products/#multi_component_dynamometer_up_to_10_k_n_9257_b, referred 28.9.2015)

[44] Shannon, Claude E., Communication in the presence of noise, Proceedings of the IRE 37.1 (1949): 10-21.

[45] Manuel Blattner, Kistler, Improving signal quality, Seminar at Chalmers University, 5.12.2013

[46] Longbottom, J. M., & Lanham, J. D. (2005). Cutting temperature measurement while machining-a review. Aircraft Engineering and Aerospace Technology, 77(2), 122-130.

[47] Julien Artozoul, Christophe Lescalier, Olivier Bomont, Daniel Dudzinski, Extended infrared thermography applied to orthogonal cutting: Mechanical and thermal aspects, Applied Thermal Engineering, Volume 64, Issues 1–2, March 2014, 441-452, ISSN 1359-4311

[48] G.G. Ye, S.F. Xue, W. Ma, M.Q. Jiang, Z. Ling, X.H. Tong, L.H. Dai, Cutting AISI 1045 steel at very high speeds, International Journal of Machine Tools and Manufacture, Volume 56, May 2012, 1-9, ISSN 0890-6955

[49] Astakhov, V. P. (2006). Tribology of metal cutting (Vol. 52). Elsevier. Appendix B: 414-417

[50] Bastian, M., Heymann, S., & Jacomy, M. (2009). Gephi: an open source software for exploring and manipulating networks. ICWSM, 8, 361-362.

[51] Bryan, K., & Leise, T. (2006). The $25,000,000,000 eigenvector: The linear algebra behind Google. Siam Review, 48(3), 569-581

[52] Blondel, V. D., Guillaume, J. L., Lambiotte, R., & Lefebvre, E. (2008). Fast unfolding of communities in large networks. Journal of Statistical Mechanics: Theory and Experiment, 2008(10), P10008.
[53] Peltokorpi, J., Laakso, S., Ratava, J., Lohtander, M., & Varis, J. (2013). Relationships of factors in a manual assembly line environment. In Advances in Sustainable and Competitive Manufacturing Systems (pp. 985-996). Springer International Publishing.
[54] Peltokorpi, J., Lohtander, M., & Laakso, S. V. (2014). Effective relationships of factors in a manual assembly line environment. International Journal of Engineering Management and Economics, 4(3-4), 267-290.
[55] Bhanot, N., Rao, P. V., & Deshmukh, S. G. (2014). Sustainable Manufacturing: An Interaction Analysis for Machining Parameters using Graph Theory. Proceedings of SOM, 2014.
[56] N. Fang, I.S. Jawahir, P.L.B. Oxley, A universal slip-line model with non-unique solutions for machining with curled chip formation and a restricted contact tool, International Journal of Mechanical Sciences, Volume 43, Issue 2, February 2001, 557-580, ISSN 0020-7403
[57] Alper Uysal and Erhan Altan, Slip-line field modelling of rounded-edge cutting tool for orthogonal machining Proceedings of the Institution of Mechanical Engineers, Part B: Journal of Engineering Manufacture 0954405415577560, first published on March 27, 2015 doi:10.1177/0954405415577560

Publications

Reprinted with permission:

Laakso, Sampsa, V.A.; Peltokorpi, Jaakko; Ratava, Juho; Lohtander, Mika; Varis, Juha. 2013. Graph-based Analysis of Metal Cutting Parameters. In: Azevedo A (ed.) Advances in sustainable and competitive manufacturing systems: 23rd International Conference on Flexible Automation & Intelligent Manufacturing. Porto, Portugal, 2628 June, 2013. Springer. Lecture Notes in Mechanical Engineering, Pages 627–636. ISBN 9783319005560.

Laakso, Sampsa. V.A., Hokka, Mikko; Niemi, Esko; Kuokkala, Veli-Tapani. 2013. Investigation of the effect of different cutting parameters on chip formation of low-lead brass with experiments and simulations. Sage Journals. Proceedings of the Institution of Mechanical Engineers, Part B: Journal of Engineering Manufacture, vol. 227 no. 11 pages 16201634. DOI: 0954405413492732.

Laakso, Sampsa V.A.; Niemi, Esko. 2015. Determination of material model parameters from orthogonal cutting experiments. Sage Journals. Proceedings of the Institution of Mechanical Engineers, Part B: Journal of Engineering Manufacture, January 8, 2015, DOI: 0954405414560620.

Laakso, Sampsa, V.A.; Niemi, Esko. 2015. Using FEM Simulations of Cutting for Evaluating the Performance of Different Johnson-Cook Parameter Sets Acquired with Inverse Methods. In: Chike F. Oduoza. Proceedings of the 25th International Conference on Flexible Automation and Intelligent Manufacturing, Designing for Advanced, High Value Manufacturing and Intelligent Systems for the 21st Century, Wolverhampton, United Kingdom, June 23-26, 2015. The Choir Press. Volume 2, Pages 172-180. ISBN: 9781910864012.

Laakso, Sampsa V.A.; Niemi, Esko. 2015. Modified Johnson-Cook Flow Stress Model with Thermal Softening Damping for Finite Element Modeling of Cutting. Sage Journals. Proceedings of the Institution of Mechanical Engineers, Part B: Journal of Engineering Manufacture, ACCEPTED FOR PUBLICATION

Graph-based Analysis of Metal Cutting Parameters

Sampsa Laakso[1*], Jaakko Peltokorpi[1], Juho Ratava[2], Mika Lohtander[2] and Juha Varis[2]

[1]Department of Engineering Design and Production
Aalto University
Espoo, Finland

[2]LUT Mechanical Engineering
Lappeenranta University of Technology
Lappeenranta, Finland

ABSTRACT

In this work, the interdependencies of different metal cutting parameters are examined. In order to ensure competitiveness in the field of manufacturing, the quality, productivity and costs of the work must be in optimal balance. The parameters affecting the end result of a metal cutting process form a complex web of interdependencies. In this work, graph-based modularity analysis is applied in order to impose a structure on the network of parameters. This allows the identification of the parameters that are to be used in more thorough examination of the individual cases. Combined with an understanding of the graph topology such as parameterized relationships between different factors, this enables powerful heuristic tools such as expert systems to be created.

1. INTRODUCTION

This study makes a proposal and then presents the information required to describe the machine and device resources in a machining environment. This information is needed for the development of an analytical method for automated and highly productive production. The description of the product and device resources and their interconnectedness is the starting point for method comparison [1], the development of expenses [2], production planning [3, 4] and performing optimization [5]. According to Newness [2], budgeting during the design phase requires the presentation of factors relating to production and the product itself, as does process optimization. The manufacturing methods cannot be optimized unless the environmental variables and their interdependences are known. Furthermore, it is impossible to create an optimal technological design, as indicated by Wang [6], unless the characteristics of the processes are known.

There are at least two points of view on cost-effectiveness in the manufacturing context, namely a cost-effective total product and cost-effective manufacturing. The concept of a cost-effective total product contains the idea of the financial control of the product's life cycle, including the main levels of this cycle: design, manufacture, marketing, use, maintenance, service and recycling or materials recovery. [7] When examining the concept of cost-effective manufacturing, we have to note that economically efficient manufacturing costs form a part of life cycle management and thus of the product's all-in price, but they do not influence the product directly as much as they do the actual manufacturer. The manufacturer must receive a yield from the manufacturing activities, making their chances of profitable operations smaller than those of the bearer of the actual product or product rights. A product is made more cost-effective when as little energy as possible is used in its production. In addition to this, the product's cycle in production must be organized in such a way that no energy is wasted on unnecessary stages of operation, warehousing or transport. [7]

The product and its production should be ecological, regardless of the point of view of cost-effectiveness. Therefore it is required to commit to an ever-increasing degree to manufacturability, as well as all other activities and events during a product's life cycle. In order for this to be possible, the informational parts of each process related to the product should be under control and the relationships of the factors affecting them should be understood. [7]

One technical development trend which research and development is currently turning towards may be the integration of master production scheduling and detailed capacity planning of separate design functions, such as drafting, operation, mechanics or production design, under one overall system in order to improve future profitability. However, whatever the development trend, it is almost certain that the portion of automatic and semi-intelligent

* Corresponding author: Tel.: +358 40 705 5039; E-mail: sampsa.laakso@aalto.fi

systems will inevitably grow. The development of smarter systems requires several separate functions, practices and disciplines to be gone through in order to prepare systems that are able to present the information people need at the right time and with suitable accuracy.

When a product is designed in such a way that the capabilities and machine properties of production are taken into account throughout, a significantly higher degree of value added can be produced in a product than by acting in a traditional way, where the focus is first on functional structure and only then are the manufacturing possibilities charted [7]. Today, manufacturing companies must be agile under conditions of global competition in order to do business successfully. In western countries, one typical response to decreasing cost-effectiveness is to transfer or outsource the non-core-competence actions to a lower-cost location and concentrate on the most-value-adding actions, in which production efficiency also plays a major role. Such a contrast could be discerned between manufacturing bulk products and assembling low-volume mass-customized products.

2. METHODS

Cutting is one of the most complex physical problems in industry. In order to improve the performance of a cutting system, changes must be made to the cutting parameters. However, changing one parameter has multiple outcomes; for example, increasing the cutting speed leads to a higher output of products but it can lead to lower profit as a result of an increased rate of tool wear. This makes optimizing cutting parameters difficult. Optimizing cutting on the basis of a limited set of parameters can achieve good results, but may have unexpected side-effects. Optimizing the cutting speed and tool wear on the basis of income can lead to bad product quality and therefore loss of profit as a result of rejected products. Understanding a cutting system requires an advanced level of expertise in the subject, which is a relatively rare and thus expensive commodity in the industry. In this paper, the proposal is to build a knowledge base with a network analysis tool in order to empower decision makers to analyze different outcomes of parameter adjustment.

The data for this research are collected from multiple research papers considering machining problems. The data are simplified into the form of a binary matrix that indicates the relationships between different parameters. The Gephi network analysis software[*] is used to automatically rearrange the network of parameters to visualize the weight of different parameters and to group the parameters. [8] Data for Gephi are prepared in human-readable form in Microsoft Excel using the NodeXL extension[†] [9]. Both pieces of software are published with an open source license and are freely available. Modularity analysis conducted with Gephi demonstrates how different parameters are connected and what kind of groups they form. This makes it possible to measure how well a network decomposes into modular communities. [10]

Several approaches have been used for the optimal cutting parameter value selection problem in cutting. If the model is known, there are several solvers that are available commercially, such as LINGO for linear programming problems. Well-known algorithms can be implemented for a customized solution. In addition, there are expert systems that were developed to find a suitable tool and cutting parameters [11, 12, 13]. For black-box models (where the objective space surface is not known) genetic algorithms and neural networks are very popular, such as in [14], though particle swarm optimization (PSO) methods have also been used [15]. Some cutting parameters may also be adjusted while the machining process is under way [16, 17, 18, 19]. The methods applied prior to machining may take considerable amounts of time, depending on the complexity of the problem or the exact configuration of the solver, but the methods used while the machining is under way must understandably be very computationally cheap. However, in order to achieve the required accuracy for the model to be optimized, it is crucial that the effects between different factors are understood and the most relevant parameters are identified.

3. RESEARCH

The cutting speed is the relative motion between the cutting tool and the workpiece. The cutting speed affects the magnitude of the cutting force, as well as the cutting temperature. The cutting temperature has been widely studied but because the connection between the cutting speed and temperature is highly case-sensitive, no generic models exist. [20] The effect of the cutting speed on tool wear rate is one of the most traditional research topics in machining. Usually, tool wear rate increases with increasing cutting speed. Though the field is well established, there are many new studies considering wear because nearly all tool-workpiece material couples require tool life testing since no universal

[*] Available from https://gephi.org/
[†] Available from http://nodex1.codeplex.com/

model exists. [21] The cutting speed affects the power consumption of a machine tool; generally, at higher speeds power consumption is higher. In addition, higher cutting speeds lead to a better surface quality, except some examples such as specific stainless steels. [22, 23] The effect of the cutting speed on the cutting time is obvious but the effects on residual stresses and tolerances are more difficult to determine. In some cases there is a clear effect on tolerances, for example when the velocity of mass deforms a workpiece moving at high speed, causing inaccuracies in the intended geometry. The cutting speed has a clear effect on residual stresses, as demonstrated by numerous studies, but the trends are highly case-sensitive. [24]

The cutting feed is the speed at which the cutting tool advances through the workpiece. The cutting feed has an almost linear effect on the cutting force, as the area of the tool-chip contact area increases with increasing feed. This has been concluded in numerous studies, such as Kienzle and Victor's commonly referenced study [25].The cutting feed has an impact on the cutting temperature, as presented in Bacci and Wallbank's review [26]. The impact of the cutting feed on tool wear and the tool wear rate has been investigated by researchers such as Astakhov [27]; it is concluded that the effect of the feed is dependent on other variables, such as the cutting temperature and cutting speed. The cutting feed has only a minor effect on the power consumption. [10, 28] The effect of the cutting feed on surface roughness is case-sensitive but clearly exists [10, 29, 30]. The cutting feed has an inverse linear relation to the cutting time. The feed has an effect on residual stresses, as reported in [21] and affects tolerances, at least through increased amounts of tool deflection at high feeds. [31]

The cutting depth is a set value that defines the depth of the cut. Since the tool-chip contact area is determined by the cutting depth and feed, the cutting depth has a similar nearly linear relation to cutting forces as the cutting feed. [32] The temperature of the tool-chip contact surface increases slightly with an increase in the depth of the cut. [33] The cutting depth is linear to the cutting volume, which directly increases tool wear, but if the machining is carried out under the optimum cutting regime an increase in the depth of the cut should not change the tool wear rate. [9, 24] The power consumption increases with an increase in the depth of the cut. [25] The cutting depth affects the number of passes needed to finish a workpiece, and therefore the cutting time decreases with an increase in the depth of the cut. Tensile residual stresses are increased with increasing tool-chip contact surface; when low tensile stress values at the surface of the workpiece are desired, the cutting depth should be small. [21] The depth of the cut affects the forces acting on the tool and therefore the tool deflection; this has an effect on the tolerances of the workpiece. [27]

The cutting force is the reaction to the cutting action. The force equals the energy required to remove material from the workpiece. The cutting force acts on the cutting tool. It can be viewed as resulting from three force components. These components point in the radial and tangential directions in relation to the machined surface and the opposite direction to the feed. Therefore, the cutting force directly affects the choice of tool. The cutting force also affects the tool wear mechanism and tool wear rate. [34] The cutting force is the primary contributor to power consumption. The cutting force can affect surface quality by changing the contact conditions at the tool-chip interface but no general trends have been discovered. [27, 35] The cutting force indicates the amount of friction and plastic deformation in the cutting zone and therefore the level of residual stresses generated.

The power consumption of a machine tool is the amount of energy the machine needs to perform cutting operations. The maximum power of a machine tool is a limiting criterion when selecting the cutting speed, feed and depth; therefore, its also affects the maximum allowable cutting force. Electricity is getting more expensive and the excessive use of power is seen as bad PR in view of the prevailing green philosophy policies. A simplified equation for calculating power requirements is

$$P = R\,v \tag{1}$$

where P is the power consumption, R is the resultant cutting force and v is the cutting speed.

Tolerances are the accepted range of dimensions of the ready workpiece. Machine tools and the tolerances achievable by them must be considered when choosing requirements for tolerance and quality in the design phase. As already noted, the tolerances of the workpiece are affected by the cutting force through tool and workpiece deflection.

A cutting tool is a geometrically defined shape that is strong and hard enough to mechanically remove material from a workpiece. A cutting tool has a major effect on the maximum applicable cutting speed, feed and depth. These values are provided by the tool manufacturers for each type of workpiece material. The recommended optimal cutting parameters for a 15-minute tool life are usually found in the catalogs of the tool manufacturers. Cutting tool performance is determined by the mechanical, tribological and thermal properties of the tool material. The performance is often measured by the tool life, maximum achievable material removal rate and cost of the tool. The geometry of the cutting tool has a major impact on cutting forces, cutting temperature, surface quality and tolerances. [10, 20, 21]

Tool wear is the flow of material away from the cutting tool as a result of adhesion, abrasion, plastic deformation and electrochemical phenomena. Tool wear obviously affects the cutting tool and its costs and performance, which is reflected in increased cutting forces. [36] Tool wear has an effect on the surface quality; the flank wear profile in particular is seen on the surface of the workpiece. [37] Tool wear and the cutting temperature have a strong omnidirectional effect on each other and the cause-effect relationship should be investigated experimentally more thoroughly. [38] The tool wear rate is the speed at which the tool wears. The wear rate affects how long one tool can be used continuously and therefore the cutting time is affected. Tolerances are critical with regard to tool wear rate because if the wear is fast, then the tool compensation changes quickly and is inaccurate, therefore leading to poor tolerances.

Cutting fluid is a lubricant and its major functions are removing cutting waste and chips, cooling the tool and workpiece and lubrication. The lubricating properties of cutting fluids have been questioned because there are indicators that the cutting fluid cannot access the tool-chip contact surface as a result of the high pressure in that area. The cutting fluid has an effect on surface quality and tool wear, as presented, for example, in Xavior and Adithan's work [39]. The cooling properties of cutting fluids are evident and strongly correlated by the thermal properties of the fluid. [40]

The cutting temperature is generated from the friction and adhesion between the tool and the workpiece and from the plastic deformation of the workpiece material. The cutting temperature has a significant effect on the cutting tool wear rate. [41] Thermal softening and thermal elongation of the workpiece and tool also affect the cutting forces and tolerances. Residual stresses are caused by the joint effect of elastic and plastic deformation and changes in temperature. [42]

The cutting time is the time needed for the cutting action. The cutting time affects the choice of cutting tool and the cumulative temperature generated and conducted to the workpiece and tool. The cutting time is the primary measurement for tool life and therefore tool wear should be considered. The cutting time affects the total power consumption of the process, labor costs and machine costs.

The surface quality is the topology of the already-machined surface layer of the workpiece. The surface quality affects the tolerances if the surface average roughness value Ra is high. The quality and tolerance requirements are also affected by a bad surface or very high costs of reaching good surface quality. Residual stresses are the remaining stresses in the workpiece after the cutting is done. The surface quality and tolerances can change if the residual stresses are released and therefore distort the workpiece. Quality and tolerance requirements are engineering-driven qualities that are critical for the workpiece to function properly in its intended surroundings. The requirements for the product also have a major impact on product costs, because if the requirements are unnecessarily high, then producing over quality in the sense of surface roughness, and the tolerances, tool, labor and machine costs are higher. Additionally, if the tolerance requirements are high, this requires the surface roughness requirements to be high too.

Tool costs mainly comprise the retail price of tool bits. If tool costs are critical in the cost structure of the product, this can affect the choice of cutting tool. Labor costs are calculated from the time the machinist must attend to the machine tool for each workpiece. Machine costs include maintenance and down payments.

Table 1 and Figure 1 present the relationships between different variables in the cutting process.

Table 1: Connections between different cutting variables

	Cutting Speed	Cutting Feed	Cutting Depth	Cutting Fluid	Cutting Tool	Cutting Force	Cutting Temperature	Tool Wear	Tool Wear Rate	Power Consumption	Surface Quality	Cutting Time	Residual Stresses	Tolerances	Tool Costs	Labor Costs	Machine Costs	Quality Requirements	Tolerance Requirements
Cutting Speed	0	0	0	0	0	1	1	0	1	1	1	1	1	1	0	0	0	0	0
Cutting Feed	0	0	0	0	0	1	1	1	1	1	1	1	1	1	0	0	0	0	0
Cutting Depth	0	0	0	0	0	1	1	1	0	1	0	1	1	1	0	0	0	0	0
Cutting Fluid	0	0	0	0	0	0	1	0	1	0	1	0	0	0	0	0	0	0	0
Cutting Tool	1	1	1	0	0	1	1	1	0	0	1	0	1	1	1	0	0	0	0
Cutting Force	0	0	0	0	1	0	0	1	1	1	1	0	1	1	0	0	0	0	0
Cutting Temperature	0	0	0	0	1	1	0	0	1	0	0	0	1	1	0	0	0	0	0
Tool Wear	0	0	0	0	1	1	1	0	0	0	1	0	0	0	1	0	0	0	0
Tool Wear Rate	0	0	0	0	0	0	0	1	0	0	0	1	0	1	0	0	0	0	0
Power Consumption	1	1	1	0	0	1	0	0	0	0	0	0	0	0	0	0	1	0	0
Surface Quality	0	0	0	0	0	0	0	0	0	0	0	0	0	1	0	0	0	1	1
Cutting Time	0	0	0	0	1	0	1	1	0	1	0	0	0	0	0	1	1	0	0
Residual Stresses	0	0	0	0	0	0	0	0	0	0	1	0	0	1	0	0	0	0	0
Tolerances	0	0	0	0	0	0	0	0	0	0	0	0	0	0	0	0	0	1	1
Tool Costs	0	0	0	0	1	0	0	0	0	0	0	0	0	0	0	0	0	0	0
Labor Costs	0	0	0	0	0	0	0	0	0	0	0	0	0	0	0	0	0	0	0
Machine Costs	0	0	0	0	0	0	0	0	0	0	0	0	0	0	0	0	0	0	0
Quality Requirements	0	0	0	0	0	0	0	0	0	0	1	0	1	1	1	1	1	0	1
Tolerance Requirements	0	0	0	0	0	0	0	0	0	0	1	0	1	1	1	1	1	1	0

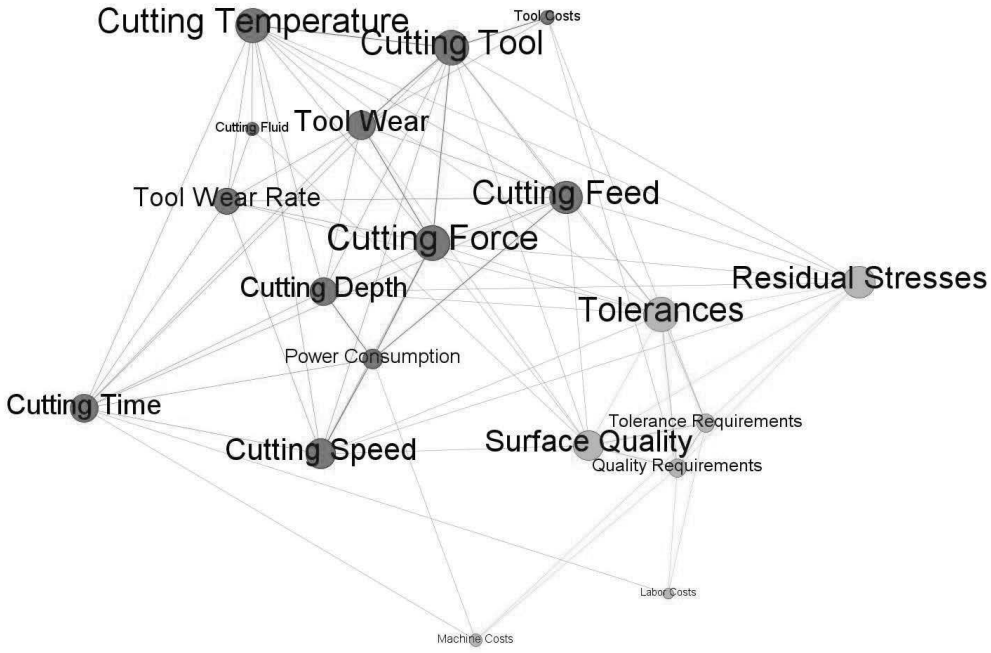

Figure 1: Relationships between factors affecting the metal cutting process

4. CONCLUSIONS

Optimizing workpiece quality, machining costs and productivity is essential for competitive manufacturing. In order to optimize cutting processes, different parameters are adjusted to achieve desirable outcomes. However, as a result of the complex nature of the cutting process and the various coupled effects of different parameters, it is difficult to predict different outcomes resulting from a parameter change. This research was conducted to inspect a graph-based approach to the creation of an expert system for assessing the outcomes of different cutting parameter changes. This is done by applying a simplified model based solely on known relationships between different parameters in cutting.

The analysis shows that cutting parameters are divided into two groups, namely “machine parameters” and “design parameters”. The division is based on Gephi modularity analysis. First, it is interesting to note that the modularity analysis led to sensible groups. Additionally, it seems to be sensible to use the network approach in order to visualize such a practical problem. Depending on the case to be optimized, different parameter loops can be identified and thus taken into account during the design of the machining routine. This approach does not give automatic optimization solutions for these cases, but helps to identify the parameters that are to be used in more thorough analysis. This kind of an expert system can be upgraded by inducing topology in the form of functions between different parameters. However, because of the high level of variation in the materials used for tools and workpieces, universal models of cutting parameters have not been created. This makes it difficult to formulate such functions. Regardless of this, the observation of two distinctive parameter groups (design and machine parameters) eases the design of the machining process through the creation of a clearer distinction between objectives and means.

REFERENCES

[1] *D. Lutters, E. ten Brinke, A.H. Streppel, and H.J.J. Kals: "Computer aided process planning for sheet metal based on information management", Journal of Materials Processing Technology, vol. 103, pp. 120-127, 2000.*

[2] *L.B. Newness, A.R. Mileham, and H. Hosseini-Nasab: "On-screen real-time cost estimating", International Journal of Production Research, vol. 45, no. 7, pp. 1577-1594, 2007.*

[3] *J. Cuirana, I. Ferrer, and J.X. Gao: "Activity model and computer aided system for defining sheet metal process planning", Journal of Materials Processing Technology, vol. 173, pp. 213-222, 2006.*

[4] *C. Hayes: "P3 : A process planner for manufacturability analysis", IEEE Transactions of Robotics and Automation, vol. 12, no. 2, 1996.*

[5] *D.K.J. Singh and C. Jebara: "Feature-based design for process planning of machining processes with optimisation using genetic algorithms", International Journal of Production Research, vol. 43, no. 18, pp. 3855-3887, 2005.*

[6] *G.G. Wang and S.Q. Xie: "Optimal process planning for a combined punch-and-laser cutting machine using ant colony optimization", International Journal of Production Research, vol. 43, no. 11, pp. 2195-2216, 2005.*

[7] *M. Lohtander: On the development of object functions and restrictions for shapes made with a turret punch press, Lappeenranta University of Technology, 2010.*

[8] *M. Bastian, S. Heymann, and M. Jacomy: "Gephi: An Open Source Software for Exploring and Manipulating Networks", 3rd International AAAI Conference on Weblogs and Social Media, San Jose, CA, USA, 2009.*

[9] *M. Smith, B. Schneiderman, N. Milic-Frayling, E.M. Rodrigues, V. Barash, C. Dunne, T. Capone, A. Perer, and E. Gleave: "Analyzing (Social Media) Networks with NodeXL", Proceedings of the Fourth International Conference on Communities and Technologies, State College, PA, USA, 2009.*

[10] *V. D. Blondel, J.-L. Guillaume, R. Lambiotte, and E. Lefebvre: "Fast unfolding of communities in large networks", Journal of Statistical Mechanics: Theory and Experiment 2008, no. 10, p. 1000, 2008.*

[11] *N.R. Abburi and U.S. Dixit: "A knowledge-based system for the prediction of surface roughness in turning process", Robotics and Computer-Integrated Manufacturing, vol. 22, no. 4, pp. 363-372, 2006.*

[12] *K. Huh and C. Pak: "Unmanned Turning Force Control with Selecting Cutting Conditions", IEEE, American Control Conference, Denver, CO, USA, 2003.*

[13] *D. Karayel: "Prediction and control of surface roughness in CNC lathe using artificial neural network", Journal of Materials Processing Technology, vol. 209, pp. 3125-3137, 2009.*

[14] *Y.H. Peng: "On the performance enhancement of self-tuning adaptive control for time-varying machining processes", International Journal of Advanced Manufacturing Technology, vol. 24, pp. 395-403, 2004.*

[15] *J. Srinivas, R. Giri, R. and S.-H. Yang: "Optimization of multi-pass turning using particle swarm intelligence", International Journal of Advanced Manufacturing Technology, vol. 40, pp. 56-66, 2009.*

[16] *J. Ratava, M. Rikkonen, V. Ryynänen, J. Leppänen, T. Lindh, J. Varis, and I. Sihvo: "An adaptive fuzzy control system to maximize rough turning productivity and avoid the onset of instability", International Journal of Advanced Manufacturing Technology vol. 53, no. 1, pp. 71-79, 2012.*

[17] *V. Ryynänen, J. Ratava, T. Lindh, M. Rikkonen, I. Sihvo, J. Leppänen, and J. Varis: "Chip control system for monitoring the breaking of chips and elimination of continuous chips in rough turning", Mechanika vol. 4 no. 78, pp. 57-62, 2009.*

[18] *V.S. Sharma, S.K. Sharma, and A.K. Sharma: "Cutting tool wear estimation for turning", Journal of Intelligent Manufacturing, vol. 19, no. 1, pp. 99-108, 2006.*

[19] *O. Yilmaz, G. Görür, and T. Dereli: "Computer Aided Selection of Cutting Parameters by Using Fuzzy Logic", Proceedings of the International Conference, 7th Fuzzy Days on Computational Intelligence, Theory and Applications, Dortmund, Germany, 2001.*

[20] *H. Saglam, S. Yaldiz, and F. Unsacar: "The effect of tool geometry and cutting speed on main cutting force and tool tip temperature", Materials & Design, vol. 28, no. 1, pp. 101-111, 2007.*

[21] *X. Cui, J. Zhao, Y. Dong: "The effects of cutting parameters on tool life and wear mechanisms of CBN tool in high-speed face milling of hardened steel", International Journal of Advanced Manufacturing Technology, July 2012.*

[22] *A. Bhattacharya, S. Das, P. Majumder, A. Batish: "Estimating the effect of cutting parameters on surface finish and power consumption during high speed machining of AISI 1045 steel using Taguchi design and ANOVA," Production Engineering, vol. 3, no. 1, pp. 31-40, 2009.*

[23] *A. Hamdan, A.A.D. Sarhan, and M. Hamdi: "An optimization method of the machining parameters in high-speed machining of stainless steel using coated carbide tool for best surface finish," International Journal of Advanced Manufacturing Technology, vol. 58, no. 1-4, pp. 81-91, 2012.*

[24] *V.G. Navas, O. Gonzalo, and I. Bengoetxea: "Effect of cutting parameters in the surface residual stresses generated by turning in AISI 4340 steel", International Journal of Machine Tools and Manufacture, vol. 61, pp. 48-57, 2012.*

[25] O. Kienzle and H. Victor: "Die Bestimmung von Kräften und Leistungen an spanenden Werkzeugmaschinen", VDI-Z, vol. 94, no. 11-12, pp. 155-171, 1952.

[26] M.B. da Silva and J. Wallbank: "Cutting temperature: prediction and measurement methods - a review", Journal of Materials Processing Technology, vol. 88, no. 1-3, pp. 195-202, 1999.

[27] V.P. Astakhov: "Effects of the cutting feed, depth of cut, and workpiece (bore) diameter on the tool wear rate", International Journal of Advanced Manufacturing Technology, vol. 34, no. 7-8, pp. 631-640, 2007.

[28] R.K. Bhushan: "Optimization of cutting parameters for minimizing power consumption and maximizing tool life during machining of Al alloy SiC particle composites", Journal of Cleaner Production, vol. 39, pp. 242-254, 2013.

[29] N. S. Kumar, A. Shetty, A. Shetty, Ananth K, and H. Shetty: "Effect of Spindle Speed and Feed Rate on Surface Roughness of Carbon Steels in CNC Turning", Procedia Engineering, vol. 38, pp. 691-697, 2012.

[30] H. Aouici, M.A. Yallese, K. Chaoui, T. Mabrouki, and J.-F. Rigal: "Analysis of surface roughness and cutting force components in hard turning with CBN tool: Prediction model and cutting conditions optimization", Measurement, vol. 45, no. 3, pp 344-353, 2012.

[31] T.S. Ong and B.K. Hinds, "The application of tool deflection knowledge in process planning to meet geometric tolerances", International Journal of Machine Tools and Manufacture, volume 43, no. 7, pp. 731-737, 2003.

[32] V. Sivaraman, S. Sankaran, and L. Vijayaraghavan: "The Effect of Cutting Parameters on Cutting Force During Turning Multiphase Microalloyed Steel", Procedia CIRP, vol. 4, pp. 157-160, 2012.

[33] L.B.Abhang and M. Hameedullah: "Chip-Tool Interface Temperature Prediction Model for Turning Process", International Journal of Engineering Science and Technology, vol. 2, no. 4, 382-393, 2010.

[34] S.K Choudhury and K.K Kishore, "Tool wear measurement in turning using force ratio", International Journal of Machine Tools and Manufacture, vol. 40, no. 6, pp. 899-909, 2000.

[35] G. Bartarya and S.K. Choudhury: "Effect of Cutting Parameters on Cutting Force and Surface Roughness During Finish Hard Turning AISI52100 Grade Steel", Procedia CIRP, vol. 1, pp. 651-656, 2012.

[36] K.-M. Li and S.Y. Liang: "Modeling of cutting forces in near dry machining under tool wear effect", International Journal of Machine Tools and Manufacture, vol. 47, no. 7-8, pp. 1292-1301, 2007.

[37] R. Pavel, I. Marinescu, M. Deis, and J. Pillar, "Effect of tool wear on surface finish for a case of continuous and interrupted hard turning", Journal of Materials Processing Technology, vol. 170, no. 1-2, pp. 341-349, 2005.

[38] M.U. Ghani, N. A. Abukhshim, and M. A. Sheikh: "An investigation of heat partition and tool wear in hard turning of H13 tool steel with CBN cutting tools", International Journal of Advanced Manufacturing Technology, vol. 39, no. 9-10, pp 874-888, 2008.

[39] M.A. Xavior and M. Adithan: "Determining the influence of cutting fluids on tool wear and surface roughness during turning of AISI 304 austenitic stainless steel", Journal of Materials Processing Technology, vol. 209, no. 2, pp. 900-909, 2009.

[40] J.M. Vieira, A.R. Machado, and E.O. Ezugwu: "Performance of cutting fluids during face milling of steels", Journal of Materials Processing Technology, vol. 116, no. 2-3, pp. 244-251, 2001.

[41] D. Jianxin, Z. Hui, W. Ze, L. Yunsong, X. Youqiang, and L. Shipeng: "Unlubricated friction and wear behaviors of Al2O3/TiC ceramic cutting tool materials from high temperature tribological tests", International Journal of Refractory Metals and Hard Materials, vol. 35, pp. 17-26, 2012.

[42] N. Guillemot, M. Winter, A. Souto-Lebel, C. Lartigue, and R. Billardon: "3D Heat Transfer Analysis for a Hybrid Approach to Predict Residual Stresses After Ball-End Milling", Procedia Engineering, vol. 19, pp. 125-131, 2011.

Original Article

Institution of MECHANICAL ENGINEERS
Journal of ENGINEERING MANUFACTURE

Proc IMechE Part B:
J Engineering Manufacture
227(11) 1620–1634

DOI: 10.1177/0954405413492732
pib.sagepub.com
SAGE

Investigation of the effect of different cutting parameters on chip formation of low-lead brass with experiments and simulations

Sampsa VA Laakso[1], Mikko Hokka[2], Esko Niemi[1] and Veli-Tapani Kuokkala[2]

Abstract

Poor chip breakage causes problems in machining of low-lead brass. To improve chip breakage, finite element model simulations were implemented in cutting tool design. Finite element model simulations enable high number of experiments that would be expensive and slow to perform by conventional cutting tests. Compression tests and cutting experiments under different temperatures and strain rates were performed for lead-free brass, to acquire material parameters for the finite element model. It was observed that the coupled effect of thermal softening and rate sensitivity of the material was difficult to take into account with the existing material model. Furthermore, it was found that there are no reported material models that can take rate sensitivity–temperature coupling into account. This was counteracted by fitting the model with least square method to the stress–strain data at the cutting temperature, although this causes error in simulations with temperatures higher or lower than the supposed cutting temperature. Nevertheless, the simulated results proved accurate enough to model the chip breakage. Based on the simulations and experiments, the use of a positive rake angle, high cutting speed and low cutting feed rate improve chip breakage from continuous chip to a chip of average length of 4 mm.

Keywords

Cutting, material modelling, finite element model, low-lead brass, chip breakage

Date received: 27 November 2012; accepted: 14 May 2013

Introduction

Health and environmental issues are growing concerns for companies and governmental decisions. In the United States, the state of California has banned plumbing products containing lead more than 0.25%.[1] The restriction took effect on 1 January 2010 despite the opposition of The Plumbing Manufacturers Institute.[2] Exposure to lead is a commonly known major health hazard, as it can cause anaemia and provoke other health issues.[3] The restriction affects especially brass components, which are typically machined from cast billets. Typical cast brass alloys with good machinability contain lead between 1.5% and 3%.[4] Some companies have decided to substitute lead with bismuth, although there are references according to which bismuth could also be toxic.[5,6] Finnish faucet and plumbing industry has decided to use lead-free brass (<0.25 Pb%) in their production. The decision has caused difficulties in machining, especially because poor chip breakage of lead-free casting brass causes jamming of the machine tool and bad-quality products because the chips are tearing the final product. This article studies chip breakage of lead-free brass in machining operations with the help of finite element simulations and extensive material characterization. The goal of this study is to develop a method for cutting lead-free brass products without generating continuous chip.

[1]Department of Engineering Design and Production, Aalto University School of Engineering, Espoo, Finland
[2]Department of Materials Science, Tampere University of Technology, Tampere, Finland

Corresponding author:
Sampsa VA Laakso, Department of Engineering Design and Production, School of Engineering, Aalto University, Puumiehenkuja 3, 02150 Espoo, Finland.
Email: sampsa.laakso@aalto.fi

In previous research by Laakso,[7] finite element modelling of cutting was evaluated by comparing simulated results to experimental data acquired for stainless steel, carbon steel and aluminium in different machining processes. Simulation software used in the study were Third Wave Systems AdvantEdge and Parametric Forming Technologies Deform. Although it was concluded that simulations generally give fair approximation (< 30% error in cutting forces), the qualitative behaviour of cutting simulations is in line with experimental results. Therefore, it is reasonable to assume that simulations can predict the effect of different cutting parameters to chip breakage accurately enough. From the study, it was concluded that the material model has the most significant impact on accuracy apart from the geometrical accuracy of the tool and the friction model. Other studies report similar results. Yen et al. studied the effect of tool geometry on cutting forces and temperature. Good correlation between experimental and simulated forces was found with different cutting edge radiuses. The error in the forces was between 5% and 13%. The cutting force increases as the radius increases. Temperature was concluded to be directly proportional to amount of plastic deformation, which is directly proportional to tool edge radius. Therefore, temperature is proportional to cutting force.[8] Mackerle[9,10] has listed research articles about finite element simulations of metal cutting from 1976 to 2002 in his bibliography review. Childs included upper yield stress to power law material model. It was concluded that for steels, the effect of upper yield stress is significant, and the standard error in cutting, which is underestimated cutting force in simulations, was not found when using the improved model.[11,12] This implicates that other material phenomenon such as temperature and rate sensitivity coupling considered to be negligible in metal cutting could prove to be significant factor in simulation accuracy. Coupled effect of rate sensitivity and temperature was reported in the studies by Suery and Baudelet[13] and Jiang et al.,[14] but it was not emphasized how important the effect is on machining. Also, as discussed in the study by Childs,[15] the friction in cutting process does not follow the Coulomb friction law. Few attempts to correct this have been reported.[16–18]

Materials and methods

The AdvantEdge[19] cutting simulation software was used for the simulations. The software was first presented in the study by Marusich and Ortiz.[20] The software is based on a dynamic explicit Lagrangian finite element model (FEM), which employs adaptive remeshing to avoid element distortions. The model is based on equations of motion and thermo-mechanically coupled material model.[20,21] The casting brass investigated in this article is not standardized, but is close to standard EN CW511L. The composition of the brass is presented

Table 1. Chemical composition of the lead-free brass investigated in this article (wt%).

Sn	Pb	P	Fe	Si	As	Sb	Al	Cu	B	Fe	Zn
0.15–0.25	0.2 maximum	0.01 maximum	0.05–0.10	0.02 maximum	0.04 maximum	0.03–0.06	0.60–0.65	62.5–63.5	10–14 ppm	0.35 maximum	Difference

inTable 1. A material model based on the power law equation was implemented to mathematically reproduce the constitutive behaviour of the material. The model is built-in in the AdvantEdge FEM software. To implement the model, material behaviour and parameters were determined from a series of compression tests and cutting experiments performed at different strain rates and temperatures.

Material model

A mathematical formulation of the flow stress model is presented in equations (1) (4) (AdvantEdge User Manual, 20). This model takes into account strain hardening, thermal softening and strain rate hardening. The stress strain relationship is composed of three parts: strain hardening multiplier,[2] thermal softening multiplier[3] and strain rate hardening multiplier.[4] Each of these multipliers takes the corresponding input parameter. Multipliers adjust the value of yield stress (flow stress) to the measured stress strain curve in different conditions. The input parameters are strain ε, temperature T and strain rate $\dot{\varepsilon}$. The material parameters determine the effect of the input parameters; these are strain hardening exponent n, thermal softening parameters c_i and rate hardening exponents m_1 and m_2. Other parameters determine the flow stress properties of the material: the cut-off value of strain ε_{cut} after which the material flow stress does not increase with increasing strain, the point T_{cut} where thermal softening starts to linearly increase towards melting point and strain rate $\dot{\varepsilon}_t$ that begins what is considered high-strain rate hardening zone. Chip breakage is calculated in two-dimensional (2D) simulations using the routine based on fracture criteria K_{IC} determined by Third Wave Systems in AdvantEdge software[19,22]

$$\text{Stress–strain relationship: } \sigma(\varepsilon^P, \dot{\varepsilon}, T) = \sigma_{yield} g(\varepsilon^P) \Gamma(\dot{\varepsilon}) \Theta(T) \quad (1)$$

$$\text{Strain hardening: } g(\varepsilon^P) = \left(1 + \frac{\varepsilon^P}{\varepsilon_0^P}\right)^{1/n},$$

$$\text{if } \varepsilon^P < \varepsilon_{cut}^P \quad g(\varepsilon^P) = g(\varepsilon_{cut}^P), \quad \text{if } \varepsilon^P \geqslant \varepsilon_{cut}^P \quad (2)$$

$$\text{Thermal softening: } \Theta(T) = \sum_{i=0}^{n} c_i T^i,$$

$$\text{if } T < T_{cut} \quad \Theta(T) = \Theta(T_{cut})\left[1 - \frac{T - T_{cut}}{T_{melt} - T_{cut}}\right],$$

$$\text{if } T \geqslant T_{cut} \quad (3)$$

$$\text{Strain rate hardening: } \Gamma(\dot{\varepsilon}) = \left(1 + \frac{\dot{\varepsilon}}{\dot{\varepsilon}_0}\right)^{\frac{1}{m_1}},$$

$$\text{if } \dot{\varepsilon} \leqslant \dot{\varepsilon}_t \quad \Gamma(\dot{\varepsilon}) = \left(1 + \frac{\dot{\varepsilon}}{\dot{\varepsilon}_0}\right)^{\frac{1}{m_2}} \left(1 + \frac{\dot{\varepsilon}_t}{\dot{\varepsilon}_0}\right)^{\frac{1}{m_1} - \frac{1}{m_2}},$$

$$\text{if } \dot{\varepsilon} > \dot{\varepsilon}_t \quad (4)$$

Material testing

Material testing was conducted by a series of compression tests at different temperatures and strain rates from 10^{-3} to 3200 s^{-1}. The range of strain rates used is limited by the capabilities of the testing platform available. Testing temperatures are selected to room temperature, expected cutting temperature and the highest temperature achievable by the testing oven. A few tensile tests were also conducted to observe if any significant differences between tension and compression exist. The low-strain rate tests ($\leqslant 10^{-1}$ s^{-1}) were conducted using a servo hydraulic material testing machine with an induction heating system. The high-strain rate tests were done using a Split Hopkinson Pressure Bar device equipped with a special high-temperature set-up. These compression tests were done at strain rates ranging from 1000 up to 3200 s^{-1} at room temperature and at elevated temperatures of 200 °C and 450 °C. For example, the devices used in this work are described in more detail in the studies by Apostol et al.[23–25]

Simulations

The simulations were carried out by the AdvantEdge software running on a server-based PC with twenty-four 3.6-GHz Intel Xeon Cores, 32 GB of memory, Nvidia Quadro FX 1800 graphics card and 3500 GB hard drives on RAID 5 configuration to enhance read/write performance. A 2D mode turning operation was employed for the simulations, which were conducted with three different cutting speeds (50, 150 and 300 m/min), three different feed rates (0.1, 0.2 and 0.4 mm/r) and rake angles of +5° and −5°. Cutting tool angle of 90° was used due to orthogonal condition of the 2D simulations. Cutting forces, temperatures and chip thicknesses were recorded as output. Chip breakage was evaluated by the number of near breaking points and chip breakage at chip root as presented in Figure 8 of Balaji et al.'s[26] study.

Cutting experiments

Strain rates above 10^4 s^{-1} are very difficult to achieve using the Hopkinson Bar techniques, and therefore, cutting experiments were conducted to obtain stress strain data at these strain rates. A manual lathe and force measuring equipment, KISTLER 9257A piezoelectric sensor and 5019A charge amplifier, were used in the experiments. The forces to the direction of primary cutting motion, F_c, and to the direction of feed, F_f, are measured. Due to the lack of valid analytical models for cutting, an inverse analysis between force measurements and FEM analysis was conducted to acquire the stress strain relationship. Inverse routine starts by fitting the material flow stress model presented in equations (1) (4) to compression test data, then using the model to simulate some specific cutting experiment and improving the model by comparing the simulated

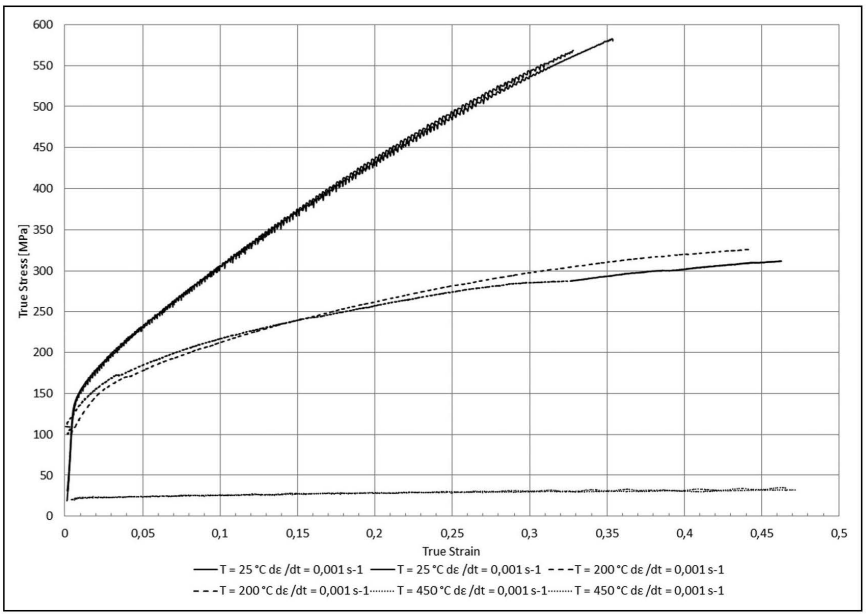

Figure 1. Compression stress–strain curves obtained at different temperatures and at the strain rate of 10^{-3} s^{-1}.

results to experimental results. Usually, cutting force is used in evaluation, but also chip thickness is used in some cases. The model is then adjusted to produce better values. The parameters to adjust are ε_{cut}, $\dot{\varepsilon}_t$ and the strain hardening exponents. Strain hardening exponents are selected with the method of least squares comparing the simulation data to cutting experiments and material testing. For each adjustment of ε_{cut}, new simulation is needed, so long iterative adjustment is not an option but rather deterministic approach to adjusting the values should be taken. The performance of the model is determined by qualitative and quantitative behaviours. Quantitative performance is error in cutting forces and chip thickness, or chip compression ratio. Qualitative behaviour is how well the simulation predicts the change in forces or chip thickness after the change of cutting parameters. There is no universal exact value for the required performance but in this research, error in cutting forces under 10% is considered to be good correlation. A nearly orthogonal cutting set-up was used to achieve a good correlation with simulations as possible. The cutting tool angle was 90° due to orthogonal cutting set-up. The cutting parameters were the same as in simulations, with the exception of the number of different feed rates and cutting speed values was higher. Each experiment was conducted with new tool to prevent tool wear affecting the results. The feed rate values were 0.1, 0.2, 0.3 and 0.4 mm/r, and cutting speeds were 50, 100, 150 and 300 m/min. Rake angle of 0° was not used. All experiments were repeated twice to ensure repeatability. Three experiments are needed for deviation plot of the cutting forces, but it was concluded that it is not worth of more experimental work because of validating nature of the experiments. Chip thicknesses were also measured. Comparative visual inspections of the chip length were the main criteria for evaluating chip breakage.

Results

First, the results of the compression tests and cutting experiments are given. Then, the material model fitting and analysis of it are presented. The simulated results are presented after the modelling details, because they are prerequisites for simulations. The last part compares the results obtained from the simulations and experiments.

Compression tests

Figure 1 shows the results of the compression tests done at strain rates of 10^{-3} s^{-1}. The yield strength of the material at room temperature is around 145 MPa. Yield strength does not depend much on strain rate, which can be seen by comparing Figure 1 with Figure 2. This is a typical behaviour of a simple face-centred cubic (FCC) metal. Also, strain hardening rate seen as the slope of the curve is fairly strong and nearly constant with respect to strain, up to fairly large strains. When the temperature is increased to 200 °C, the yield strength of the material does not change much, but the strain hardening rate decreases significantly. Also, the strain rate sensitivity of the material increases especially at larger strains, which is an indication of increasing amount of thermally activated dislocation glide

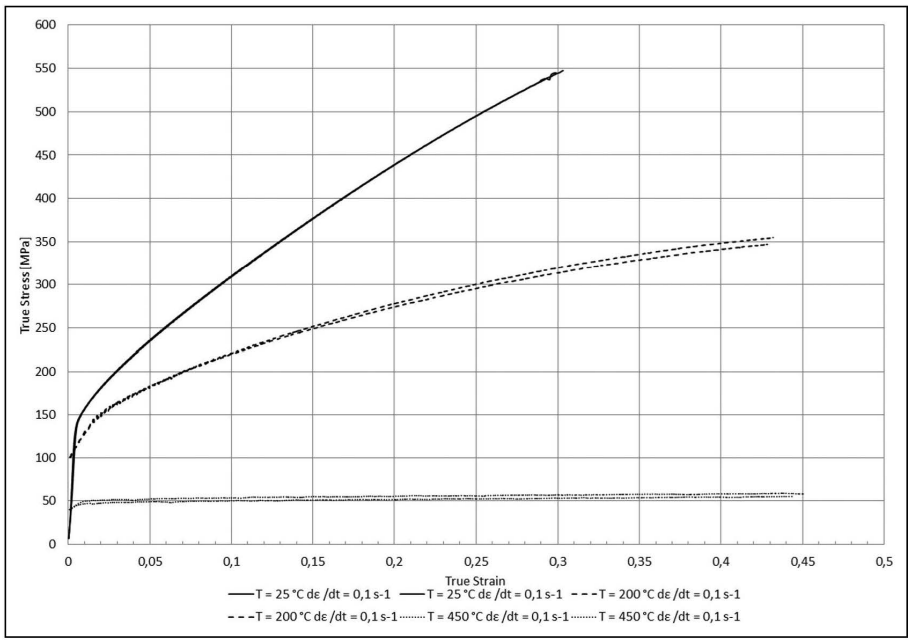

Figure 2. Compression stress–strain curves obtained at different temperatures and at the strain rate of 10^{-1} s^{-1}.

obstacles.[27] For a FCC metal, the most significant thermally activated event is the cutting of forest dislocations, the number of which increases with strain. Even at higher temperature, not only the strain hardening rate drops further but also the yield strength decreases significantly. This might be an indication of recrystallization and/or grain growth at this temperature.

Figures 3 and 4 present the results of the compression tests done at high strain rates. The yield strength of the material seems to be fairly insensitive to strain rate, and only a modest increase to about 170 MPa is observed at the highest strain rates. The strain hardening rate, however, increases strongly compared to the low-strain rate tests. At high strain rates, the temperature seems to have much less effect on the strength and strain hardening behaviour of the material when compared to that observed at low strain rates. The yield strength of the material decreases only from 170 to about 145 MPa at 450 °C and at 1300 s^{-1}, and also the strain hardening rate is only slightly decreased at higher temperatures. This is an important result, because material models generally do not take this behaviour into account.

Similar rate sensitivity and temperature behaviour were observed for 60/40 brass in research conducted by Suery and Baudelet. Yield stress at 600 °C increased from 50 to over 200 MPa when strain rate increased from 10^{-2} to $0.4\,s^{-1}$.[15] Jiang et al. conducted experiments on 7050-T7451 aluminium to simulate turning with power law material model. Similar procedure as in this article was done to acquire material parameters. Split Hopkinson tests revealed that yield stress of aluminium at 300 °C increases from 350 to 500 MPa when strain rate increases from 10^{-3} to $6200\,s^{-1}$. The increase of yield stress with increasing strain rate is not significant at room temperature.[16]

Cutting experiments

Results of the cutting experiments are presented in Table 2. The forces are presented as the resultant of the cutting force acting in the direction of primary cutting motion and the tangential force acting in the direction of feed. The resultant cutting forces increase almost linearly with the increase of cutting feed rate. Cutting speed does not have a significant impact, except a minor decrease of cutting forces at the highest speeds with a negative rake angle. Similar results were also observed with chip thicknesses. Cutting forces are clearly higher in the negative rake angle experiments. Chip breakage was observed by visual appearance and the length and thickness of the chip. The best results in chip breakage were observed at low feed rates. High cutting speed was also observed to improve surface roughness, although this was not measured as it was not in the scope of the research.

Material parameters

Material parameter values in Table 3 were determined to fit the model (equations (1)–(4)) to the stress–strain data obtained from the compression tests. Material parameters were fitted by the method of least squares. Other parameters needed by the simulation software are elastic modulus, Poisson's ratio, thermal conductivity, heat capacity and density. All these values are found in engineering reference books or databases.

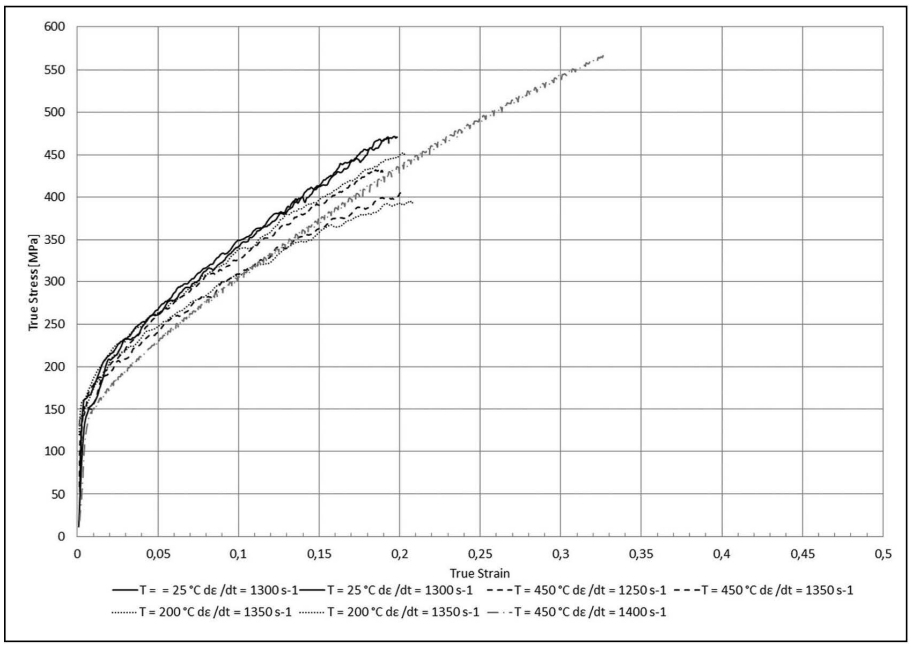

Figure 3. Compression stress–strain curves obtained at different temperatures at the strain rate of ~1300 s^{-1}.

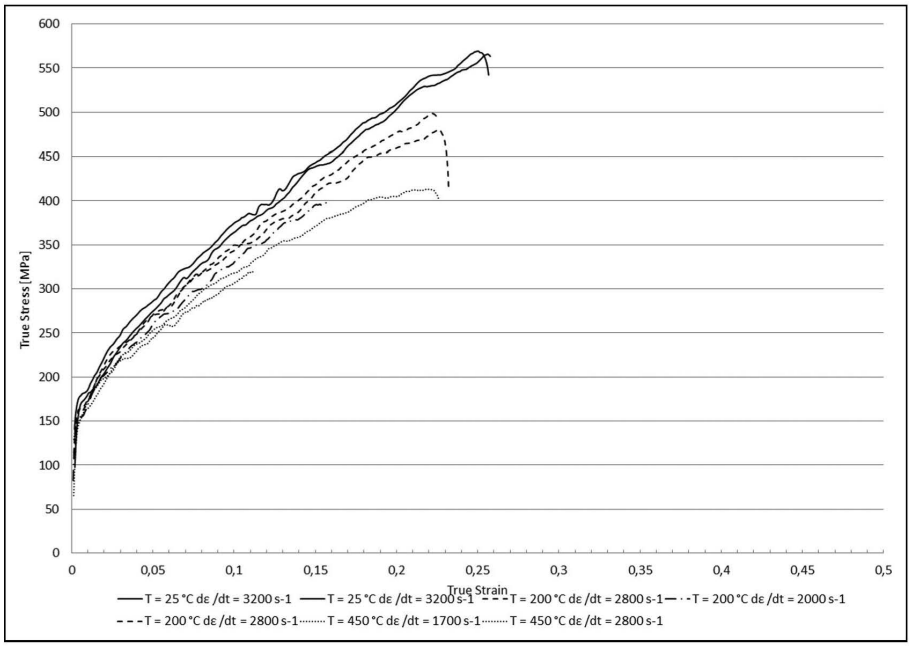

Figure 4. Compression stress–strain curves obtained at different temperatures at the strain rates of 1700–3200 s^{-1}.

Figures 5 and 6 present the multipliers for strain rate hardening and thermal softening. After the compression tests, ε_{cut} was set to 0.2. Simulated results while using this value showed greatly underestimated values for the resultant cutting forces so the value was increased to 0.3. After that, the forces were in much better agreement. Jiang et al. discussed the determining of strain cut-off value from orthogonal turning

Table 2. Resultant cutting forces and chip thicknesses from the experiments.

	Feed				
Cutting speed	$\gamma = +5$	0.1 mm/r	0.2 mm/r	0.3 mm/r	0.4 mm/r
	50.0 m/min	434.8 N	672.9 N	865.2 N	1086.0 N
		0.333 mm	0.515 mm	0.663 mm	0.863 mm
	100.0 m/min				1039.6 N
					0.743 mm
	150.0 m/min				1039.2 N
					0.783 mm
	300.0 m/min	430.1 N	677.2 N	850.9 N	1039.9 N
		0.343 mm	0.495 mm	0.665 mm	0.828 mm
	$\gamma = -5$	0.1 mm/r	0.2 mm/r	0.3 mm/r	0.4 mm/r
	50.0 m/min	584.0 N	878.7 N	1082.1 N	1127.0 N
		0.288 mm	0.460 mm	0.593 mm	0.765 mm
	100.0 m/min				1249.0 N
					0.748 mm
	150.0 m/min				1250.3 N
					0.693 mm
	300.0 m/min	519.7 N	790.3 N	1030.7 N	1155.7 N
		0.318 mm	0.478 mm	0.563 mm	0.678 mm

Table 3. Material parameters.

σ_{yield} (MPa)	132
ε_0	0.0012
N	4
ε_{cut}	0.3
c_0	0,79
c_1	-1.2×10^{-3}
c_2	2.4×10^{-7}
T_{ref} (°C)	5
T_{melt} (°C)	920
T_{cut} (°C)	460
m_1	1000
m_2	8
$\dot{\varepsilon}_0$	0.001
$\dot{\varepsilon}_t$	50
E (GPa)	116
ν	0.3754
k (W/m °C)	109
C (J/kg °C)	380
ρ (kg/m^3)	8550

experiments by comparing simulated and experimental chip thicknesses and cutting forces. They concluded that strain cut-off value has major impact on simulated cutting forces and chip thickness.[16] The strain rate coefficients were chosen on the basis of the compression test results: the high-strain rate hardening zone seems to be as low as 50 s^{-1}; therefore, the compression tests at the range used were adequate to model the strain rate hardening. Thermal softening was the most difficult to model because there are two distinctly different softening curves depending on the strain rate. The observed reduced thermal softening at high strain rates caused some difficulties in modelling the behaviour, as the model does not take such behaviour into account. The softening parameters were chosen as medium of the two different softening curves. Therefore, the model was fitted to the results obtained at 200 °C, which is the expected cutting temperature.

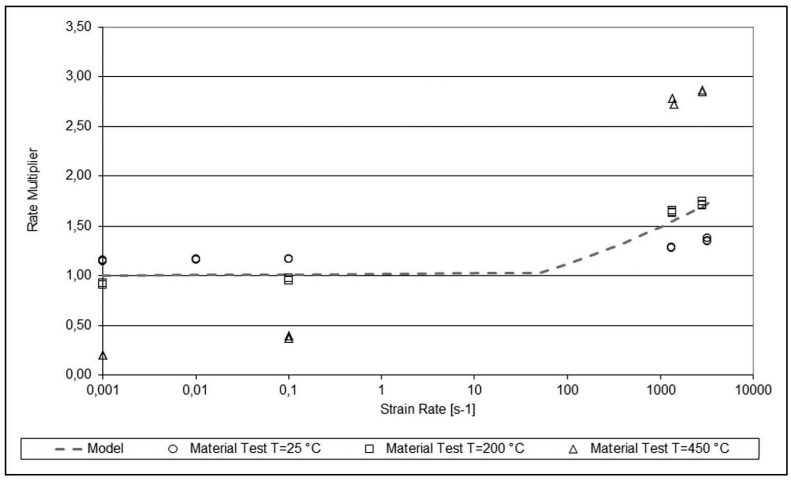

Figure 5. Rate multiplier fit by the method of least squares; the high deviation is caused by the material constitutive model, not by fitting method; the model is fitted to data in 200 °C.

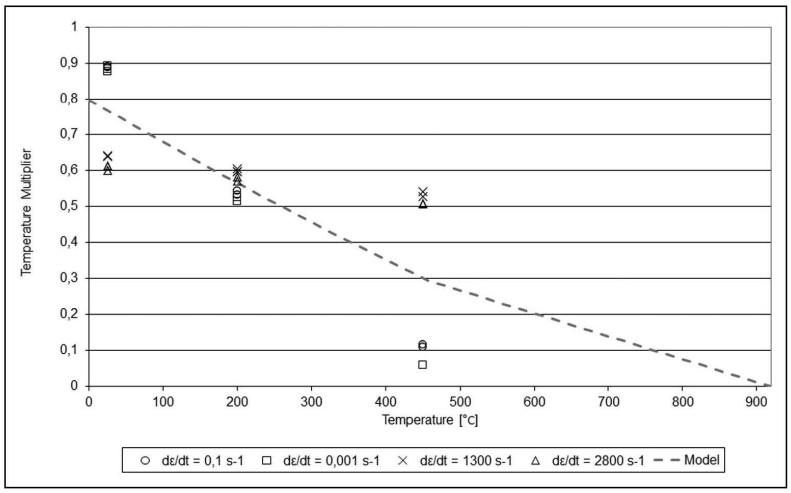

Figure 6. Temperature multiplier fit by the method of least squares; the high deviation is caused by the material constitutive model, not by fitting method; material flow stress reduces to 0 at the melting temperature of 920 °C as defined by the material model.

Table 4. Resultant cutting forces and chip thicknesses from simulations.

	Feed			
Cutting speed	$\gamma = +5$	0.1 mm/r	0.2 mm/r	0.4 mm/r
	50.0 m/min	321.2 N	533.8 N	901.3 N
		0.220 mm	0.400 mm	0.730 mm
	150.0 m/min	317.8 N	547.8 N	948.6 N
		0.160 mm	0.350 mm	0.680 mm
	300.0 m/min	319.8 N	550.2 N	982.3 N
		0.200 mm	0.310 mm	0.660 mm
	$\gamma = -5$	0.1 mm/r	0.2 mm/r	0.4 mm/r
	50.0 m/min	377.3 N	662.0 N	1129.4 N
		0.200 mm	0.380 mm	0.710 mm
	150.0 m/min	380.7 N	652.9 N	1162.9 N
		0.250 mm	0.450 mm	0.820 mm
	300.0 m/min	378.3 N	644.0 N	1142.3 N
		0.160 mm	0.290 mm	0.640 mm

This can be seen in Figures 5 and 6 as deviation of the model from the data points in temperatures lower or higher than 200 °C. The thermal softening effect is extreme after the material reaches cut-off value of 460 °C, after which the material flow stress goes linearly towards 0 and reaches it at the melting temperature.

Simulations

The simulated resultant cutting forces and chip thicknesses are presented in Table 4. Machinability is generally measured not only by chip thickness ratio but also by chip compression ratio. In this article, the chip thickness is used as measure for simulation error, not as criterion of machinability. The resultant cutting forces and chip thicknesses increase with increasing feed rate, but cutting speed does not have a major influence. The results show higher forces with negative rake angles. This is not unusual behaviour as it has been presented in many textbooks of the field. The higher forces are caused by the larger amount of plastic deformation in the chip formation zone.[28–30] Chip breakage was best at high feed rates and speeds as explained in Appendix 1. The highest number of breaking and near breaking points was observed at 300 m/min with feed rate of 0.1 mm/r and +5° rake angle where 1 breaking and 1 near breaking points were observed at cutting length of 10 mm. The second best breakage was observed with same cutting parameters but with −5° rake angle; there were two near breaking points. Only three other cutting conditions lead to any breakage at all in 10 mm length of cut; these were at 150 m/min and 0.1 mm/r feed rate with + 5° rake angle and at 300 m/min and 0.2 mm/r with both positive and negative rake angles. All of the simulation images are found in Appendix 1. Visualization of the chip breakage in Figure 7 is done by giving a score of 0.5 for one near breaking point and 1 for breaking point and summing it up as a score for each cutting condition.

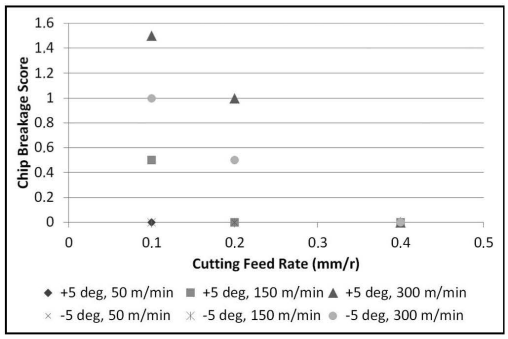

Figure 7. Chip breakage comparison, higher the score the better chip breakage.

Comparison

Figures 8 and 9 present the simulated and tested resultant cutting forces. It can be seen that the forces are in best agreement at high feed rate values. The higher difference at low feed rates can be explained by the lack of accuracy of the friction model.[17] Friction models tend to underestimate friction force in cutting. Friction force is a component in each of the three primary cutting force and therefore also a part of resultant force. Therefore, in higher feed rates, the force induced by friction between tool and chip is small in relation to the primary cutting force caused by the energy consumed in plastic deformation. That is the friction model tends to underestimate the resultant force in small values of feed rate, so the error is not as significant in the resultant cutting force in high feed rates as it is in lower feed rates. Also, as the simulations are 2D, the lack of a third force component tends to underestimate the resultant force. The error is in an acceptable range (average of <17%), compared to traditional analytical models (errors of >50% are not unusual). Qualitative behaviour of the simulations is more important than the exact values of the cutting force. A similar behaviour was perceived on chip thicknesses; the measured and simulated thicknesses were in best agreement with high feed rates (Figures 10 and 11). The best chip breakage was observed at low feed rates. Chip lengths at different cutting speeds and feed rates are presented in Figure 12. High cutting speed has also a minor positive impact on chip breakage. Although a better agreement in forces could have been achieved by adjusting model parameters, by changing the yield stress value higher or increasing the strain hardening exponent, the physical validity of the simulations would not have been correct. Therefore, qualitative behaviour would not have been correct either. Also, it should be mentioned that currently, there are no material models reported, which can take into account the coupled effect of rate sensitivity and temperature. Therefore, a new material model should be built around the test data, to improve the simulations and to observe the model's impact on accuracy. Also, as many researchers have already suggested, a method to acquire the material parameters directly from cutting experiments should be developed.[31] Friction model should also be improved to reach better agreement with forces as the Coulomb friction is not valid in cutting because it has been shown that there is sliding between the chip and the tool.[32]

Discussion

Smallest chip is formed in high cutting speed. This can be explained with the material testing results. Chip is ductile in high temperatures because low-lead brass is highly thermal softening. The softening effect is less

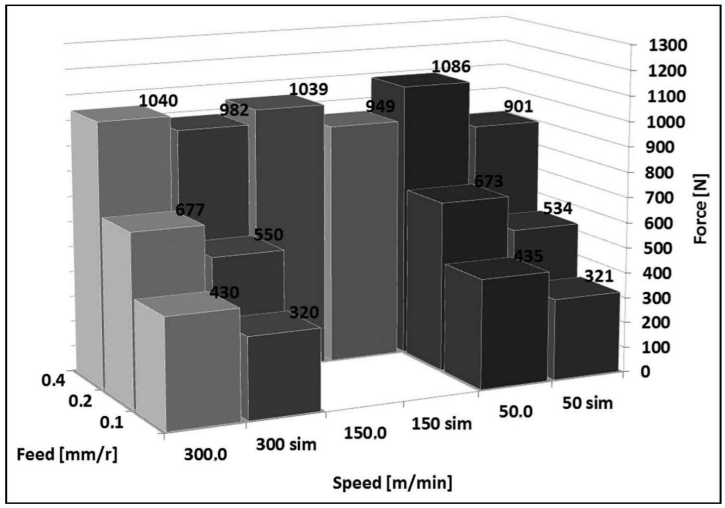

Figure 8. Comparison of simulated and tested resultant cutting forces for a positive rake angle; experimental forces are averages of two experiments.

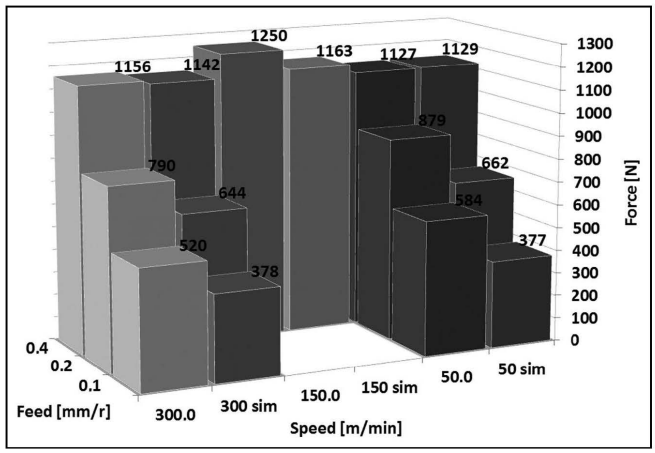

Figure 9. Comparison of simulated and tested resultant cutting forces for a negative rake angle; experimental forces are averages of two experiments.

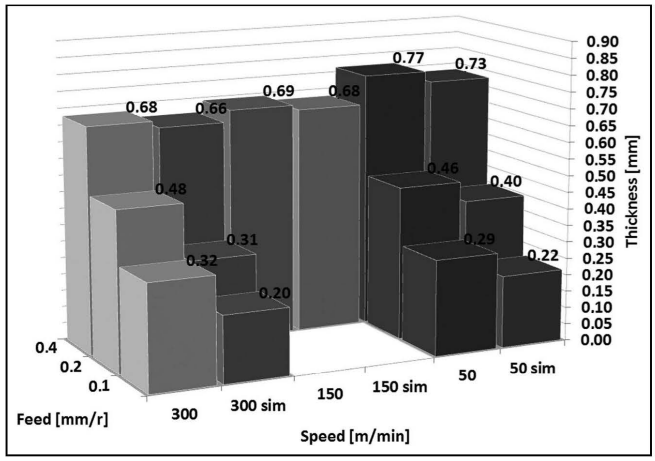

Figure 10. Comparison of simulated and measured chip thicknesses for a positive rake angle; experimental thicknesses are averages of five different chips.

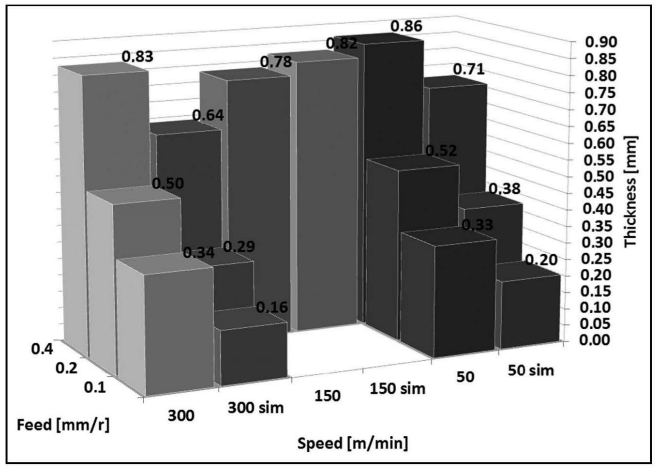

Figure 11. Comparison of simulated and measured chip thicknesses for a negative rake angle; experimental thicknesses are averages of five different chips.

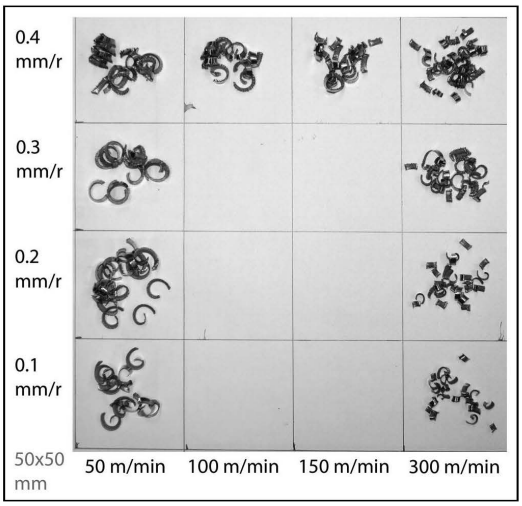

Figure 12. Experimental chip lengths at different cutting speeds and feed rates.

drastic in high strain rates, so the chip forms more brittle in high cutting speeds. Other results can also be explained with chip temperature; therefore, heat generation in cutting is investigated. Heat generation during cutting is caused mainly by two factors: plastic deformation and friction between tool and chip. To control the cutting temperature, plastic deformation and friction should be minimized. If all mechanical works are assumed to turn into heat, then heat generation can be approximated by the following equations (5) and (6) where F and F_μ are the primary cutting force and friction force, v is cutting speed and λ is chip thickness ratio. To minimize heat generation, F and v should be minimized and λ maximized[33]

$$\text{Heat generation in primary shear zone: } Q_s = Fv \quad (5)$$

$$\text{Heat generation in secondary shear zone: } Q_R = \frac{F_\mu v}{\lambda} \quad (6)$$

To minimize cutting forces F and F_μ, a positive rake angle should be used.[30,34] To reduce friction force, the contact area between tool and chip should be relatively low; this can be achieved by reducing cutting feed rate and/or cutting depth. Low feed is also beneficial for surface finish.[35] Also, as shown in the study by Astakhov,[29] as the normal stress at contact surface increases, the mean contact temperature is lower.[29] Additionally, reducing cutting feed increases the chip thickness ratio λ, as shown in Figure 13, and therefore reduces the heat generation in secondary shear zone. Values of chip thickness used for Figure 13 are presented in Table 2.

Conclusion

Chip breakage of low-lead brass can be improved using high cutting speed, small feed rate and positive rake angle because of the following reasons: the material is thermal softening so the chip should stay as cool as possible for it to break. Positive rake angle leads to lower forces and therefore decreased heat generation. Cutting speed should be high, as the thermal softening effect is reduced in high strain rates. Low feed rate

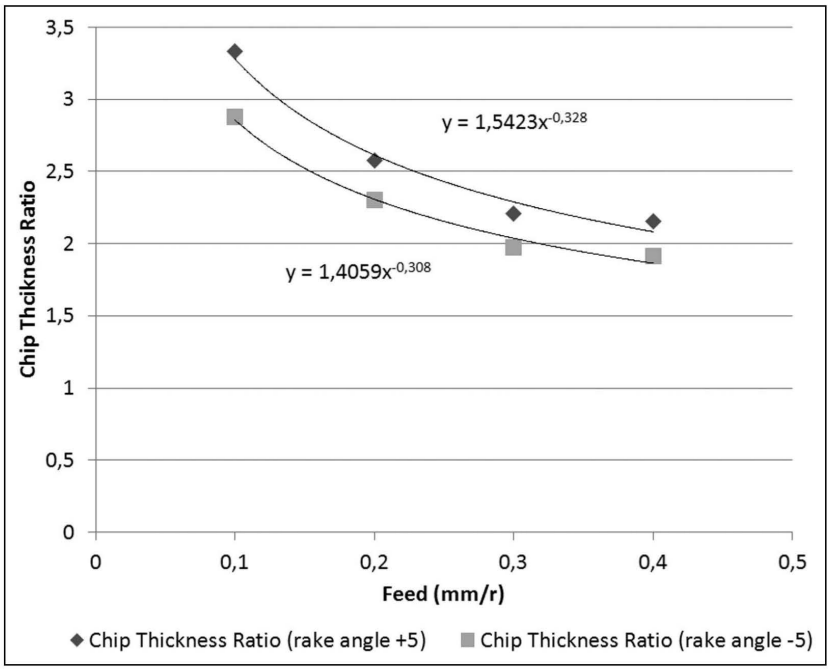

Figure 13. Chip thickness ratio.

increases chip thickness ratio and decreases contact surface area. Increasing chip thickness ratio leads to lower heat generation. Reducing contact surface area using a chip breaking groove increases contact stress and therefore reduces cutting temperature. Also, cutting fluid with good cooling properties should be used to reduce cutting temperature. These observations were verified by FEM simulations and cutting experiments. It was observed that the material model used in this study was not able to predict the material behaviour in all temperature ranges.

Declaration of conflicting interests

The authors declare that there is no conflict of interest.

Funding

This research received no specific grant from any funding agency in the public, commercial or not-for-profit sectors.

References

1. California Department of Toxic Substances Control, Recent Legislation. *Lead in plumbing*, http://www.dtsc.ca.gov/PollutionPrevention/LeadInPlumbing.cfm#Recent_Legislation (accessed 6 October 2010).
2. Penton Media, Inc. Faucet fitting companies battle California lead ban. *The Contractor Magazine*, 1 August 2006, http://www.contractormag.com/bathkitchen/cm_newsarticle_953/index.html (accessed 6 October 2010).
3. Tong S, von Schirnding YE and Prapamontol T. Environmental lead exposure: a public health problem of global dimensions. *B World Health Organ* 2000; 79(9): 1068–1077.
4. Vilarinho C, Davim JP, Soares D, et al. Influence of the chemical composition on the machinability of brasses. *J Mater Process Tech* 2005; 170(1–2): 441–447.
5. Ovaska H, Wood DM, House I, et al. Severe iatrogenic bismuth poisoning with bismuth iodoform paraffin paste treated with DMPS chelation. *Clin Toxicol* 2008; 46: 855–857.
6. Fahey NSC. *The use of science in environmental policy making and the implications for health: a case study of bismuth shotshells*. Master's Thesis, University of Waterloo, Canada, 2005.
7. Laakso SVA. *Finite element modeling of cutting – applications and usability*. Master's Thesis, Helsinki University of Technology, Finland, 2009 (in Finnish).
8. Yen Y, Jain A and Altan T. A finite element analysis of orthogonal machining using different tool edge geometries. *J Mater Process Tech* 2004; 146(1): 72–81
9. Mackerle J. Finite element analysis and simulation of machining: a bibliography (1976–1996). *J Mater Process Tech* 1998; 86(1): 17–44.
10. Mackerle J. Finite element analysis and simulation of machining: an addendum: a bibliography (1996–2002). *Int J Mach Tool Manu* 2003; 43(1): 103–114.
11. Childs THC. Modelling orthogonal machining of carbon steels, part I: strain hardening and yield delay effects. *Int J Mech Sci* 2009; 51(5): 402–411.
12. Childs THC and Rahmad R. Modelling orthogonal machining of carbon steels. Part II: Comparisons with experiments. *Int J of Mech Sci* 2009; 51(6): 465–472.
13. Suery M and Baudelet B. Flow stress and microstructure in superplastic 60/40 brass. *J Mater Sci* 8(3): 363–369.
14. Jiang F, Li J, Sun J, et al. Al7050-T7451 turning simulation based on the modified power-law material model. *Int J Adv Manuf Tech* 2010; 48(9–12): 871–880.
15. Childs THC. Friction modelling in metal cutting. *Wear* 2006; 260(3): 310–318.
16. Arrazola PJ, Ugarte D and Domínguez X. A new approach for the friction identification during machining through the use of finite element modeling. *Int J Mach Tool Manu* 2008; 48(2): 173–183.
17. Arrazola PJ and Özel T. Investigations on the effects of friction modeling in finite element simulation of machining. *Int J Mech Sci* 2010; 52(1): 31–42.
18. Bonnet C, Valiorgue F, Rech J, et al. Improvement of the numerical modeling in orthogonal dry cutting of an AISI 316L stainless steel by the introduction of a new friction model. *CIRP J Manuf Sci Technol* 2008; 1(2): 114–118.
19. http://www.thirdwavesys.com/ (accessed 21 September 2011).
20. Marusich TD and Ortiz M. Modeling and simulation of high speed machining. *Int J Numer Meth Eng* 1995; 38(21): 3675–3694.
21. Marusich TD and Askari E. Modeling residual stress and workpiece quality in machined surfaces. In: *Proceedings of the fourth CIRP international workshop modeling of machining operations*, Delft Technological University, Delft, The Netherlands, August 2001, pp.105–109.
22. Marusich TD, Thiele JD and Brand CJ. *Simulation and analysis of chip breakage in turning processes*, http://www.thirdwavesys.com/pdfs/tech/chipbreaking.pdf (accessed 6 February 2012).
23. Apostol M, Vuoristo T and Kuokkala VT. High temperature high strain rate testing with a compressive SHPB. *J de Phys IV* 2003; 110: 459–464.
24. Apostol M, Kuokkala VT and Vuoristo T. High temperature high strain rate behavior of OFHC copper with a compressive high temperature recovery split hopkinson pressure bar. ICEM12 - 12th International Conference on Experimental Mechanics, 29 August - 2 September, 2004, Politecnico di Bari, Italy. 2004, pp. 172–179.
25. Apostol M. *Strain rate and temperature dependence of the compression behaviour of FCC and BCC metals: development of experimental techniques and their application to materials modelling*. PhD Thesis, Tampere University of Technology, Finland, 2007.
26. Balaji AK, Ghosh R, Fang XD, et al. Performance-based predictive models and optimization methods for turning operations and applications: part 2 – assessment of chip forms/chip breakability. *J Manuf Process* 2006; 8(2): 144–158.
27. Klepaczko J and Chiem C. On the rate sensitivity of FCC metals, instantaneous rate sensitivity and rate sensitivity of strain hardening. *J Mech Phys Solids* 1986; 34: 29–54.
28. Klocke F. *Manufacturing processes 1: cutting*. Springer, 2011.
29. Astakhov VP. *Tribology of metal cutting, tribology and interface engineering series*. London: Elsevier, 2006.
30. Günay M, Korkut İ, Aslan E, et al. Experimental investigation of the effect of cutting tool rake angle on main cutting force. *J Mater Process Tech* 2005; 166(1): 44–49.
31. Sartkulvanich P. *Determination of material properties for use in FEM simulations of machining and roller burnishing*. PHD Dissertation, Ohio State University, USA, 2007.

32. Ackroyd B, Akcan NS, Chhabra P, et al. Exploration of contact conditions in machining. *Proc IMechE, Part B: J Engineering Manufacture* 2001; 215: 493–507.
33. Saglam H, Unsacar F and Yaldiz S. Investigation of the effect of rake angle and approaching angle on main cutting force and tool tip temperature. *Int J Mach Tool Manu* 2006; 46(2): 132–141.
34. Abukhshim NA, Mativenga PT and Sheikh MA. Heat generation and temperature prediction in metal cutting: a review and implications for high speed machining. *Int J Mach Tool Manu* 2006; 46(7–8): 782–800.
35. Suresh R, Basavarajappa S, Gaitonde VN, et al. State-of-the-art research in machinability of hardened steels. *Proc IMechE, Part B: J Engineering Manufacture*. Epub ahead of print 4 January 2013. DOI: 10.1177/095440541 2464589.

Appendix 1

Chip breakage was not observed on any simulations with low cutting speeds (Figures 14–19). Simulations with average cutting speeds and positive rake angle show one near breaking point on lowest feed rate (Figures 20–22). No chip breaking was observed in simulations with medium cutting speed and negative rake angle (Figures 23–25). Simulations with high cutting speed and positive rake angle show chip breakage and near breaking points in low and medium feed rates (Figures 26–28). Near breaking points were observed in simulations with high cutting speed, negative rake angle and low or medium feed rates (Figures 29–31).

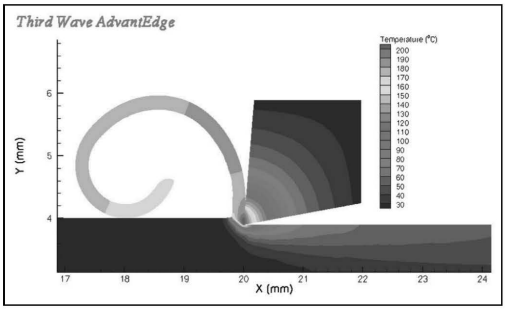

Figure 14. Cutting speed of 50 m/min, rake angle of 5° and feed of 0.1.

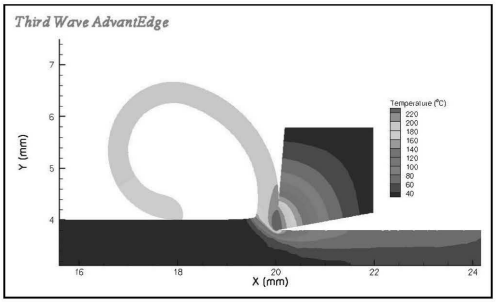

Figure 15. Cutting speed of 50 m/min, rake angle of 5° and feed of 0.2.

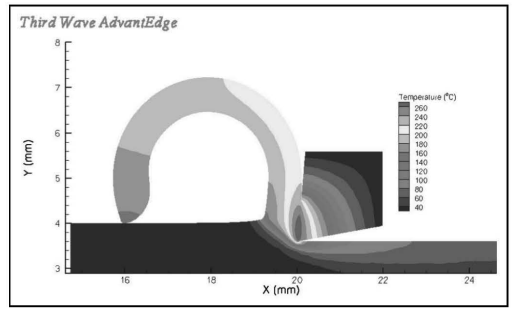

Figure 16. Cutting speed of 50 m/min, rake angle of 5° and feed of 0.4.

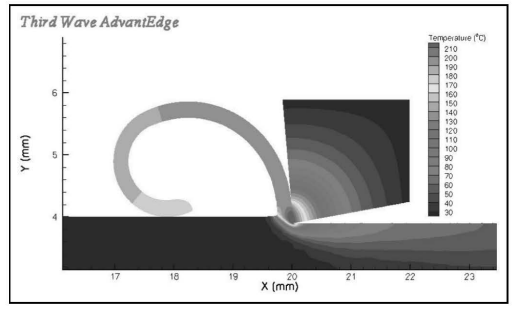

Figure 17. Cutting speed of 50 m/min, rake angle of −5° and feed of 0.1.

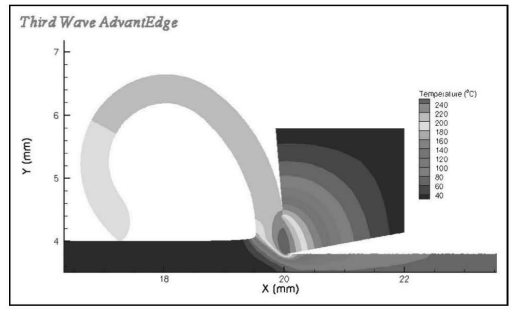

Figure 18. Cutting speed of 50 m/min, rake angle of −5° and feed of 0.2.

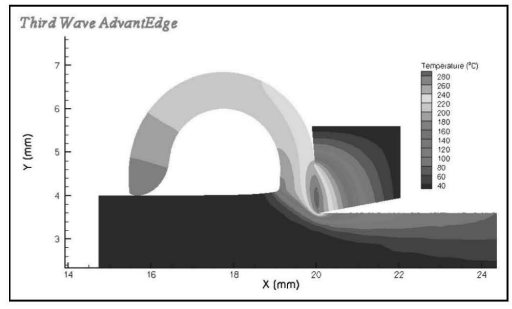

Figure 19. Cutting speed of 50 m/min, rake angle of −5° and feed of 0.4.

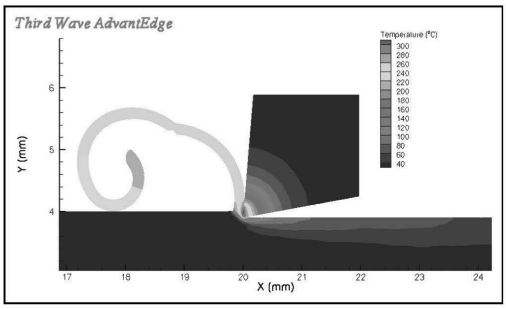

Figure 20. Cutting speed of 150 m/min, rake angle of 5°, feed of 0.1 and one near breaking point.

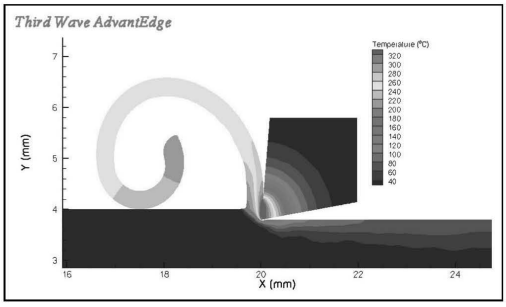

Figure 21. Cutting speed of 150 m/min, rake angle of 5° and feed of 0.2.

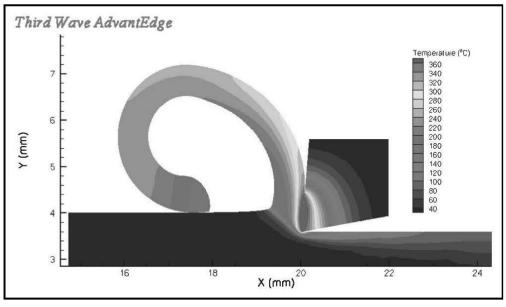

Figure 22. Cutting speed of 150 m/min, rake angle of 5° and feed of 0.4.

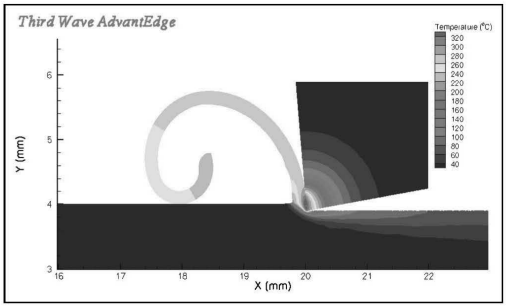

Figure 23. Cutting speed of 150 m/min, rake angle of −5° and feed of 0.1.

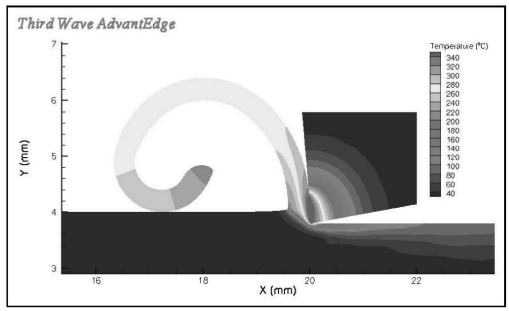

Figure 24. Cutting speed of 150 m/min, rake angle of −5° and feed of 0.2.

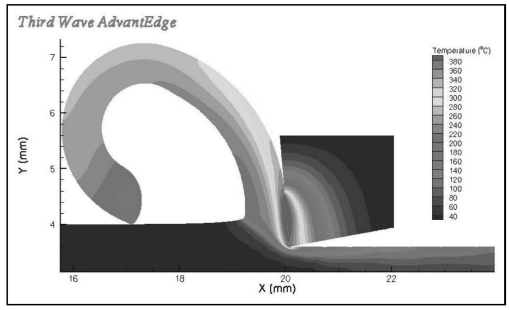

Figure 25. Cutting speed of 150 m/min, rake angle of −5° and feed of 0.4.

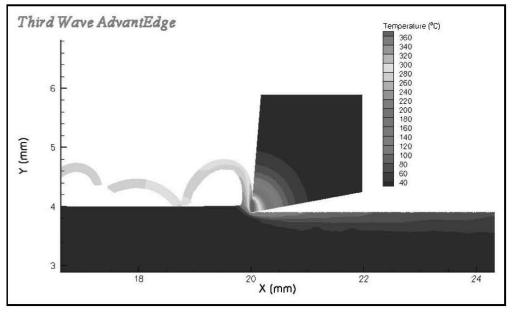

Figure 26. Cutting speed of 300 m/min, rake angle of 5°, feed of 0.1 and one breakage and one near breaking point.

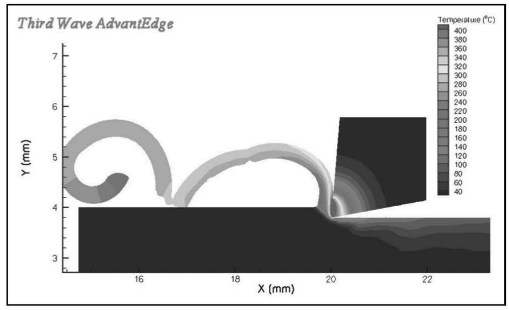

Figure 27. Cutting speed of 300 m/min, rake angle of 5°, feed of 0.2 and two near breaking points.

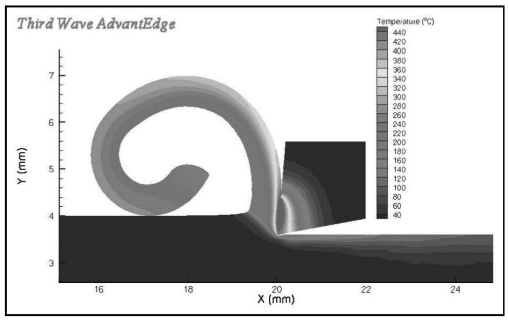

Figure 28. Cutting speed of 300 m/min, rake angle of 5° and feed of 0.4.

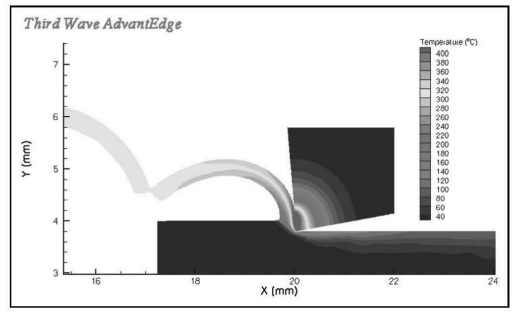

Figure 30. Cutting speed of 300 m/min, rake angle of −5°, feed of 0.2 and one near breaking point.

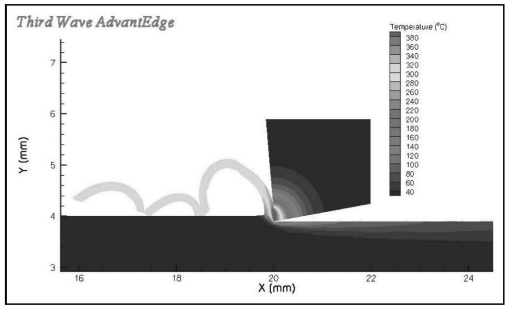

Figure 29. Cutting speed of 300 m/min, rake angle of −5°, feed of 0.1 and two near breaking points.

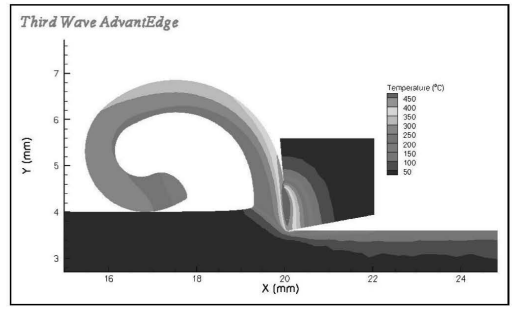

Figure 31. Cutting speed of 300 m/min, rake angle of −5° and feed of 0.4.

Original Article

Institution of MECHANICAL ENGINEERS
Journal of ENGINEERING MANUFACTURE

Proc IMechE Part B:
J Engineering Manufacture
1–10

DOI: 10.1177/0954405414560620
pib.sagepub.com
SAGE

Determination of material model parameters from orthogonal cutting experiments

Sampsa Vili Antero Laakso and Esko Niemi

Abstract

Flow stress models in finite element analysis of metal cutting require material parameters that are essential considering the accuracy of the simulations. This article presents a method to acquire material parameters from cutting experiments using the extended Oxley's shear zone theory. The novelty in this approach is to use measured chip geometry and temperature instead of determining them analytically to calculate strain and strain rate. These values are used to calculate the resultant cutting forces with the extended Oxley's model and Johnson–Cook flow stress model. Flow stress model parameters are optimized to fit the calculated forces to those measured from cutting experiments. The Johnson–Cook parameters acquired with this method perform better than those found in the literature.

Keywords

Flow stress, inverse analysis, cutting experiments, strain, strain rate, finite element method, AISI 1045

Date received: 13 May 2014; accepted: 27 October 2014

Introduction

Finite element analysis of metal cutting has been established as a research and development method in the field of machining research.[1] The accuracy of the simulations is dependent on the material model used.[2] In its simplest form, a model approximates the relationship between stress and strain, such as Hooke's law. The power law equation between stress and strain was used by Oxley[3] in his widely referred machining theory. More sophisticated material models include the influence of strain rate and temperature on the stress–strain relationship. One such model is the common Johnson–Cook model.[4] In addition, damage models add the effect of mechanical and thermal damage to the model which is required, for example, to simulate serrated chip.[5,6] By including elasticity to the simulations, residual stresses can be calculated.[7] Also, more specific behavior such as yield delay can be taken into account.[8]

One general outcome in the research articles is that the modeling of the stress–strain behavior itself is not the problem, but rather the determination of the material parameters for each model.[9] Determination of the material parameters for a model is difficult because testing conditions do not match the real cutting conditions. For example, during a compression test, the material is under a much slower strain rate and a lower temperature than during machining. The contact conditions in cutting are more or less unique, so by acquiring the material parameters by means of materials testing much of the relevant data are left out. To avoid the above-mentioned difficulties, few improvements in testing have been made. To gain flow stress at a high deformation rate, split Hopkinson's pressure bar (SHPB) testing is used.[10] Nevertheless, the strain rate and in some cases the temperature are too low compared to cutting conditions. Strain rate values as high as 20,000 s^{-1} can be achieved by SHPB testing, whereas cutting involves strain rates up to 10^6 s^{-1}. By using a preheated test specimen, SHPB testing can be done in temperatures as high as 900 °C which is high enough for most materials. The most common approach is to compile the material parameters from data gathered from materials testing and orthogonal cutting tests.[11] Apart from the cutting forces, different phenomena occurring during cutting are difficult to measure

Department of Engineering Design and Production, School of Engineering, Aalto University, Espoo, Finland

Corresponding author:
Sampsa Vili Antero Laakso, Department of Engineering Design and Production, School of Engineering, Aalto University, Puumiehenkuja 3, Espoo 02150, Finland.
Email: sampsa.laakso@aalto.fi

because of high speeds and loads. For that, determining the real stress strain relationship of a material based only on direct measurement is complicated. Even though it is difficult to measure flow stress or hardening effects from cutting tests, they are the most reliable source of acquiring material parameters. Therefore, inverse analysis with simulations or analytical models is often used. Inverse analysis with simulations means running the simulations and using a full-factorial analysis on each parameter or optimizing the results parameter by parameter deductively.[12,13] Inverse analysis with analytical model means calculating theoretical values of strain, strain rate and flow stress from measurable factors such as cutting forces, chip thickness and shear angle to obtain parameters for material models by fitting the model curve to the measured values.[14] The most used analytical model is the parallel sided shear zone model, often referred to as Oxley's model, which has been developed in parts by Piispanen,[15] Eugene Merchant[16] and Oxley,[3] among others.

Parallel sided shear zone theory

The orthogonal cutting model proposed by Oxley is based on a model where deformation of the material takes place in a parallel sided zone that follows the shear angle. The geometrical definition of the model is presented in Figure 1, and equations (1) (8) present the relevant model details.[3] Boothroyd and Knight[17] have developed a temperature prediction model presented in equations (9) (12). Lalwani et al.[18] proposed an extension that enables Oxley's model to be used with other than the Power law material model. The strain hardening exponent n and strain rate constant C_0 require modifications, which are presented in equations (13) and (14) for the Johnson Cook model.

Resultant force[19]

$$R = \sqrt{F_C^2 + F_T^2} = \frac{k_{AB} t_1 w}{\sin\phi \cos\theta} \tag{1}$$

Specific cutting force[3]

$$k_{AB} = \frac{1}{\sqrt{3}} \sigma_{yield} = \sigma_{flow}(\varepsilon, \dot{\varepsilon}, T) \tag{2}$$

Shear angle[16]

$$\phi = \tan^{-1} \frac{\cos\alpha}{\zeta - \sin\alpha} \tag{3}$$

Chip compression ratio (CCR)[20]

$$\zeta = \frac{t_2}{t_1} \tag{4}$$

Oxley's model[3]

$$\theta = \tan^{-1} \frac{\cos\alpha}{\zeta - \sin\alpha} + \tan^{-1} \frac{F_T}{F_C} \tag{5}$$

Shear strain[16]

$$\gamma_{AB} = \frac{1}{2\sin\phi \cos(\phi - \alpha)} \tag{6}$$

Equivalent strain[3]

$$\varepsilon = \frac{\gamma_{AB}}{\sqrt{3}} \tag{7}$$

Strain rates in tool chip interface and shear sone[3]

$$\begin{aligned} \dot{\varepsilon}_{int} &= \frac{U\cos\alpha}{\cos(\phi-\alpha)} \frac{1}{\Delta s_2 \sqrt{3}} = \frac{V_c}{\Delta s_2 \sqrt{3}} \\ \dot{\varepsilon}_{AB} &= C_0 \frac{V_S}{t\sqrt{3}} \end{aligned} \tag{8}$$

Shear zone temperature[17]

$$T = T_W + \Delta T_{SZ} \tag{9}$$

Temperature rise in shear zone[17]

$$\Delta T_{SZ} = \frac{1-\beta}{\rho S t_1 w} \frac{F_S \cos\alpha}{\cos(\phi - \alpha)} \tag{10}$$

Proportion of heat conducted to workpiece[17]

$$\beta = a_{\%} + b_{\%} \log(R_T \tan\phi) \tag{11}$$

Dimensionless thermal number[17]

$$\begin{aligned} R_T &= \frac{\rho S U t_1}{K} \\ R_T \tan\phi &\leqslant 10 \\ a_{\%} &= 0.5 \; b_{\%} = -0.35 \\ R_T \tan\phi &> 10 \\ a_{\%} &= 0.3 \; b_{\%} = -0.15 \end{aligned} \tag{12}$$

Mod. strain hardening exponent[18]

$$n_{eq} = \frac{d\sigma_{AB}}{d\varepsilon_{AB}} \left(\frac{\varepsilon_{AB}}{\sigma_{AB}} \right) = \frac{nB\varepsilon_{AB}^n}{\left(A + B\varepsilon_{AB}^n\right)} \tag{13}$$

Mod. strain rate constant[18]

$$C_0 = 1 + 2\left(\frac{\pi}{4} - \phi\right) - \frac{\tan\theta}{n_{eq}} \tag{14}$$

Different measures of strain and strain rate

In this article, three measures of strain are investigated, which are proposed by Oxley, Merchant and Astakhov. Strain proposed by Oxley is presented in equation (6). Merchant's strain is presented in equation (15) and Astakhov's and Shvets'[21] strain is presented in equation (16). All strains can be expressed in terms of shear angle and rake angle, or rake angle and CCR. One noteworthy observation is that Oxley's strain is exactly the same as Merchant's strain, but it is divided by $2\sqrt{3}$, and there is a geometrical explanation for this in equation (17). Oxley's strain is divided by 2 because it is assumed that half of the deformation has taken place when the material reaches the AB-line and $\sqrt{3}$ comes from von Mises' equivalent strain definition. Strains are plotted in Figure 2 with a rake angle range of ±20°. Oxley's and Astakhov's strains are closer to each other since they represent an equivalent strain in a major

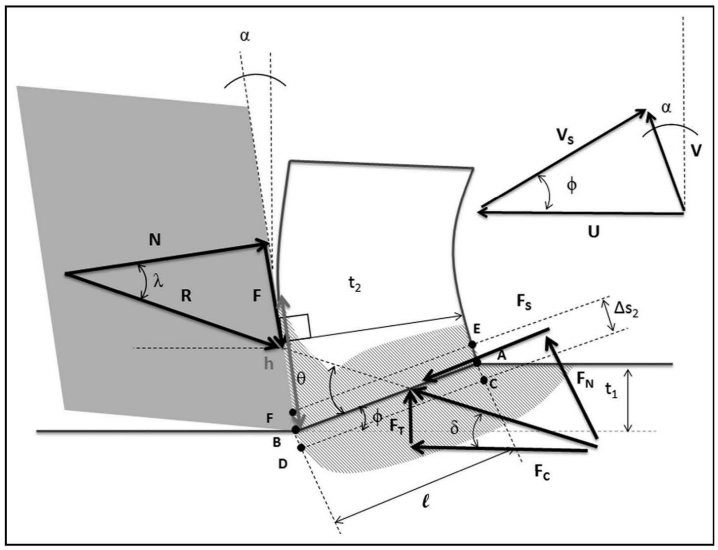

Figure 1. Parallel sided shear zone model.

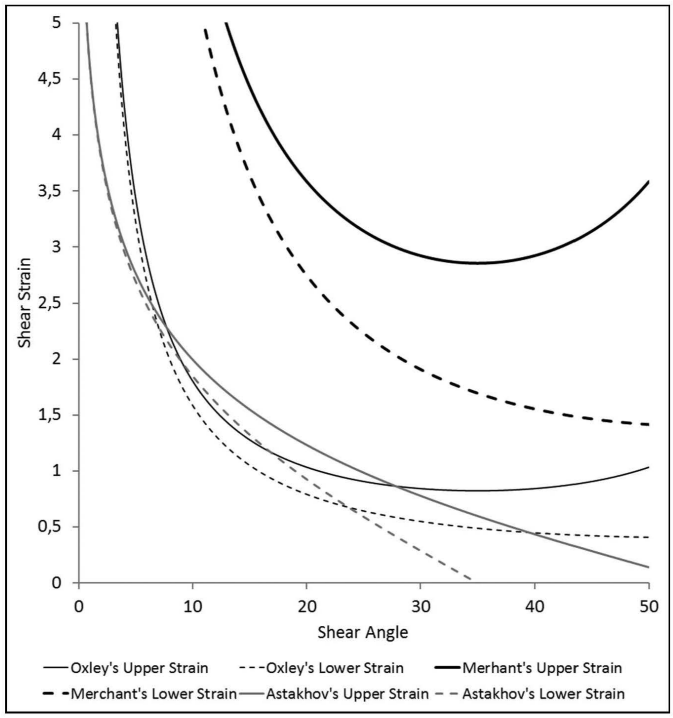

Figure 2. Different strains plotted against shear angle with rake angles of ±20°.

shear zone, whereas Merchant's strain is a presentation of the total strain in a chip formation zone. Astakhov and Shvets[21] argue that Merchant's presentation of strain is invalid because when the CCR is 1, there is no geometrical deformation, so the strain should be 0 at this point, which is not the case with Merchant's model. Figure 3 shows the strain plotted against CCR, which shows Astakhov's argument about a non-zero strain at a CCR value of 1. Merchant's definition of strain and strain rate is evaluated in Davim and Maranhão[22] using simulations. Finite element method (FEM) results support Merchant's model, but the article unfortunately

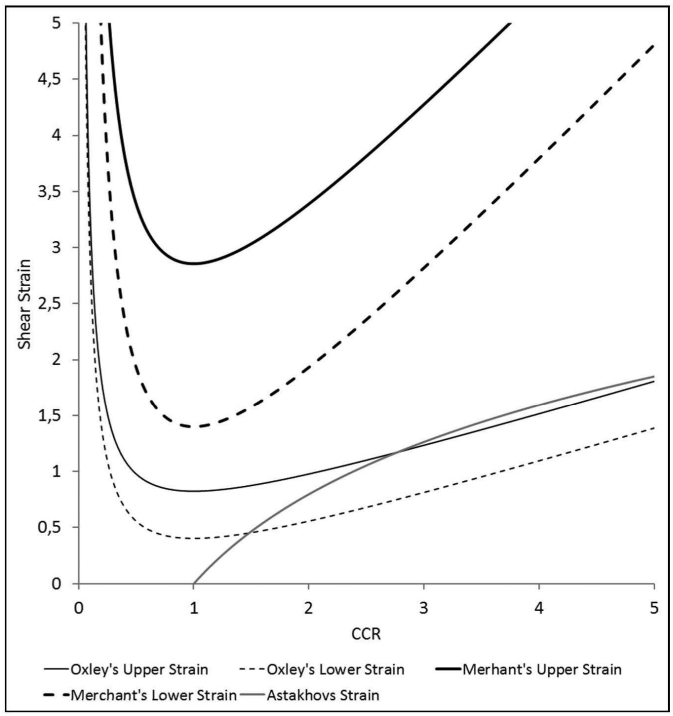

Figure 3. Different strains plotted against CCR with rake angles of ±20°.

does not provide simulated temperatures or cutting forces to evaluate the accuracy of the simulations. For extended Oxley's model to produce results that are aligned with the theory, the original Oxley's definition of strain should be used. Otherwise the flow stress is overestimated by a magnitude of 100%–200%.

Merchant's strain

$$\varepsilon = \cot(\phi) + \tan(\phi - \alpha) \tag{15}$$

Astakhov's strain

$$\varepsilon = 1.15 \ln \zeta \tag{16}$$

Geometrical explanation

$$\zeta = \frac{\cos \alpha}{\tan \phi} + \sin \alpha = \frac{\cos(\phi - \alpha)}{\sin \phi} \tag{17}$$

Flow stress models

Flow stress is normally presented as a function of strain, strain rate and temperature, although the form of the function varies. The Johnson–Cook model[4] (equation (18)) is formulated for materials under high strain rate and is one of the most used models in the field of metal cutting. The most common flow stress models used in cutting simulations are presented in Appendix 2, equations (19)–(24). Zerilli and Armstrong model[23] (equation (23)) is special since it has different equations for BCC and FCC materials. Another unusual model is Maekawa's model because of strain path dependency.[24]

Research objectives

In order to take advantage of cutting simulations in academia or industry, material modeling must be efficient time and cost vice. This research article investigates a robust method of acquiring material model parameters directly from cutting experiments. If this method performs as expected, the material parameter acquisition will be more efficient than with high-speed compression tests. The results show whether analytical models are viable option to be used in an inverse analysis routine and whether further development of the method is advisable. The results are evaluated in the framework of previous studies on the same material.

Challenges in experimental setup

Forces, chip thicknesses and cutting parameters are easy to obtain reliably from cutting experiments, but temperatures, actual strain and strain rate are difficult to measure. Approaches with thermal couple, thermal sensors and pyrometers or infrared (IR) imaging have been tried with a variety of results.[25–29] A thermal couple measures the largest temperature difference between a tool and a workpiece; thermal sensors and pyrometers can be set to measure the surface temperatures of

a newly machined layer or a tool. Thermal imaging can measure anything in theory, but practicalities such as imaging frame rate and different emissivity of surfaces cause challenges. Strain and strain rate can be measured using analytical models, quick stop experiments with metallography or digital image correlation during machining.[30] Analytical models are only accurate in an orthogonal cutting setup and only for some materials and cutting parameters. Quick stop experiments provide reliable results but are slow and expensive to conduct and the quick stop device or setup is never infinitely fast so the obtained sample does not fully represent the actual cutting condition. Digital image correlation is a promising method, but frame rate and optics resolution need to be improved to measure strain and strain rate in real cutting speeds (> 100 m/min).[30]

Experimental inverse analysis routine

In this article, an inverse analysis routine is formulated to acquire Johnson Cook parameters from cutting experiments. This approach is different from that presented by Sartkulvanich et al.[14] since in their OXCUT model inputs are cutting conditions and material properties but no experimentally determined strain, strain rate and temperature values. The novelty in this approach is to use experimental values for chip thickness and temperature to avoid error caused by the analytical model. Chip geometry and temperature are measured from cutting experiments. Chip thickness is measured and CCR is calculated with equation (4). Rake angle together with CCR give shear zone angle with equation (3). Next, the strain and strain rate are calculated from chip geometry using definitions from the parallel sided shear zone theory. Then, using these values of the strain, strain rate and temperature instead of those determined from the analytical model, the extended Oxley's model is used to calculate cutting forces. These cutting force values are compared to the experimental values of AISI 1045 that can be found in the literature. Using the obtained data set, a flow stress model (Johnson Cook) is calibrated by optimizing the parameters of the model to fit it to the obtained flow stress strain strain rate temperature data set. The results are compared to other Johnson Cook parameter sets found from the literature.

Materials and methods

The inverse analysis routine is based on extended Oxley's model with Johnson Cook flow stress model. Flowchart of the whole routine is presented in Figure 4. The resultant cutting force is calculated with equation (1). For this, flow stress and chip geometry are needed. Flow stress is calculated from the flow stress model, which needs strain, strain rate and temperature as input parameters. The strain and strain rate are calculated from the chip geometry with Oxley's model equations (7) and (8). Input parameters for the model are cutting speed, feed, width and rake angle. Also, experimentally obtained values of chip thickness, shear zone angle and temperature are used as input parameters. The predicted resultant forces are evaluated against experimentally obtained values, and flow stress model parameters are adjusted for a better fit until the optimal solution. The optimization routine minimized the error of the normalized resultant cutting forces with the least squares method. Experiment data and parameters are presented in Table 1. The resultant force is calculated as the root of the sum of squares of each force component. Experimental data for the cutting of AISI 1045 are acquired from literature sources: A1 A8 from Ivester et al. and B1 B4 from Iqbal et al.[31 34] and Ivester et al. used orthogonal turning for their tests. The tool used was a Kennametal K68, an uncoated general-purpose tungsten carbide insert with rake angles of $+5°$ and $-7°$. Cutting forces were measured with a Kistler 9257B 3-component piezoelectric dynamometer and 9403 mount. Cutting temperatures were measured with an intrinsic thermocouple and selected experiments with IR-microscopy. The experiments were conducted twice for each cutting parameter set in four different laboratories to ensure repeatability. Resultant forces from Ivester et al. are average of all the experiments except clearly anomalous results were discarded from the average. Iqbal et al. conducted similar experiments with a lathe and a Kistler 9263A dynamometer using uncoated Sandvik TCMW 16T304 grade 5015 inserts. The article does not report how many repetitions were conducted so it is assumed that no repetitions have been done. Experimental data by Ivester have been used as well in Lalwani et al.[18] and Ding and Shin,[35] but the temperature values used in these articles are for some reason twice as high as those in Ivester's articles. The original values presented by Ivester are used in this article. This decision is encouraged by the temperature results in Davies et al.[26] and their thermal imaging experiments, where the results are similar to those in Ivester et al. Temperatures for experiments B1 B4 are determined from the simulations of Ding and Shin and considering Ivester's results because Iqbal et al. did not present any temperature measurements for their experiments.

Johnson–Cook model parameters for AISI 1045

The Johnson Cook model includes strain hardening parameters A, B, n and rate hardening parameter C and thermal softening parameter m. The Johnson Cook parameter sets acquired from inverse analysis and the literature are presented in Table 2. The errors in Table 2 are calculated as average, minimum and maximum of the percentile errors for each individual cutting condition between average resultant forces acquired from experiments and analytical method. The experimental values used are the average of each parameter's set. Sets 1 3 are from inverse analysis. Set 1 was optimized by varying only C and m, set 2 was optimized by

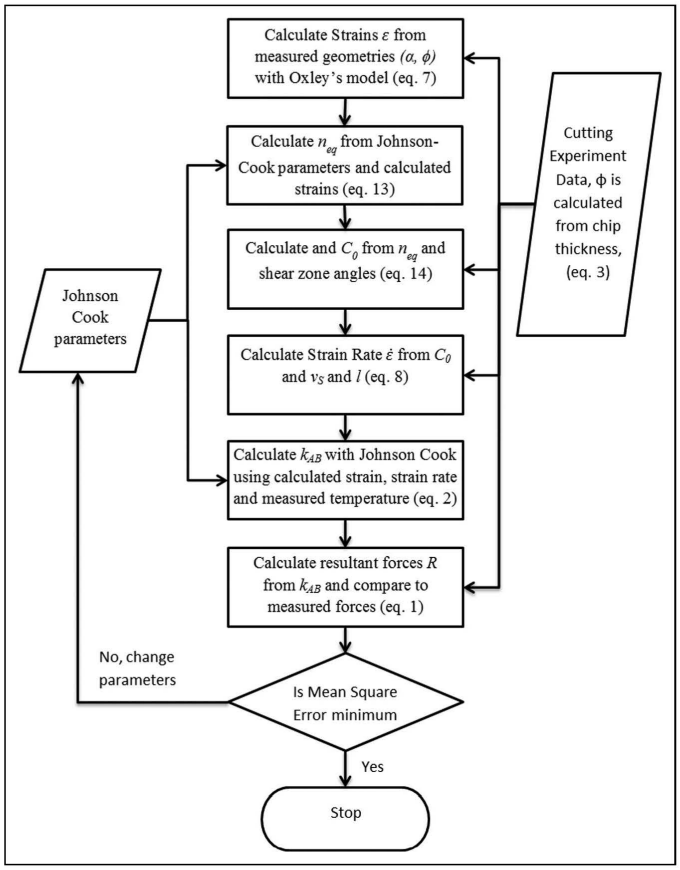

Figure 4. Inverse analysis routine flowchart.

Table 1. Experimental data and parameters.

No.	v (m/min)	f (mm/r)	α	w (mm)	R_{exp} (N)	T_{AB} (°C)
A1	200	0.15	5	1.6	2900	561
A2	300	0.15	5	1.6	2564	618
A3	200	0.15	−7	1.6	3285	544
A4	300	0.15	−7	1.6	3234	653
A5	200	0.3	5	1.6	2222	600
A6	300	0.3	5	1.6	1954	653
A7	200	0.3	−7	1.6	2590	586
A8	300	0.3	−7	1.6	2531	535
B1	198	0.1	0	2.5	2812	564
B2	399	0.1	0	2.5	2538	613
B3	628	0.1	0	2.5	2314	620
B4	879	0.1	0	2.5	2339	628

varying all parameters with the reference strain rate at 7500 s^{-1} and set 3 was similarly optimized with the reference strain rate at 0.001 s^{-1}. Parameter A is bounded between 290 and 660 MPa because A represents yield stress in the model. Other variables are bounded between [0; 10] except B, which is between [0; 1000]. Set 4 is from Lalwani et al.[18] and set 5 is from Klocke et al.[12] Lalwani et al. used the Johnson–Cook parameters found in Jaspers and Dautzenberg[36] and the experimental results of Ivester. Jaspers et al. used SHPB experiments to determine their values. Lalwani et al. did not perform any inverse analysis in their work. Buchkremer et al. used the Johnson–Cook parameters A, B and n from Abouridouane et al.[37] and for C and m they performed a full-factorial analysis, basically running simulations of all combinations of the factors. The cutting

Table 2. Johnson–Cook parameters from different sources and accompanying errors.

No.	1	2	3	4	5
A	550	**391**	**290**	553	546
B	600	**217**	**283**	601	487
n	0.234	**0.340**	**0.249**	0.234	0.250
C	**0.025**	**0.003**	**0.004**	0.013	0.027
m	**0.741**	**3.283**	**3.365**	1.000	0.631
T_{melt}	1460	1460	1460	1460	1460
T_{ref}	20	20	20	20	20
$(d\varepsilon/dt)_{ref}$	7500	7500	0.001	7500	0.001
Average (%)	5.3	5.0	5.0	20.4	13.4
Maximum (%)	12.6	9.9	9.9	34.9	28.4
Minimum (%)	0.0	1.1	1.1	7.5	0.8
ΣE^2	0.06	0.04	0.04	0.57	0.29

Values in bold: values that have been used as free variables in optimization routine.

experiments were done at RWTH Aachen University with a Broaching Machine, a Kistler dynamometer and a two-color pyrometer. The cutting experiment data set is with feed 0.1–0.4 and 50 and 100 m/min for cutting speed.

Results and discussion

Using the proposed method, an average error of less than 6% is achieved, whereas parameters obtained from the literature produce an average error of 20% and 13%. All parameters are relatively of the same magnitude with the greatest variation in the values of C and m. Figure 5 presents the normalized resultant forces from experiments and predicted values using all four different flow stress parameter sets. Sets 1–3 follow experimental results well. Sets 2 and 3 estimate the effect of rate sensitivity lower and thermal softening higher than sets 1, 4 and 5. A noteworthy point is that the data are from multiple sources and from a wide cutting parameter scope (e.g. a cutting speed from 200 to 870 m/min), but despite that the model follows the data well. One point to consider is the uniqueness of the solutions since parameter sets 1–3 produce results that are very close to each other, but the parameters are clearly different. It could be that cutting has too fuzzy mechanistic properties for cutting experiments to clearly differentiate hardening mechanisms from each other. For example, an increase in cutting speed leads

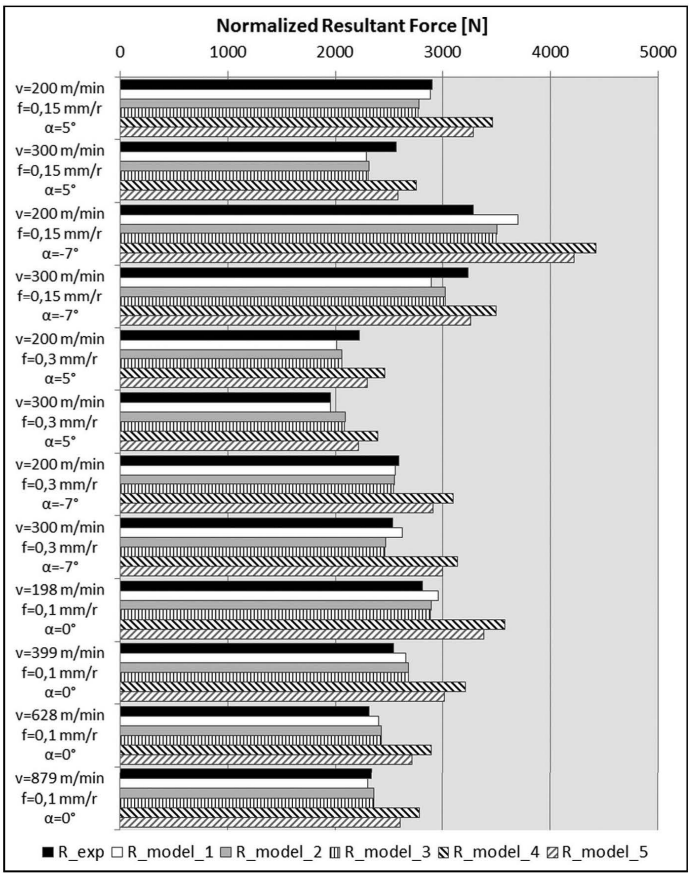

Figure 5. Comparison of experimental resultant forces with modeled resultant forces.

to an increase in strain rate and temperature, and the cause of the proportional increase in the resultant force in this case cannot be determined unambiguously. This was also implied by a graph analysis of metal cutting parameters in Laakso et al.[38] A linear relationship between strain, strain rate or temperature and machining parameters cannot be formed. Therefore, the role of compression experiments or SHPB experiments could be irreplaceable, because in these experiments, one variable can be changed while other variables are controlled.

Conclusion

In this article, an inverse analysis of flow stress model parameters was conducted to optimize the model performance. The following important points were observed:

1. The method produces better performing flow stress model parameter values for an analytical model than those found in the literature

$$\sigma_{flow} = \left(550 + 600\varepsilon^{0.234}\right)\left[1 + \frac{1}{40}\ln\left(\frac{\dot{\varepsilon}}{7500}\right)\right]\left[1 - \left(\frac{T-20}{1460-20}\right)^{0.741}\right]$$

2. A clear relationship between flow stress model variables and cutting parameters is difficult to form; therefore, a wide range of cutting parameters should be used.
3. There are many local optimal solutions for flow stress model parameters. Therefore, it is advisable to use compression test values for setting the reference frame for the model parameters.
4. The method is promising and further study is required to identify more delicate material behavior related to thermal effects.

Declaration of conflicting interests

The authors declare that there is no conflict of interest.

Funding

This research received no specific grant from any funding agency in the public, commercial, or not-for-profit sectors.

References

1. Marusich TD and Ortiz M. Modeling and simulation of high speed machining. *Int J Numer Meth Eng* 1995; 38(21): 3675–3694.
2. Laakso SVA. *Finite element modeling of cutting—applications and usability*. Master's Thesis, Helsinki University of Technology, Helsinki, 2009 (in Finnish).
3. Oxley PLB. *The mechanics of machining: an analytical approach to assessing machinability* (Ellis Horwood series in mechanical engineering). West Sussex, UK: Market Cross House, 1989.
4. Johnson GR and Cook WH. A constitutive model and data for metals subjected to large strains, high strain rates and high temperatures. In: *Proceedings of the 7th international symposium on ballistics*, The Hague, 19–21 April 1983, vol. 21, pp.541–547. Hague, Netherlands: International Symposium on Ballistics, American Defense Preparedness Association, and Koninklijk Instituut van Ingenieurs.
5. Pantalé O, Bacaria JL, Dalverny O, et al. 2D and 3D numerical models of metal cutting with damage effects. *Comput Method Appl M* 2004; 193(39): 4383–4399.
6. Guo YB and Yen DW. A FEM study on mechanisms of discontinuous chip formation in hard machining. *J Mater Process Tech* 2004; 155–156: 1350–1356.
7. Marusich TD and Askari E. Modeling residual stress and workpiece quality in machined surfaces. In: *Proceedings of the fourth CIRP international workshop modeling of machining operations, Delft Technological University, Delft*, 17–18 August 2001, pp.105–109.
8. Childs THC. Modelling orthogonal machining of carbon steels. Part I: strain hardening and yield delay effects. *Int J Mech Sci* 2009; 51(5): 402–411.
9. Sartkulvanich P. *Determination of material properties for use in FEM simulations of machining and roller burnishing*. PhD Dissertation, Ohio State University, Columbus, OH, 2007.
10. Apostol M, Vuoristo T and Kuokkala VT. High temperature high strain rate testing with a compressive SHPB. *J Phys IV* 2003; 110: 459–464.
11. Laakso SVA, Hokka M, Niemi E, et al. Investigation of the effect of different cutting parameters on chip formation of low-lead brass with experiments and simulations. *Proc IMechE, Part B: J Engineering Manufacture* 2013; 227(11): 1620–1634.
12. Klocke F, Lung D and Buchkremer S. Inverse identification of the constitutive equation of Inconel 718 and AISI 1045 from FE machining simulations. *Proced CIRP* 2013; 8: 212–217.
13. Sartkulvanich P, Lopez AM, Rodriguez C, et al. Inverse analysis methodology to determine flow stress data for finite element modeling of machining. In: *11th CIRP conference on modeling of machining operation*, Gaithersburg, MD, 16–18 September 2008, http://nsm.eng.ohio-state.edu/CIRPNIST_paper_inverse_machining_2008.pdf (accessed 15 April 2014).
14. Sartkulvanich P, Koppka F and Altan T. Determination of flow stress for metal cutting simulation—a progress report. *J Mater Process Tech* 2004; 146(1): 61–71.
15. Piispanen V. Theory of formation of metal chips. *J Appl Phys* 1948; 19: 876–881, http://dx.doi.org/10.1063/1.1697893
16. Eugene Merchant M. Mechanics of the metal cutting process. I. Orthogonal cutting and a type 2 chip. *J Appl Phys* 1945; 16: 267–275, http://dx.doi.org/10.1063/1.1707586
17. Boothroyd G and Knight WA. *Fundamentals of machining and machine tools*. 2nd ed. New York: Marcel Dekker, Inc., 1989.
18. Lalwani DI, Mehta NK and Jain PK. Extension of Oxley's predictive machining theory for Johnson and

Cook flow stress model. *J Mater Process Tech* 2009; 209(12–13): 5305–5312.
19. Taylor FW. *On the art of cutting metals*. New York: Transactions of ASME, 1907.
20. Zorev NN. *Metal cutting mechanics*. Oxford: Pergamon Press, 1966.
21. Astakhov VP and Shvets S. The assessment of plastic deformation in metal cutting. *J Mater Process Tech* 2004; 146(2): 193–202.
22. Davim JP and Maranhão C. A study of plastic strain and plastic strain rate in machining of steel AISI 1045 using FEM analysis. *Mater Design* 2009; 30(1): 160–165.
23. Zerilli FJ and Armstrong RW. Dislocation mechanics based constitutive relations for materials dynamics calculations. *J Appl Phys* 1987; 61(6): 1816–1825.
24. Maekawa K, Shirakashi T and Usui E. Flow stress of low carbon steel at high temperature and strain rate (part 2)—flow stress under variable temperature and variable strain rate. *B Jpn Soc Prec Eng* 1983; 17(3): 167–172.
25. Abhang LB and Hameedullah M. Chip-tool interface temperature prediction model for turning process. *Int J Eng Sci Tech* 2010; 2(4): 382–393.
26. Davies MA, Cooke AL and Larsen ER. High bandwidth thermal microscopy of machining AISI 1045 steel. *CIRP Ann: Manuf Techn* 2005; 54(1): 63–66.
27. Heisel U, Storchak M, Eberhard P, et al. Experimental studies for verification of thermal effects in cutting. *Prod Engineer* 2011; 5(5): 507–515.
28. Longbottom JM and Lanham JD. Cutting temperature measurement while machining—a review. *Aircr Eng Aerosp Tec* 2005; 77(2): 122–130.
29. Artozoul J, Lescalier C, Bomont O, et al. Extended infrared thermography applied to orthogonal cutting: mechanical and thermal aspects. *Appl Therm Eng* 2014; 64: 441–452.
30. Mahadevan D. *Experimental determination of velocity and strain rate fields in metal cutting of OFHC copper*. Master's Thesis, Wichita State University, 2007, http://soar.wichita.edu/handle/10057/1522 (accessed 15 April 2014).
31. Ivester RW, Kennedy M, Davies M, et al. Assessment of machining models: progress report. *Mach Sci Technol* 2000; 4(3): 511–538.
32. Ivester RW and Kennedy M. Comparison of machining simulations for 1045 steel to experimental measurements. SME paper TPO4PUB336, 2004, pp.1–15.
33. Iqbal SA, Mativenga PT and Sheikh MA. Characterization of machining of AISI 1045 steel over a wide range of cutting speeds. Part 1: investigation of contact phenomena. *Proc IMechE, Part B: J Engineering Manufacture* 2007; 221(5): 909–916.
34. Iqbal SA, Mativenga PT and Sheikh MA. Characterization of machining of AISI 1045 steel over a wide range of cutting speeds. Part 2: evaluation of flow stress models and interface friction distribution schemes. *Proc IMechE, Part B: J Engineering Manufacture* 2007; 221(5): 917–926.
35. Ding H and Shin YC. A metallo-thermomechanically coupled analysis of orthogonal cutting of AISI 1045 steel. *J Manuf Sci E: T ASME* 2012; 134(5): 051014.
36. Jaspers SPFC and Dautzenberg JH. Material behaviour in conditions similar to metal cutting: flow stress in the primary shear zone. *J Mater Process Tech* 2002; 122(2–3): 322–330.
37. Abouridouane M, Klocke F, Lung D, et al. A new 3D multiphase FE model for micro cutting ferritic–pearlitic carbon steels. *CIRP Ann: Manuf Techn* 2012; 61(1): 71–74.
38. Laakso SVA, Peltokorpi J, Ratava J, et al. Graph-based analysis of metal cutting parameters. In: Azevedo A (ed.) *Advances in sustainable and competitive manufacturing systems* (Lecture Notes in Mechanical Engineering). Berlin: Springer, 2013, pp.627–636.

Appendix 1

Notation

$a_{\%}$	Boothroyd's thermal model parameter 1
A	J-C yield equivalent
$b_{\%}$	Boothroyd's thermal model parameter 2
B	J-C strain hardening multiplier
C_0	strain rate constant
F_C	cutting force
F_T	tangential force
k_{AB}	specific cutting force
K	thermal conductivity
n	J-C strain hardening exponent
n_{eq}	strain hardening exponent
R	resultant force
R_T	thermal number
S	specific heat
t_1	uncut chip thickness
t_2	chip thickness
T	temperature
T_{AB}	temperature in shear zone
T_W	workpiece temperature
U	cutting speed
V_s	cutting speed in shear direction
w	width of cut
α	rake angle
β	heat partition coefficient
γ_{AB}	shear strain in shear zone
Δs_2	shear zone thickness
ΔT_{SZ}	increase in temperature in shear zone
ε	strain
$\dot{\varepsilon}$	strain rate
$\dot{\varepsilon}_{AB}$	strain rate in shear zone
$\dot{\varepsilon}_{int}$	tool chip interface strain rate
θ	angle between resultant force and shear zone
ρ	density
σ_{AB}	stress in shear zone
σ_{flow}	flow stress
σ_{yield}	yield stress
ϕ	shear zone angle

Appendix 2

Flow stress models

Johnson Cook[4]

$$\sigma = (A + B\varepsilon^n)\left[1 + C\ln\left(\frac{\dot{\varepsilon}}{\dot{\varepsilon}_{ref}}\right)\right]\left[1 - \left(\frac{T - T_{ref}}{T_{melt} - T_{ref}}\right)^m\right] \quad (18)$$

Power law[3]

$$\sigma = C\dot{\varepsilon}^{n}\dot{\varepsilon}^{m} \tag{19}$$

Macgregor/Oxley[3]

$$\begin{aligned} \sigma &= C\dot{\varepsilon}^{n(T_{mod})}T_{mod} \\ T_{mod} &= T\left(1-\nu\ln\frac{\dot{\varepsilon}}{\dot{\varepsilon}_{ref}}\right) \end{aligned} \tag{20}$$

Extended power law (Marusich and Askari[7])

$$\sigma = \sigma_{yield}\, g(\varepsilon)\Gamma(\dot{\varepsilon})\Theta(T)$$

$$g(\varepsilon) = \left(1+\frac{\varepsilon}{\varepsilon_{ref}}\right)^{\frac{1}{n}}$$

$$\Gamma(\dot{\varepsilon}) = \begin{cases} \left(1+\frac{\dot{\varepsilon}}{\dot{\varepsilon}_{ref}}\right)^{\frac{1}{m_1}} & \text{when} \quad \dot{\varepsilon}\leqslant\dot{\varepsilon}_t \\ \left(1+\frac{\dot{\varepsilon}_t}{\dot{\varepsilon}_{ref}}\right)^{\frac{1}{m_1}}\left(1+\frac{\dot{\varepsilon}_t}{\dot{\varepsilon}_{ref}}\right)^{\frac{1}{m_1}-\frac{1}{m_2}} & \text{when} \quad \dot{\varepsilon}>\dot{\varepsilon}_t \end{cases}$$

$$\Theta(T) = \begin{cases} \sum_{i=0}^{k} c_i T^i & \text{when} \quad T < T_{cut} \\ \left(\sum_{i=0}^{k} c_i T_{cut}^i\right)\left[1-\frac{T-T_{cut}}{T_{melt}-T_{cut}}\right] & \text{when} \quad T\geqslant T_{cut} \end{cases} \tag{21}$$

Childs yield delay[8]

$$\sigma = \sigma_u, \quad \text{when} \quad \varepsilon\leqslant\varepsilon_u \tag{22}$$

Zerilli and Armstrong[23]

$$\begin{aligned} &\sigma = C_0 + C_1\, exp\left(-C_3T + C_4T\ln\dot{\varepsilon}\right) + C_5\varepsilon^n \\ &\quad \text{for BCC materials} \\ &\sigma = C_0 + C_2\varepsilon^{0.5}\, exp\left(-C_3T + C_4T\ln\dot{\varepsilon}\right) \\ &\quad \text{for FCC materials} \end{aligned} \tag{23}$$

Mackawa[14]

$$\sigma = A\left(\frac{\dot{\varepsilon}}{1000}\right)^{M} e^{aT}\left(\frac{\dot{\varepsilon}}{1000}\right)^{n}\left[\int_{\text{strain path}}\left(e^{\frac{-aT}{K}}\right)\left(\frac{\dot{\varepsilon}}{1000}\right)^{\frac{m}{K}} d\varepsilon\right]^{N} \tag{24}$$

Using FEM Simulations of Cutting for Evaluating the Performance of Different Johnson Cook Parameter Sets Acquired with Inverse Methods

Sampsa VA Laakso[1*], Esko Niemi[1]

[1]Department of Engineering Design and Production
Aalto University School of Engineering
Espoo, Southern Finland, 02150, Finland

ABSTRACT

Material model parameters are the primary source of error in the finite element analysis (FEM) of cutting processes. Expensive and time consuming material testing is required in order to describe the material's behavior in high temperature and high strain rate conditions during cutting. An alternative approach has been suggested in research papers; inverse analysis using cutting experiments together with FE analysis or analytical models. The latest approach is to combine an analytical model together with a material model capable of describing flow stress in terms of strain, strain rate and temperature, and using cutting experiments to acquire input parameters for inverse analysis, from which the material model parameters can be solved. In this paper, performance evaluation is done for five different sets of Johnson Cook parameters for AISI 1045, acquired with materials testing, inverse analysis with FEM, and the proposed combined inverse analysis with an analytical model and cutting experiments. The performance is evaluated by running simulations with a wide range of cutting parameters and comparing the simulated results of cutting forces and temperature to known experimental results found in literature. It was found that the proposed inverse method produces better performing model parameters than those found in literature.

1. INTRODUCTION

In order to use the FEM modeling of cutting in industrial applications, more robust material modeling using real cutting data is required instead of expensive materials testing data. Different approaches using inverse modeling have been suggested by Sartkulvanich et al. [1, 2, 3], Klocke et al. [4], and Laakso & Niemi [5]. Each of these methods adjusts the model parameters to fit the model to the cutting data acquired from cutting experiments. The major differences are that Sartkulvanich uses analytical models where Klocke uses simulations in iterative trials to fit the model to the data. Laakso's approach uses an analytical model as well, but instead of analytic or simulated solutions of plastic strain, strain rate and temperature, real cutting data is used as an input to the model.

These approaches have been evaluated by Laakso & Niemi [5], by using five different sets of Johnson Cook material model parameters together with a modified Oxley's chip formation model, presented in [6]. The modified Oxley's model can be used with any material model instead of the power function of yield stress (as in the original Oxley's model). The results produced using the parameters from Laakso & Niemi, Klocke et al. and Lalwani et al. were compared to the real cutting experiment data of AISI 1045 by Ivester et al. [7, 8] and Iqbal et al. [9]. The method proposed by Laakso & Niemi produced data that had, on average, a 5 % error in resultant forces, where the same results with parameters by Klocke [4] produced a 13 % error, and with parameters by Lalwani et al. [6] and Jaspers & Dautzenberg [10] they produced a 20 % error. In this paper, the same model parameters as in Laakso & Niemi [5] are used with FEM simulations to evaluate if the performance with a modified Oxley's model correlates with the performance in simulations.

2. MATERIALS AND METHODS

Third Wave Systems' AdvantEdge (*http://www.thirdwavesys.com/*) is used to simulate the orthogonal cutting of AISI 1045 with 12 different cutting conditions and five different material parameter sets. The software was first presented in a paper by Marusich and Ortiz [11]. The software is based on a dynamic explicit Lagrangian finite

* Sampsa VA Laakso: Tel.: +358(0)407055039; E-mail: sampsa.laakso@aalto.fi

element model, which employs adaptive remeshing to avoid element distortions. The model is based on equations of motion and a thermo-mechanically coupled material model. In this paper, a Johnson Cook material model is used (equation 1) [12]:

$$\sigma = (A + B\varepsilon^n)\left[1 + C\ln\left(\frac{\dot{\varepsilon}}{\dot{\varepsilon}_{ref}}\right)\right]\left[1 - \left(\frac{T - T_{ref}}{T_{melt} - T_{ref}}\right)^m\right]. \quad (1)$$

Where A = Yield Equivalent, B = Strain Hardening Multiplier, n = Strain Hardening Exponent, m = Thermal Softening Exponent, ε = Strain, Strain $\dot{\varepsilon}$, = Rate T = Temperature, T_{ref} = Reference Temperature, T_{melt} = Melting Temperature.

The cutting conditions are presented in

Table 1. A wide range of cutting conditions is used to ensure that the model is accurate beyond local cutting conditions. Also, as cutting is a complex physical problem, interaction of different cutting parameters makes measuring the effect of individual parameters difficult [13]. The cutting conditions are the same as those used by Ivester et al. (*A1–A8*) and Iqbal et al. (*B1–B4*) in their cutting experiments [7, 8, 9]. No cutting fluid was used in the simulations or in the cutting experiments by Ivester et al. or Iqbal. The friction was set to a standard 0.5 in the simulations and tool cutting edge sharpness was set to 20 µm. The length of cut was set to 5 mm to have steady state chip. 40 000 nodes were used in the simulations.

Table 1: The Cutting Conditions Used in Simulations: Cutting Speed, Feed, Rake Angle, Width of Cut, Measured Resultant Cutting Force, and Temperature in Chip Formation Zone

Nr.	v (m/min)	f (mm/r)	α	w (mm)	R_{exp} (N)	T_{AB} (C°)
A1	200	0,15	5	1,6	2900	561
A2	300	0,15	5	1,6	2564	618
A3	200	0,15	-7	1,6	3285	544
A4	300	0,15	-7	1,6	3234	653
A5	200	0,3	5	1,6	2222	600
A6	300	0,3	5	1,6	1954	653
A7	200	0,3	-7	1,6	2590	586
A8	300	0,3	-7	1,6	2531	535
B1	198	0,1	0	2,5	2812	564
B2	399	0,1	0	2,5	2538	613
B3	628	0,1	0	2,5	2314	620
B4	879	0,1	0	2,5	2339	628

The material parameters used in the simulations are presented in Table 2. Sets JC1–JC3 are from the inverse analysis presented by Laakso & Niemi [5]. Set JC1 was fitted to cutting data by varying C and m; set JC2 by varying all parameters at 7500 s-1 reference strain rate; and set JC3 was similarly fitted with the reference strain rate at 0,001 s-1. Parameter A is bound between 290–660 MPa in the fitting since A represents yield stress in the model. Other variables are bound between 0 and 10 except B, which is bound between 0 and 1000. Set JC4 is from Lalwani et al. [6] and set JC5 is from Klocke et al. [4]. Lalwani et al. [6] used the Johnson Cook parameters found in Jaspers & Dautzenberg [10] and the experimental results of Ivester et al. [7]. The high variation between the model parameters, especially regarding JC2 and JC3, can be explained by the mechanistic nature of Oxley's model. There can be many local optimums and some of them can be unrealistic. Therefore, as suggested by Laakso & Niemi [5], the model parameters that have a clear link to actual material behavior (like yield stress or a strain hardening exponent) should be kept constant and preferably be acquired from material tests. Even though the method can be used with any material model besides the Johnson Cook model, the cutting experiments might not give distinct enough differences in temperatures or strain rates to identify all material behavior – like coupled rate hardening and thermal softening identified in [14,15] – to fit more complex material models to the data.

Table 2: Material Model Parameter Sets

Parameter	JC1	JC2	JC3	JC4	JC5
A	550	391	290	553	546
B	600	217	283	601	487
n	0,234	0,340	0,249	0,234	0,250
C	0,025	0,003	0,004	0,013	0,027
m	0,741	3,283	3,365	1,000	0,631
T_{melt}	1460	1460	1460	1460	1460
T_{ref}	20	20	20	20	20
$(d\varepsilon/dt)_{ref}$	7500	7500	0,001	7500	0,001

3. RESULTS AND DISCUSSION

The simulation results are presented in Figure 1. The simulation results, cutting forces, tangential forces and temperatures are compared to the cutting experiments (the black bars). The resultant forces calculated from the cutting forces and tangential forces are also included in the comparison. More detailed simulation results are presented in Appendix 1. The errors are calculated for each test condition and the material parameter set and the average, maximum and minimum errors are presented in Table 3.

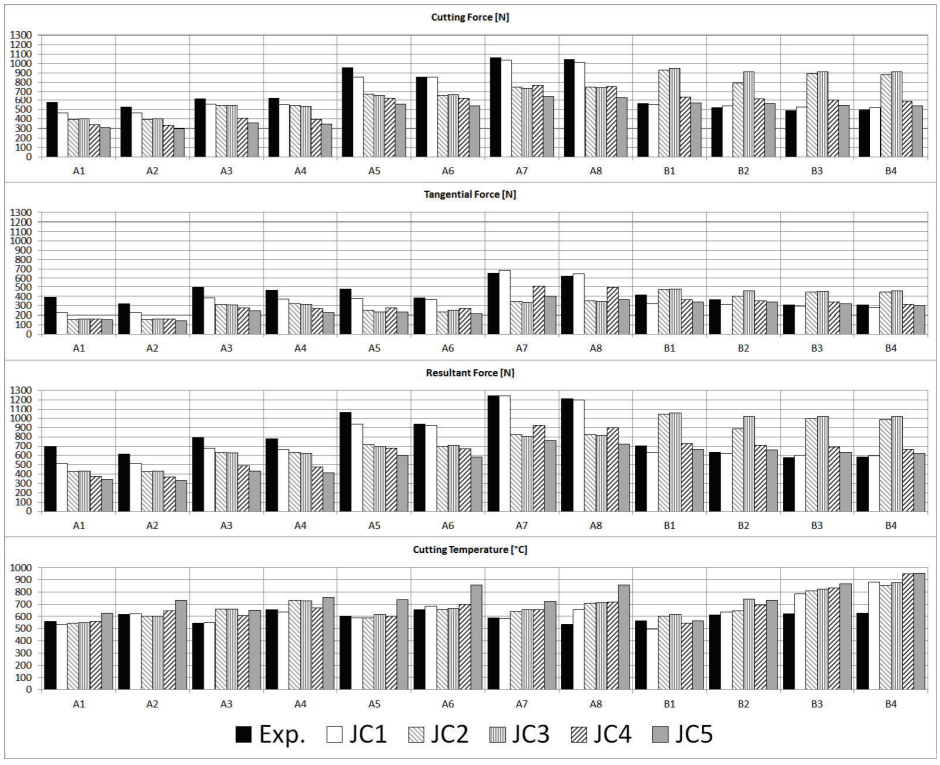

Figure 1: A Comparison of the Cutting Forces and Temperatures of the Simulations and Cutting Experiments

Table 3. Error Comparison

	JC1			JC2			JC3			JC4			JC5		
	Avg.	Max.	Min.	Avg.	Max.	Min.	Avg.	Max.	Min.	Avg.	Max.	Min.	Avg.	Max.	Min.
$\mathbf{F_C}$	7 %	20 %	0 %	39 %	82 %	11 %	42 %	86 %	11 %	28 %	41 %	12 %	30 %	47 %	1 %
$\mathbf{F_T}$	17 %	42 %	4 %	39 %	60 %	12 %	41 %	59 %	14 %	28 %	59 %	2 %	35 %	61 %	2 %
R	9 %	26 %	0 %	39 %	72 %	19 %	41 %	76 %	20 %	27 %	46 %	4 %	31 %	51 %	3 %
T	10 %	40 %	1 %	14 %	36 %	1 %	16 %	39 %	2 %	15 %	51 %	0 %	26 %	61 %	0 %

Based on these results, the JC1 parameter set clearly performs better than the parameter sets JC2–JC5. JC1 produces a less than 20 percent average error in all categories, whereas other parameters sets produce 30–40 percent average errors. The greatest differences between the models are in the model behavior under different cutting speeds. JC1, JC4, and JC5 produce better results at higher cutting speeds, but JC1 gives the best overall performance through all cutting speeds. The JC1 model is also significantly more accurate than the other models on high chip loads (large chip cross-section area, feed x width of cut) in test conditions A5–A8. JC2 and JC3 have lower performance at the higher speeds but also the worst performance in all categories. This can be explained by the model parameter *C* that affects the rate hardening. The low *C* values of JC2 and JC3 affect the model behavior, especially at high strain rates (i.e., at high cutting speeds) so that the increase of the flow stress of the material is not significant. Though this is against intuition, JC2 and JC3 produce overestimated values for the cutting forces on high cutting speeds, even when the flow stress is lower than in JC1, JC4, and JC5. This can be explained by the chip formation; the softer material forms a larger plastic deformation zone, instead of a clean chip formation zone, and the chip formation causes a higher load on the tool. This can be observed in Figure 2, where JC2 and JC3 have clear differences to other models in the size of the shear zone. JC2 and JC3 produce a much thicker chip in all simulations because the *A* and *B* values are underestimated, leading to lower flow stresses in general. Also, the thermal softening behavior determined by the parameter *m* in JC2 and JC3 is over three times the value of the other models; this leads to a slower decrease of flow stress with increasing temperature when compared to other models – though that does not affect the results as much as the rate hardening exponent.

Figure 2. Simulated Plastic Strains. B3 Cutting Conditions, JC1 to JC5 from left to right

4. CONCLUSIONS

The material model parameters acquired by the inverse analysis method proposed by Laakso & Niemi [5] are compared to other material parameter sets. The evaluation was conducted by Laakso & Niemi [5] by analytical model and the conclusion was that the inverse method proposed produces better performing parameters that those found in literature. In this paper, the model was further evaluated by implementing the model parameters in FEM simulations and comparing those to experimental results and to simulations with other material parameters. The results are similar to those of the analytical model in [5]. The material parameters proposed (set JC1) produced the most accurate results from the simulations. It is safe to say that the inverse method can be used to acquire material model parameters from cutting experiments. Though one point has been found that should be taken into account when implementing the method:

> As analytical models like Oxley's model can produce the same cutting forces with different parameters, model fitting must be done so that the parameters that are clearly bound by material properties, like yield strength, are determined from material testing to avoid unrealistic material behavior, like in the case of the JC2 and JC3 parameter sets.

REFERENCES

[1] P., Sartkulvanich Determination of material properties for use in FEM simulations of machining and roller burnishing, PHD Dissertation, Ohio State University, USA, 2007

[2] P., Sartkulvanich, A.M., Lopez, C., Rodriguez, T., Altan, Inverse Analysis Methodology to Determine Flow Stress Data for Finite Element Modeling of Machining, 11th CIRP Conference on Modeling of Machining Operation, September 16-18, 2008, Gaithersburg, MD USA, (http://nsm.eng.ohio-state.edu/CIRPNIST_paper_inverse_machining_2008.pdf, referred 15.4.2014)

[3] P., Sartkulvanich, F., Koppka, T., Altan, Determination of flow stress for metal cutting simulation—a progress report, Journal of Materials Processing Technology, Volume 146, Issue 1, 15 February 2004, Pages 61-71, ISSN 0924-0136

[4] F., Klocke, D., Lung, S., Buchkremer, Inverse Identification of the Constitutive Equation of Inconel 718 and AISI 1045 from FE Machining Simulations, Procedia CIRP, Volume 8, 2013, Pages 212-217, ISSN 2212-8271

[5] S.V.A., Laakso, E., Niemi, Determination of material model parameters from orthogonal cutting experiments, Proceedings of the Institution of Mechanical Engineers, Part B: Journal of Engineering Manufacture, 8 January 2015, DOI: 10.1177/0954405414560620

[6] D.I., Lalwani, N.K., Mehta, P.K., Jain, Extension of Oxley's predictive machining theory for Johnson and Cook flow stress model, Journal of Materials Processing Technology, Volume 209, Issues 12–13, 1 July 2009, Pages 5305-5312, ISSN 0924-0136

[7] R.W., Ivester, M., Kennedy, M., Davies, R., Stevenson, J., Thiele, R., Furness, & S., Athavale, Assessment of machining models: progress report, Machining science and technology, 4(3), 2000, 511-538

[8] R.W., Ivester, & Kennedy, M., Comparison of machining simulations for 1045 steel to experimental measurements, SME Paper TPO4PUB336, 2004, 1-15

[9] S.A., Iqbal, P.T., Mativenga, & M A., Sheikh, Characterization of machining of AISI 1045 steel over a wide range of cutting speeds. Part 1: investigation of contact phenomena, Proceedings of the Institution of Mechanical Engineers, Part B: Journal of Engineering Manufacture, 221(5), 2007, 909-916

[10] S.P.F.C., Jaspers, J.H., Dautzenberg, Material behaviour in conditions similar to metal cutting: flow stress in the primary shear zone, Journal of Materials Processing Technology, Volume 122, Issues 2–3, 28 March 2002, Pages 322-330, ISSN 0924-0136

[11] T.D., Marusich, M., Ortiz, Modeling and Simulation of High Speed Machining, International Journal for Numerical Methods in Engineering, Volume 38, Issue 21, 1995, s. 3675 3694

[12] G.R., Johnson, & W.H., Cook, A constitutive model and data for metals subjected to large strains, high strain rates and high temperatures. In Proceedings of the 7th International Symposium on Ballistics Vol. 21, pp. 541-547, 1983, April

[13] S.V.A., Laakso, J., Peltokorpi, J., Ratava, M., Lohtander, J., Varis, Graph-Based Analysis of Metal Cutting Parameters, Advances in Sustainable and Competitive Manufacturing Systems Lecture Notes in Mechanical Engineering 2013, pp 627-636, Springer

[14] S.V.A., Laakso, M., Hokka, E., Niemi, & V.T., Kuokkala, Investigation of the effect of different cutting parameters on chip formation of low-lead brass with experiments and simulations. Proceedings of the Institution of Mechanical Engineers, Part B: Journal of Engineering Manufacture, 227(11), 2013 1620-1634.

[15] F., Jiang, J., Li, J., Sun, S., Zhang, Z., Wang, L., Yan, Al7050-T7451 turning simulation based on the modified power-law material model, International Journal of Advanced Manufacturing Technology, 2010, Volume 48, Numbers 9-12, 871-880, DOI: 10.1007/s00170-009-2328-9

APPENDIX 1: SIMULATED PLASTIC STRAINS, FORCES AND TEMPERATURES

A1: v=200 m/min f=0,15 mm/r α=5°

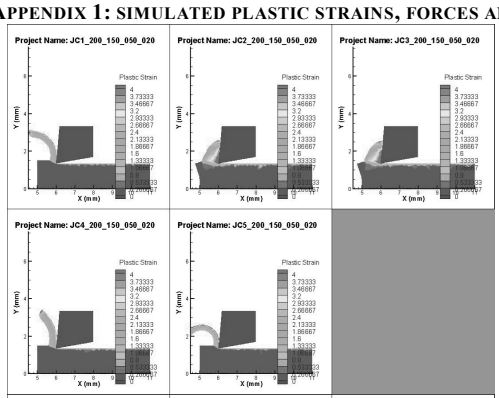

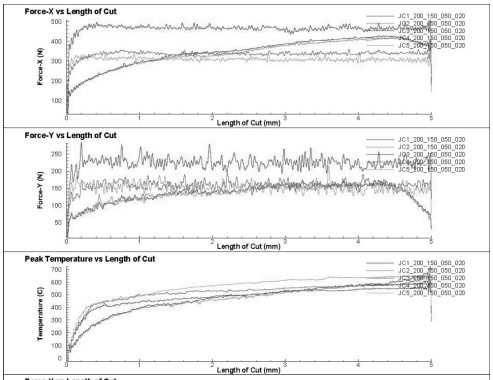

A2: v=300 m/min f=0,15 mm/r α=5°

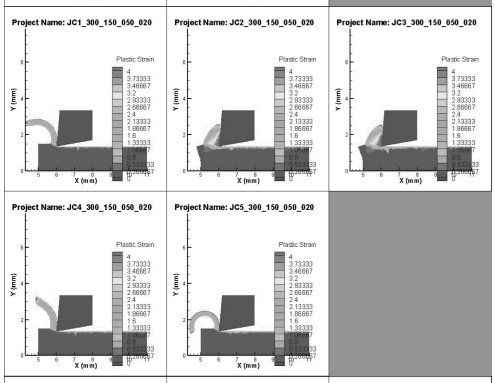

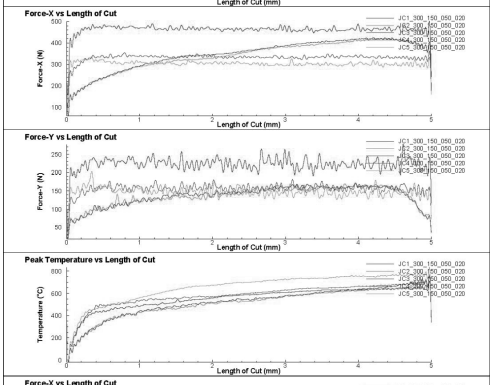

A3: v=200 m/min f=0,15 mm/r α=-7°

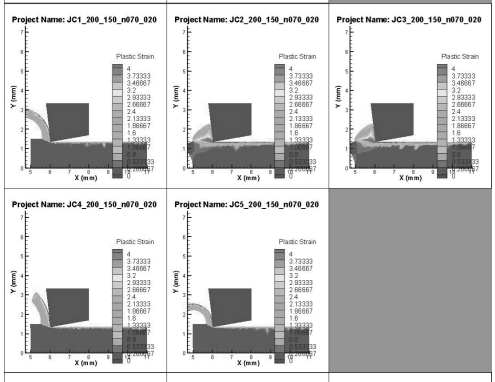

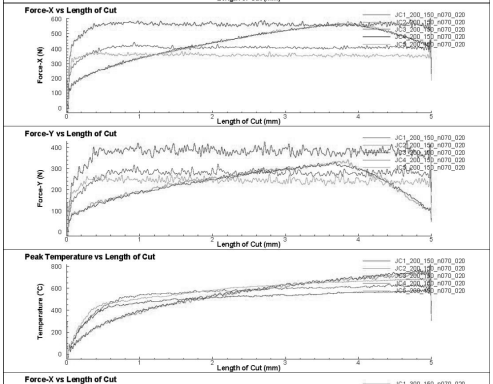

A4: v=300 m/min f=0,15 mm/r α=-7°

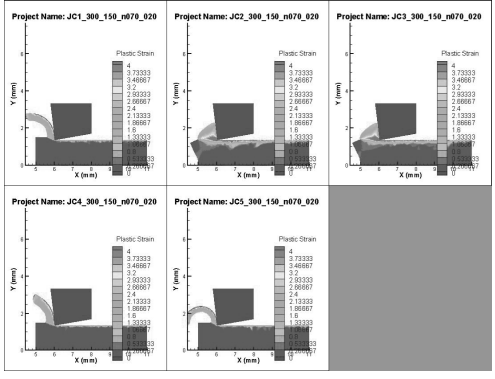

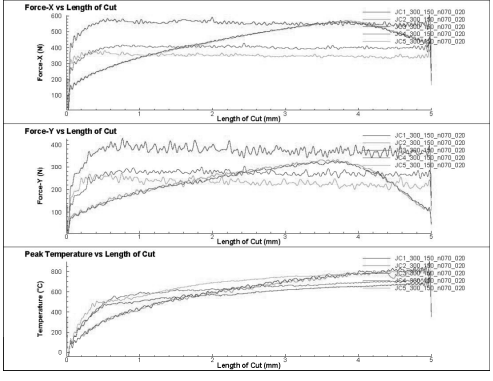

A5: v=200 m/min f=0,3 mm/r α=5°

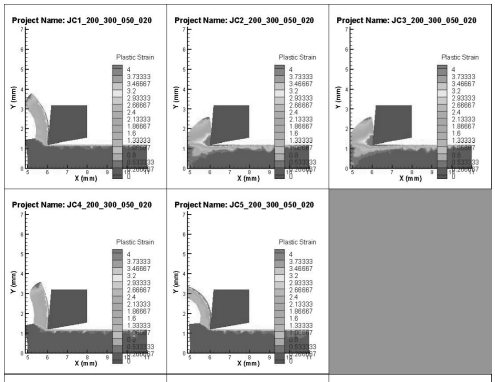

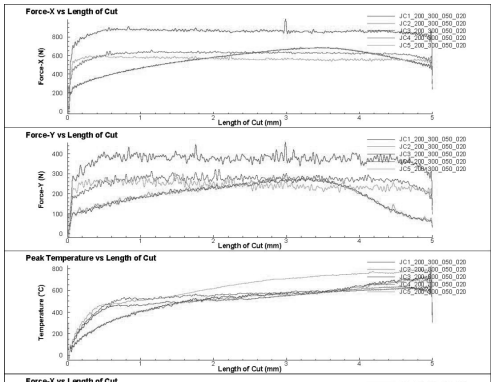

A6: v=300 m/min f=0,3 mm/r α=5°

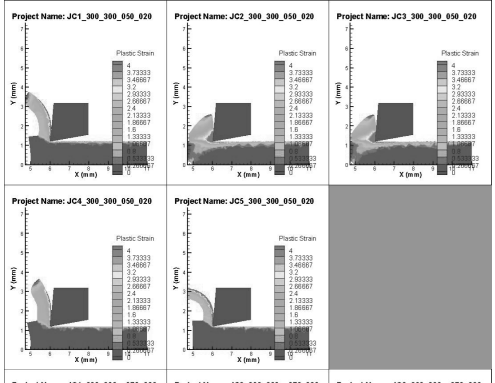

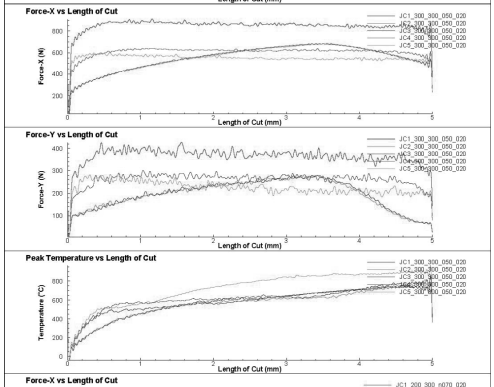

A7: v=200 m/min f=0,3 mm/r α=-7°

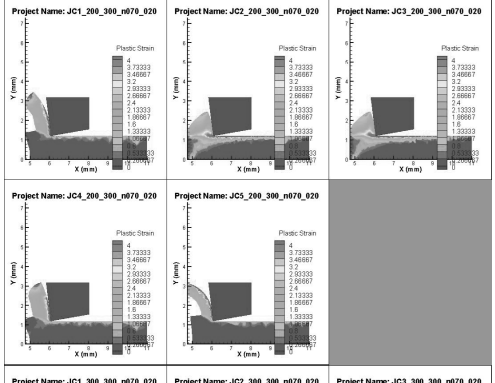

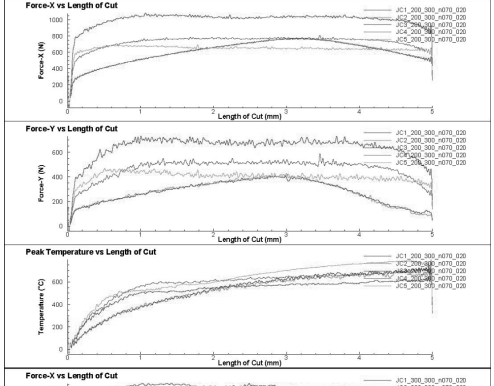

A8: v=300 m/min f=0,3 mm/r α=-7°

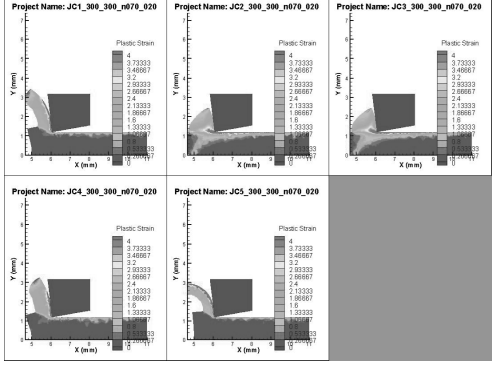

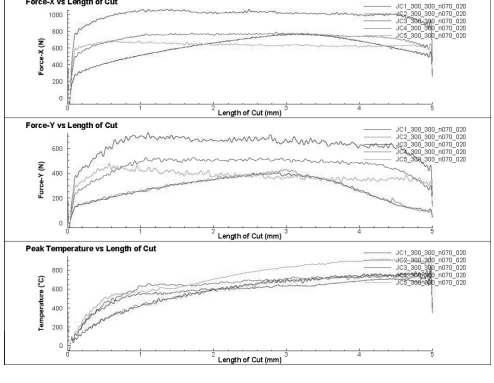

B1: v=198 m/min f=0,1 mm/r α=0°

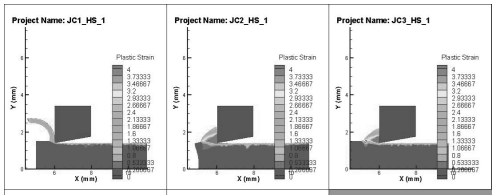

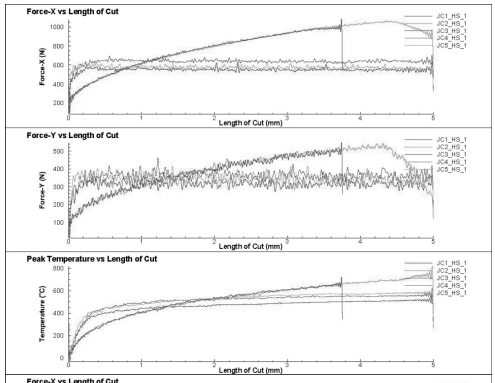

B2: v=399 m/min f=0,1 mm/r α=0°

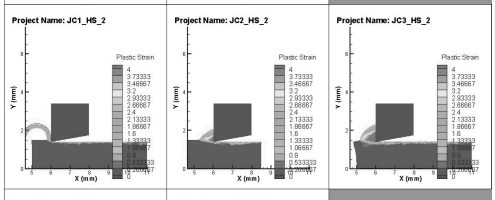

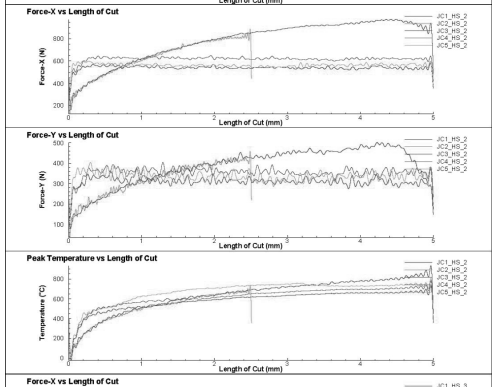

B3: v=628 m/min f=0,1 mm/r α=0°

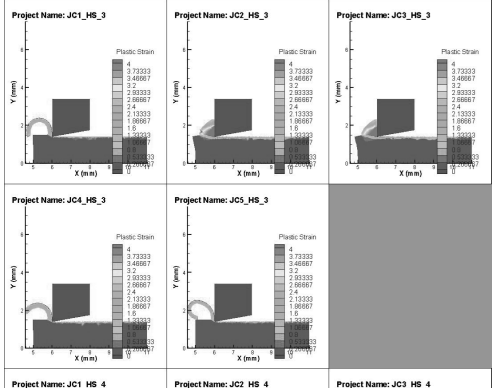

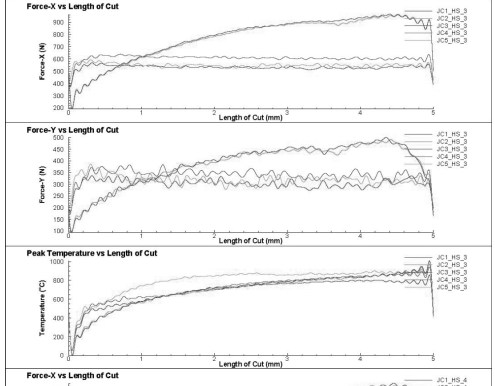

B4: v=879 m/min f=0,1 mm/r α=0°

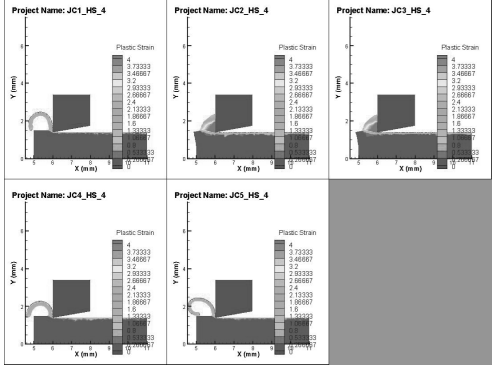

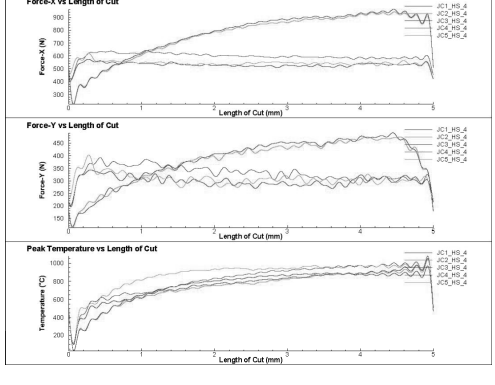

Modified Johnson-Cook Flow Stress Model with Thermal Softening Damping for Finite Element Modeling of Cutting

Sampsa Laakso[s], Esko Niemi

[s]Corresponding Author
Sampsa Vili Antero Laakso, MSc.(tech.)
Aalto University
School of Engineering
Department of Engineering Design and Production
sampsa.laakso@aalto.fi
+358407055039

Abstract

Results of materials testing for lead-free brass show that the effect of thermal softening decreases significantly when the strain rate is high. This behavior is referred to as thermal softening damping. In this paper, a flow stress model with thermal softening damping based on the Johnson-Cook flow stress model was developed. Finite element simulations with the proposed model are compared to cutting experiments to estimate the effect of damping in metal cutting.

Keywords

Cutting, Finite Element Modeling, Johnson-Cook Flow Stress Model, Thermal Softening Damping, Low Lead Brass

Introduction

Finite element simulations of cutting employ a flow stress model to predict the required stress for chip formation. Flow stress models gives the stress in respect to strain, strain rate and temperature. The most fundamental effects are strain hardening, rate sensitivity and thermal softening. Other behaviors can be observed, depending on the material, including yield delay, temperature and rate dependent strain hardening, and thermal softening dependent on strain rate. In this paper, modifications to the Johnson-Cook flow stress model[1] are made to implement the coupled effect of thermal softening and rate sensitivity. Material testing results and literature sources are presented as evidence of the existence of this behavior, and the effect of the behavior in cutting is investigated. In the proposed model, an increasing strain rate leads to a decrease in the effect of thermal softening. This is significantly different from the rate sensitivity, since the nominal flow stress is not exceeded due to the thermal softening damping multiplier approaching a predetermined cutoff value with an infinite strain rate. The rate sensitivity in the model is replaced with rate sensitivity from the modified

power law presented by Marusich.[2] Additionally, a decrease in the initial yield stress and the slope of the strain hardening with increasing temperature was identified in the material testing data, although this is not addressed in this paper in terms of modifications to the material model. These behaviors also diminish with increasing strain rate. Finite element simulations with the proposed model are compared to cutting experiments to evaluate the effect of damping behavior on cutting.

Wang et al. have modified the Johnson-Cook model so as to model the behavior of brass (Cu 79–81 %, Si 2.5–4.5 %, and the remainder of Zn) over a wide range of strain rates.[3] The rate sensitivity they observed is very similar to that of the current paper, while the effect of the strain rate is insignificant in regard to strain hardening behavior. For this reason, the rate dependent coefficient in strain hardening is left out of the scope of this paper. Xiao et al. have developed an Arrhenius-type equation for modeling H62 brass stress-strain behavior with different strains and temperature.[4] Although the experiments by Xiao et al. have limited strain rate range in regard to cutting conditions, the coupled effect of temperature and strain rate can be identified in their results. Jiang et al. modified the power law equations to simulate cutting of Al7050-T7451. The results of their materials testing show that the thermal softening damping behavior is present also in aluminum.[5]

Materials and Methods

This research has three major parts: cutting experiments, materials testing, and cutting simulations. A manual lathe is used for the cutting experiments. The cutting experiment setup is presented in Figure 1. The workpiece was a Ø55 mm cylinder with 2 mm wide flanges. The groove depth was 4 mm and the width was 3 mm. The tool was generic high speed steel with a 9 degree release angle and a zero degree rake angle. The tool holder was installed on a Kistler 9257A piezoelectric sensor for force measurements. The tool holder was set at two positions, with a rake angle of ±4 degrees and therefore a 5 and 13 degrees release angle. The cutting edge angle was 90 degrees and the tool cutting edge preparation (corner radius) was approximately 30 µm. This is observable from the microscope image (Figure 2) of the tool rake face, where it can be seen that the tool edge roundness is clearly less than one thirds of the minimum 0.1 mm range of a glass scale. The feed direction was orthogonal to the workpiece, leading therefore to almost orthogonal cutting. Cutting fluid was not used. Four sets of cutting parameters were used, two feeds 0.1 and 0.4 mm/r and two rotation speeds leading to 54–47 m/min and 216–185 m/min cutting speeds, depending on the cutting length (radial depth). The width of the cut was the same as the flange width. The chips were collected after each test and the chip thickness was measured. Each experiment was repeated three times.

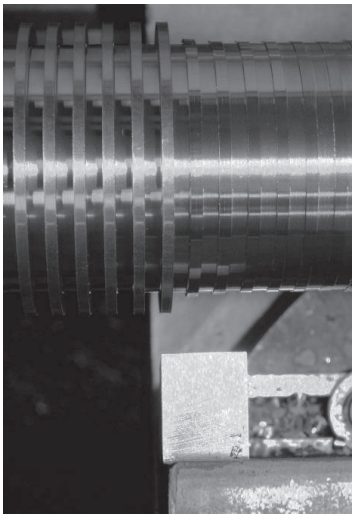

Figure 1 Cutting Experiment Setup

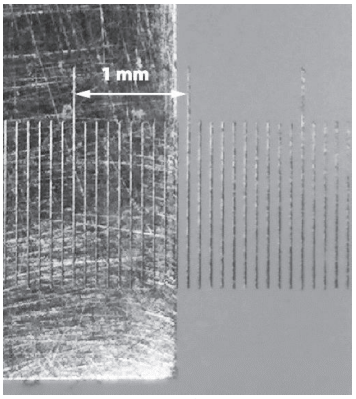

Figure 2 Cutting Tool Edge Preparation on the Rake Face (Facing Up)

The lead-free brass investigated in this paper is close to the standard CW511L. The composition of the brass is presented in Table 1. Details of the materials testing, compression tests, Split Hopkinson Pressure Bar (SHPB) tests and tensile testing have been presented in the authors' previous work (Laakso et al. 2013).[6] The most significant results from those experiments are presented in Figure 3 and Figure 4, where the thermal softening effect can be seen to diminish in high strain rate tensile testing and SHPB experiments.

Table 1 Chemical composition of the lead-free brass

Sn	Pb	P	Fe	Si	As	Sb	Al	Cu	B
0.15-0.25	0.2 max	0.01 max	0.05-0.10	0.02 max	0.02 max	0.03-0.06	0.60-0.65	61.5-63.5	10-14 ppm

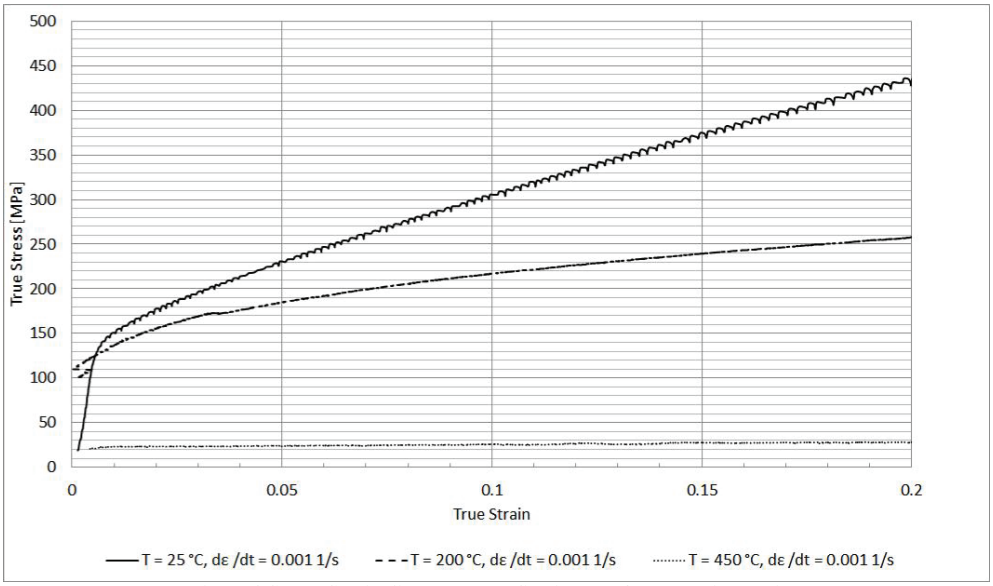

Figure 3 Stress-Strain Curve on Low Strain Rate from Tensile Testing

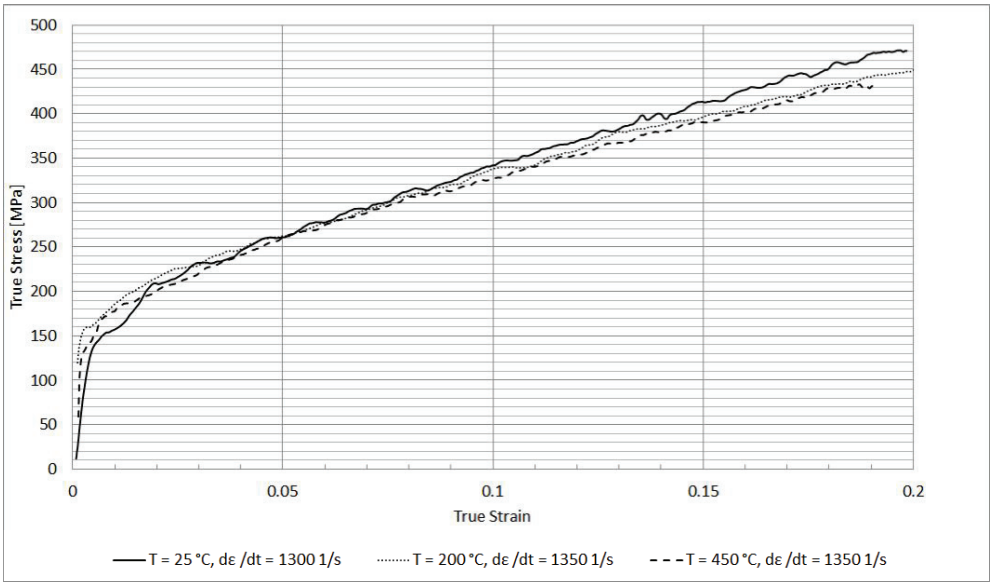

Figure 4 Stress-Strain Curve on High Strain Rate from SHPB testing

Simulations were done with Third Wave Systems AdvantEdge FEM simulation software, running on a PC with 24 3.6 GHz Intel Xeon Cores, 32 GB of memory, an Nvidia Quadro FX 1800 graphics card and 3x500 GB hard drives on RAID 5 configuration. The software uses dynamic explicit Lagrangian finite element solver and the chip formation and element distortion is handled with adaptive remeshing. The user routine for the material model was programmed with Fortran, using Microsoft Visual Studio and compiled with the Intel Fortran Compiler. The simulation setup had 30 000 elements and the workpiece was 8x2 mm. Simulations were done with the same cutting parameters as the cutting experiments, although the cutting speeds were set to 50 m/min and 200 m/min. The same simulations were done with the unmodified Johnson-cook model for comparison. Simulations with the Johnson-Cook model with a strain hardening cutoff were done to inspect the effect of thermal softening damping alone. The importance of strain hardening cutoff is discussed in Jiang et al.5 Additionally, simulations with the modified Johnson-Cook model with a damping cutoff value set to 1.0 were done to remove all sources of error between the two models.

Flow Stress Model

The flow stress model used in this paper is based on the widely used Johnson-Cook model with two modifications. The unmodified Johnson-Cook model is presented in equation 1. The modified model is presented in equation 2 as the multiplication of three individual parts that represent strain hardening (equation 3), rate sensitivity (equation 4) and thermal softening (equation 5). The strain hardening is limited by the cutoff strain, after which the stress is constant, presented in Figure 5 First modification was done on rate sensitivity that was replaced with modified power law rate sensitivity developed by Marusich[2]. The rate hardening multiplier is plotted in Figure 6. The second modification was thermal softening damping. Damping causes thermal softening to decrease with increased strain rate. The rate dependent damping function is presented in equation 6 and it is plotted in Figure 7. The damping cutoff value c_{cut} represents the ratio of thermal softening in low strain rates and thermal softening in high strain rates. Setting the value to 1.0, the damping effect is removed, whereas the maximum damping i.e. no thermal softening would occur at the value 0.0 before the cutoff temperature. The simulations were also done with the unmodified Johnson-Cook model and Johnson-Cook model with strain cutoff. In the model with the strain cutoff, the first Johnson-Cook term $A+B\varepsilon^n$ is replaced with the strain hardening presented in equation 3.

Johnson-Cook Model [1]	$\sigma_{flow} = (A + B\varepsilon^n)\left[1 + C\, ln\left(\frac{\dot{\varepsilon}}{\dot{\varepsilon}_{ref}}\right)\right]\left[1 - \left(\frac{T - T_{ref}}{T_{melt} - T_{ref}}\right)^m\right]$	1
Modified Johnson-Cook Model	$\sigma_{flow} = g(\varepsilon)\, \Gamma(\dot{\varepsilon})\, \Theta(\dot{\varepsilon}, T)$	2
Strain hardening	$g(\varepsilon) = \begin{cases} A + B\varepsilon^n \; if \; \varepsilon < \varepsilon_{cut} \\ A + B\varepsilon_{cut}{}^n \; if \; \varepsilon \geq \varepsilon_{cut} \end{cases}$	3
Rate Sensitivity multiplier	$\Gamma(\dot{\varepsilon}) = \begin{cases} \left(1 + \frac{\dot{\varepsilon}}{\dot{\varepsilon}_{ref}}\right)^{\frac{1}{m_1}} \; when \; \dot{\varepsilon} \leq \dot{\varepsilon}_t \\ \left(1 + \frac{\dot{\varepsilon}}{\dot{\varepsilon}_{ref}}\right)^{\frac{1}{m_2}} \left(1 + \frac{\dot{\varepsilon}_t}{\dot{\varepsilon}_{ref}}\right)^{\frac{1}{m_1} - \frac{1}{m_2}} \; when \; \dot{\varepsilon} > \dot{\varepsilon}_t \end{cases}$	4
Thermal Softening Multiplier	$\Theta(\dot{\varepsilon}, T) = \begin{cases} 1 \; if \; T \leq T_{room} \\ 1 - \left[\frac{T - T_{room}}{T_{cut} - T_{room}}\right]^m h(\dot{\varepsilon}) \; if \; T < T_{cut} \\ \left(1 - h(\dot{\varepsilon})\right)\left(1 - \left[\frac{T - T_{cut}}{T_{melt} - T_{cut}}\right]\right) \; if \; T \geq T_{cut} \\ 0 \; if \; T \geq T_{melt} \end{cases}$	5
Thermal Softening Damping Function	$h(\dot{\varepsilon}) = \frac{\dot{\varepsilon}_h + c_{cut}\dot{\varepsilon}}{\dot{\varepsilon}_h + \dot{\varepsilon}}$	6

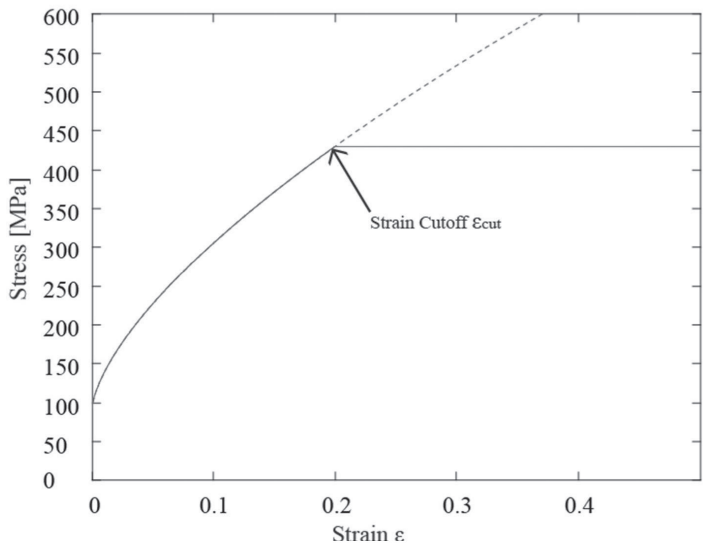

Figure 5 Strain Hardening Curve

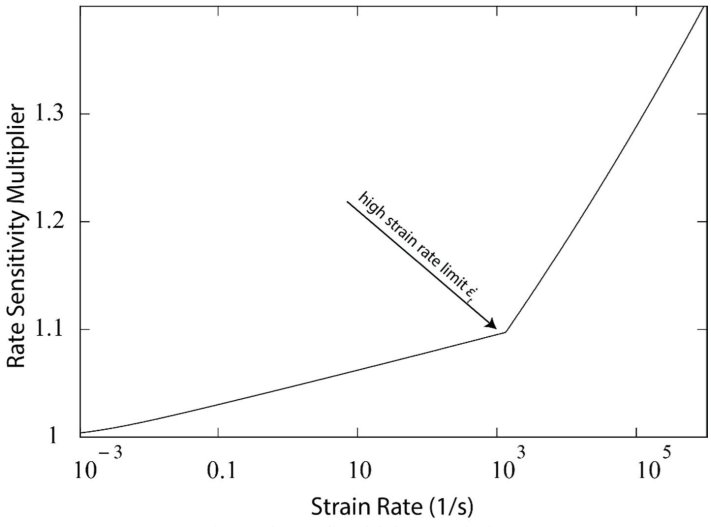

Figure 6 Rate Sensitivity Multiplier

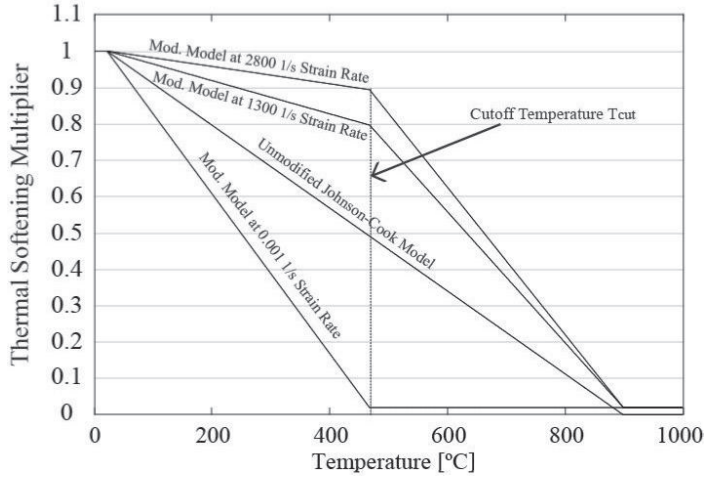

Figure 7 Thermal Softening Multiplier

Fitting the Flow Stress Model to the Materials Testing Results

The first steps in fitting the model to the materials test data were to set the strain hardening parameters, since they are considered independent in respect to strain rate and temperature. Strain hardening at a temperature of 25 °C and strain rate of 0.001 1/s were selected as the reference strain hardening curve. The model was fitted to the testing data so as to minimize the square of errors of the yield stress. The fitted model and testing data are presented in Figure 8. Figure 9 shows the similar strain hardening plot but for higher strain rate (1300 1/s) to illustrate that the model fit is also good in high strain rates.

The strain hardening model accuracy was 3.33% calculated as average deviation. The original unmodified Johnson-Cook model was similarly fitted to the testing data.

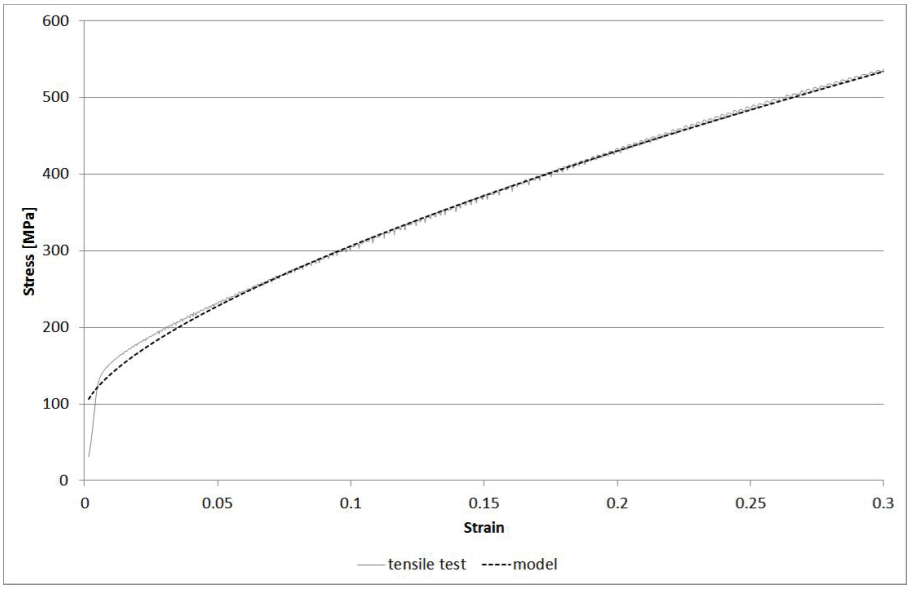

Figure 8 Strain Hardening at 0.001 1/s and 25 °C

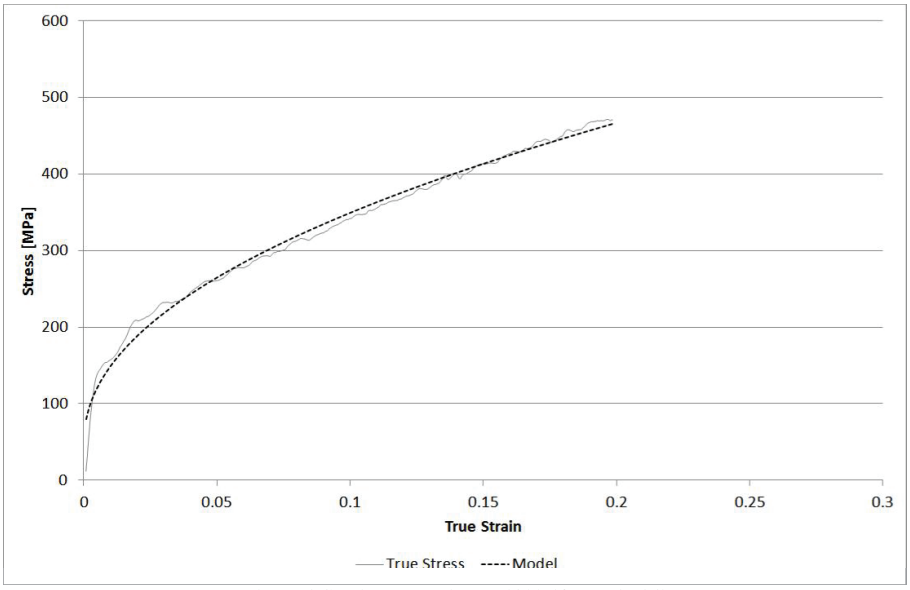

Figure 9 Strain Hardening at 1300 1/s and 25 °C

When the strain hardening is set, the materials testing data can be normalized in terms of thermal softening and rate sensitivity. A plastic strain value of 0.19 was selected as the reference point for all

material behaviors, since it is the largest strain where material testing data was obtained in all test conditions. The model was then fitted to the normalized testing data in respect to rate sensitivity and thermal softening. The strain cutoff value was selected based on the cutting experiments and simulations, though 0.2 was used as the initial value. The friction coefficient was adjusted based on the experiments and simulations, with an initial value of 0.1. The fitted model parameters are presented in Table 2. The model accuracy was 4.77%. The materials testing data and equivalent model values are presented in Figure 10. Figure 11 shows the model surface fit to the material testing data points in strain rate-temperature based system. The physical properties of the brass presented in Table 3 were acquired from the material manufacturer's brochure.[7] Parameters for the unmodified Johnson-cook model and the model with strain cutoff are presented in Table 4. The model parameters in Table 4 were also identified with model fitting by the author, as presented above. The accuracy for the Johnson-Cook model was 42.09%.

Table 2 Flow Stress Model Parameters

Strain Hardening Parameters	A	initial yield stress	Pa	93E6
	B	strain hardening stress coefficient	Pa	978E6
	n	strain hardening power coefficient	-	0.662
	ε_{cut}	cutoff strain	-	0.2
Thermal Softening Parameters	Troom	room temperature	°C	19.4
	Tmelt	melting temperature	°C	920
	m	thermal softening power coefficient	-	1
	Tcut	cutoff temperature	°C	468
Rate Sensitivity Parameters	m1	strain rate exponent 1	-	131.6
	m2	strain rate exponent 2	-	27.5
	$\dot{\varepsilon}_t$	high strain rate limit	1/s	886
	$\dot{\varepsilon}_{ref}$	reference strain rate	1/s	0.000888
Damping Parameters	$\dot{\varepsilon}_h$	high damping strain rate limit	1/s	103
	c_{cut}	damping cutoff	-	0.118

Table 3 Material Physical Properties

Heat Transfer	k	thermal conductivity	W/m°C	123
	c	heat capacity	J/kg°C	375
	ρ	density	kg/m^3	8400
	α	alpha (thermal expansion)	1/°C	2.05E-5
Elastic	E	Youngs Modulus	Pa	97E9
	ν	Poisson's Ratio	-	0.3754

Table 4 Johnson-cook Model Parameters

Strain Hardening Parameters	A	initial yield stress	Pa	93E6
	B	strain hardening stress coefficient	Pa	978E6
	n	strain hardening power coefficient	-	0.662
	ε_{cut}	cutoff strain	-	0.28
Thermal Softening Parameters	Troom	room temperature	°C	20
	Tmelt	melting temperature	°C	920
	m	thermal softening power coefficient	-	0.131
Rate Sensitivity Parameters	C	rate hardening coefficient	-	0.0935
	$\dot{\varepsilon}_{ref}$	reference strain rate	-	0.001

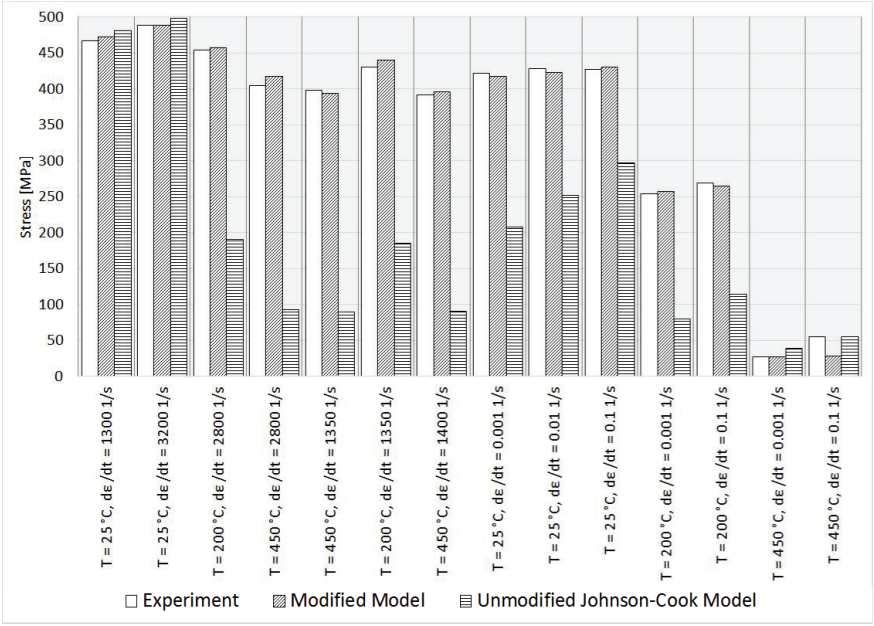

Figure 10 Material Model and Experimental Stress Values at 0.19 Strain

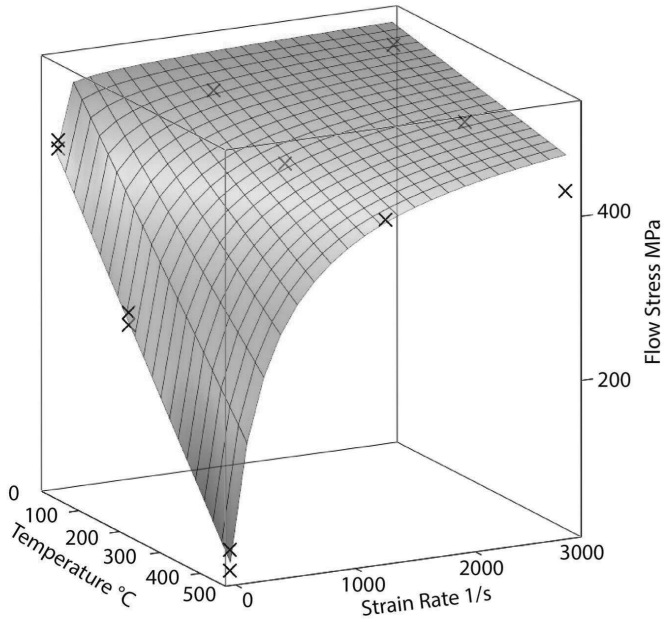

Figure 11 The Modified Johnson Cook Model Plotted as a Surface by Strain Rate and Temperature, the small X's are Material Testing Data Points for Reference

Results

The cutting experiments produced consistent results for cutting forces for each repeated experiment with an average 3.9% deviation. The cutting force results are presented in Figure 12. Chip thicknesses showed larger variation, with an average 13.3% deviation, presented in Figure 13. Simulations with the modified and unmodified Johnson-Cook model produces very different results. The unmodified Johnson-Cook model produced overestimated forces and chip thicknesses, with an error of 20.5% for tangential force, 208% for the main cutting force and 240.1% for the chip thickness. The modified Johnson-Cook model produced better results with corresponding errors of 21.4%, 35.0% and 43.9%. The comparison of the cutting forces is presented in Figure 14. Figure 15 presents the second set of simulations. Simulations with the Johnson-Cook model with the strain hardening cutoff set to 0.28 produced much better results, leading to 9.4%, 3.5% and 20.6% errors, respectively. The modified Johnson-Cook model with the damping cutoff set to 1.0 produced similarly better results, of 15.7%, 5.6% and 31.8%, respectively. The simulation results regarding temperature distribution in the shear zone and chip thickness are presented in Appendix 1.

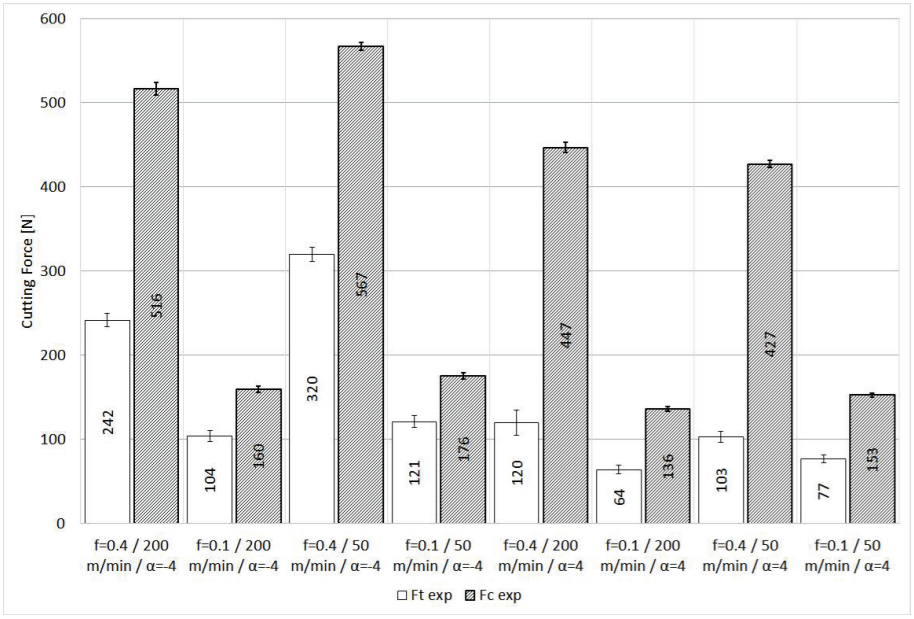

Figure 12 Measured Forces from Cutting Experiments

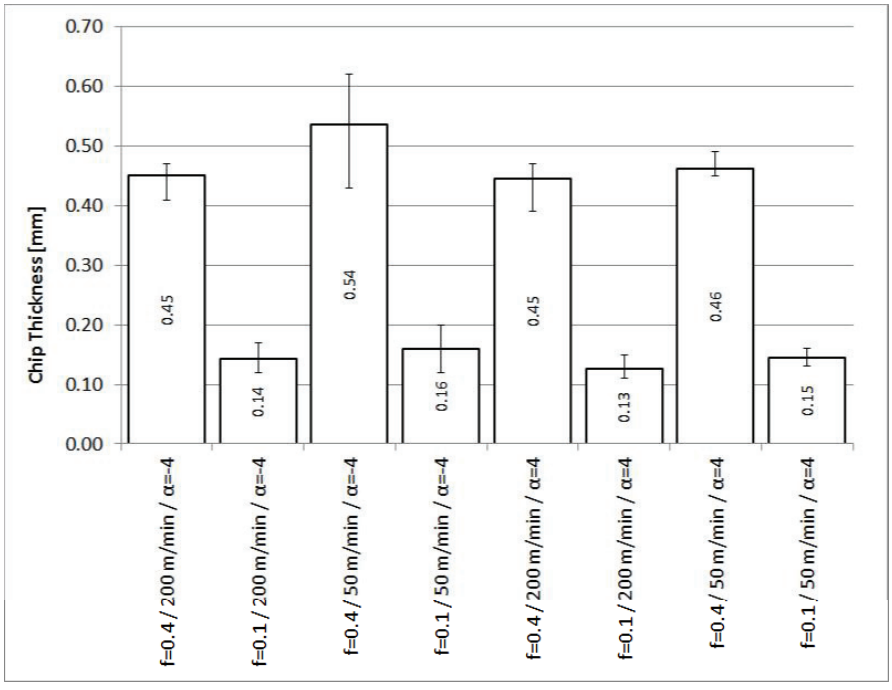

Figure 13 Measured Chip Thicknesses from Cutting Experiments, Error Bars Indicate the Measured Maximum and Minimum Values

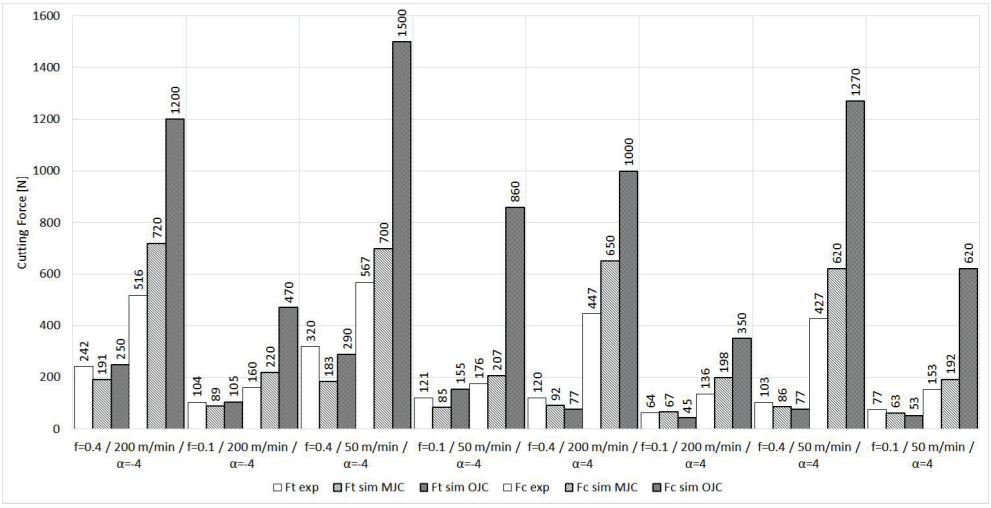

Figure 14 Cutting Forces from Simulations and Experiments (Modified Johnson-Cook, MJC, Original Johnson-Cook, OJC)

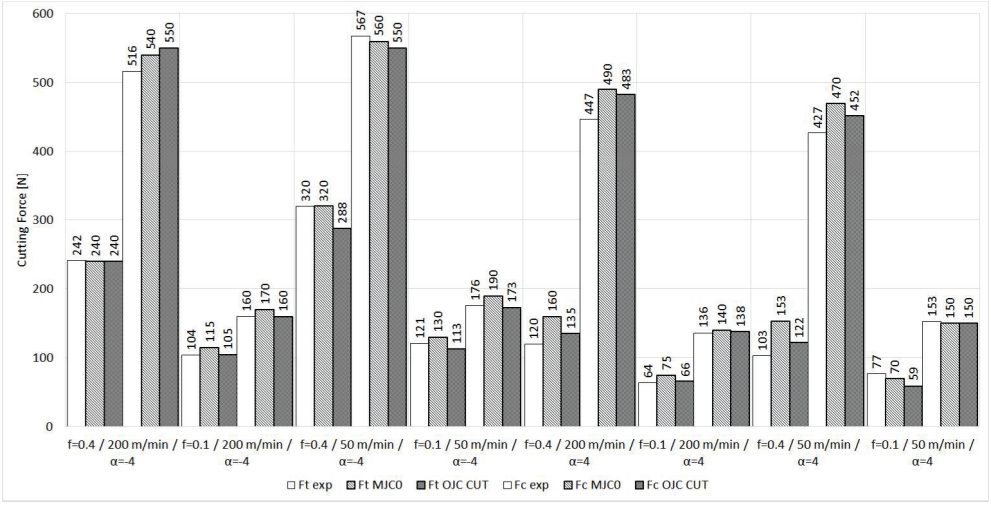

Figure 15 Cutting Forces from Simulations and Experiments, no thermal damping (Modified Johnson-Cook model with no damping effect, MJC0, Original Johnson-Cook with Strain Cutoff, OJC CUT)

Conclusions

Based on the cutting experiments and simulation results, the effect of thermal softening damping on high strain rates observed in the materials testing results did not seem to impact the cutting. There are a few possible explanations for why the materials testing data and cutting experiments contradict each other: if the thermal softening damping occurs only in a very short time interval, the effects are

negligible in a continuous cutting process. Moreover, the damping effect could diminish in high strains, as the simulations suggest that strains during cutting are 1 to 2.0 in magnitude in the shear zone, while the material model covers only strains from 0 to 0.3. The time aspect of the damping in particular needs more research, since it shares similarities with yield delay behavior and the effect on cutting as proposed by Childs et al.[8] Their conclusions were based on results of Marsh & Campbell 1963, where high speed compression experiments with low carbon steel were conducted, and the stress level was seen to be dependent on time.[9] In other words, the strain did not begin until after a certain time period, which was named the yield delay. This can also be observed in stress that is higher in the first tenths of seconds and which stabilizes after one second of loading. If this behavior were also to be found in the brass investigated in this paper, the SHPB experiments could add too high stress, since the loading cycle is too short. The absence of the damping effect in cutting implies that using analytical model and cutting experiments as inverse method to obtain flow stress model parameters as discussed in Laakso and Niemi, 2015 is plausible even with materials with more complex thermal behavior that was questioned in the paper.[10]

References:

[1] Johnson, G. R., & Cook, W. H. A constitutive model and data for metals subjected to large strains, high strain rates and high temperatures. In Proceedings of the 7th International Symposium on Ballistics Vol. 21, pp. 541-547, 1983, April

[2] Marusich T.D., Ortiz, M. Modeling and Simulation of High Speed Machining, International Journal for Numerical Methods in Engineering, Volume 38, Issue 21, 1995, s. 3675 3694

[3] Wang, Y., Zhou, Y., & Xia, Y. A constitutive description of tensile behavior for brass over a wide range of strain rates. Materials Science and Engineering, 2004, A, 372(1), 186-190.

[4] Xiao, Y. H., Guo, C., & Guo, X. Y., Constitutive modeling of hot deformation behavior of H62 brass. Materials Science and Engineering, 2011, A, 528(21), 6510-6518.

[5] Jiang, F., Li, J., Sun, J., Zhang, S., Wang, Z., Yan, L., Al7050-T7451 turning simulation based on the modified power-law material model, International Journal of Advanced Manufacturing Technology, 2010, Volume 48, Numbers 9-12, 871-880, DOI: 10.1007/s00170-009-2328-9

[6] Laakso, SVA., Hokka, M., Niemi, E., & Kuokkala, V. T. Investigation of the effect of different cutting parameters on chip formation of low-lead brass with experiments and simulations. Proceedings of the Institution of Mechanical Engineers, Part B: Journal of Engineering Manufacture, 227(11), 2013 1620-1634.

[7] KME.COM, Bluewave Brass, Technical Specifications Brochure, http://www.kme.com/assets/uploads/oldkme/file/Brochure/2010/bluewave_web_brochure.pdf, referred on 18.5.2015

[8] Childs, T.H.C., Rahmad, R., The Effect of a Yield Drop on Chip Formation of Soft Carbon Steels, 12th CIRP Conference on Modelling of Machining Operations, 2009

[9] Marsh, K.J., Campbell, J.D., The effect of strain rate on the post-yield flow of mild steel, Journal of the Mechanics and Physics of Solids, Volume 11, Issue 1, January–February 1963, Pages 49-63, ISSN 0022-5096

[10] Laakso, S.V.A., Niemi, E., Determination of material model parameters from orthogonal cutting experiments, Proceedings of the Institution of Mechanical Engineers, Part B: Journal of Engineering Manufacture, 8 January 2015, DOI: 10.1177/0954405414560620

Appendix 1: Simulation Results

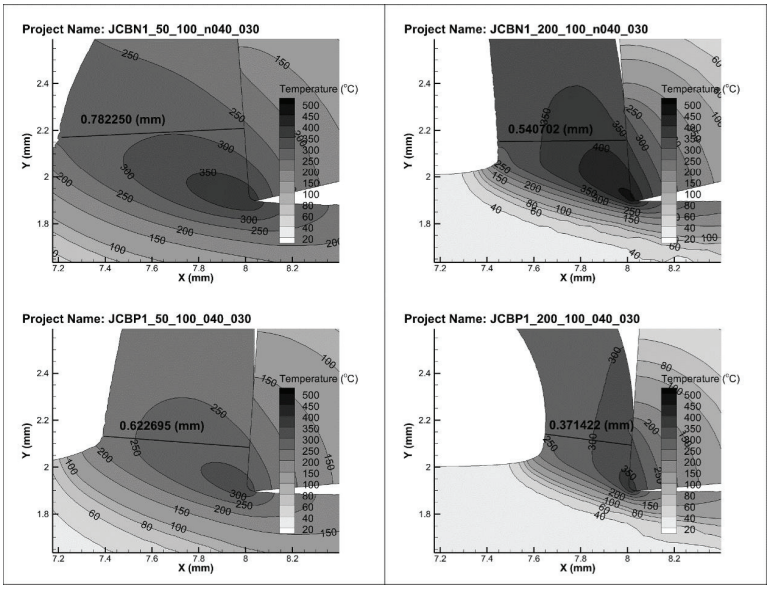

Figure 16 Simulations with the original Johnson-Cook Model with cutting speeds 50 m/min and 200 m/min and α=-4 and 4°, f = 0.1 mm/r

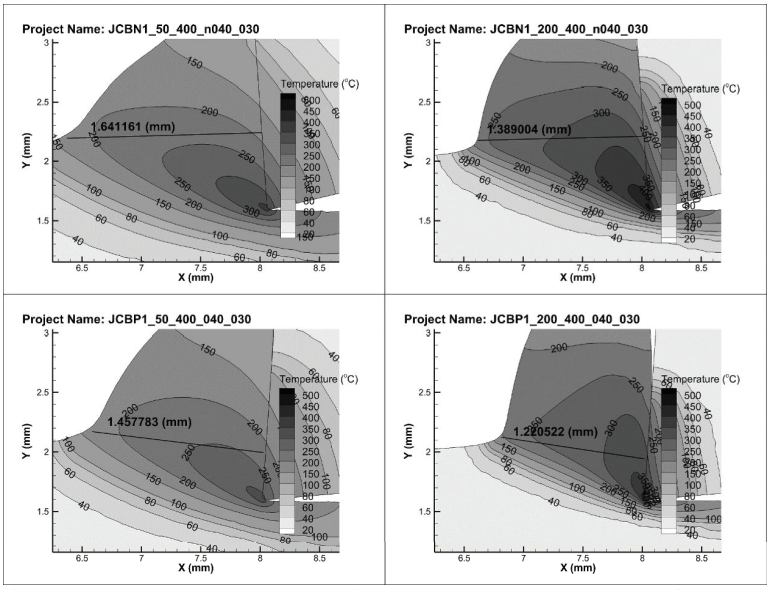

Figure 17 Simulations with the original Johnson-Cook Model with cutting speeds 50 m/min and 200 m/min and α=-4 and 4°, f = 0.4 mm/r

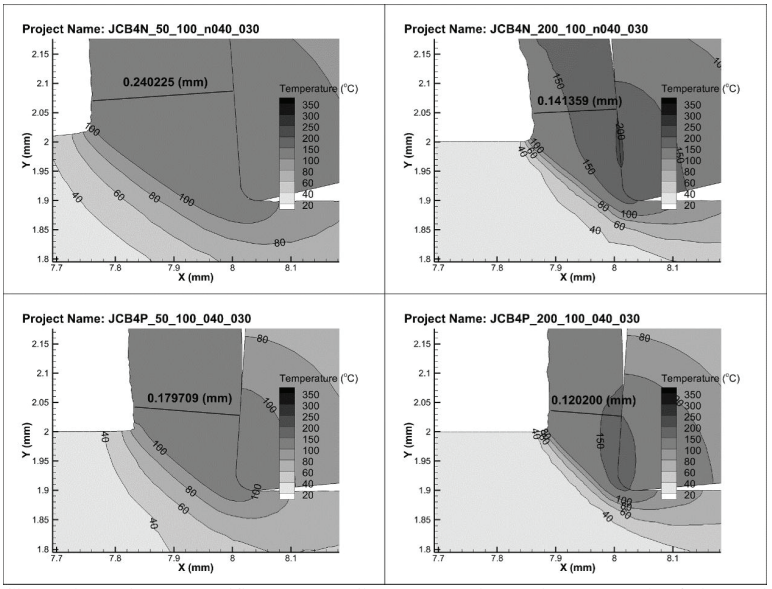

Figure 18 Simulations with the modified Johnson-Cook Model with cutting speeds 50 m/min and 200 m/min and α=-4 and 4°, feed = 0.1 mm/r

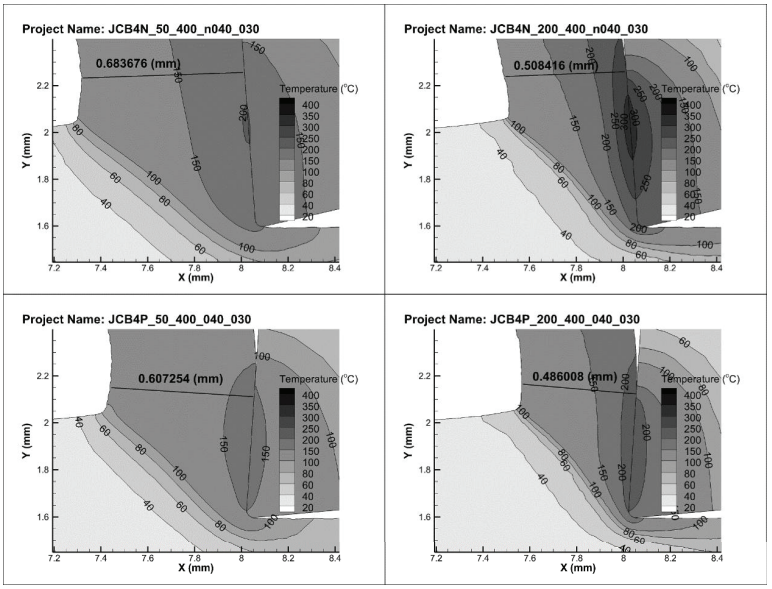

Figure 19 Simulations with the modified Johnson-Cook Model with cutting speeds 50 m/min and 200 m/min and α=-4 and 4°, feed = 0.4 mm/r

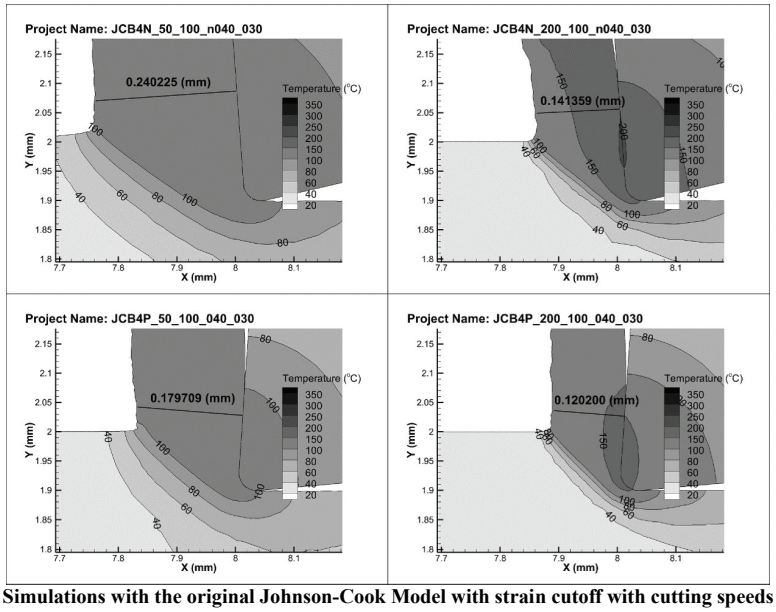

Figure 20 Simulations with the original Johnson-Cook Model with strain cutoff with cutting speeds 50 m/min and 200 m/min and α=-4 and 4°, feed = 0.1 mm/r

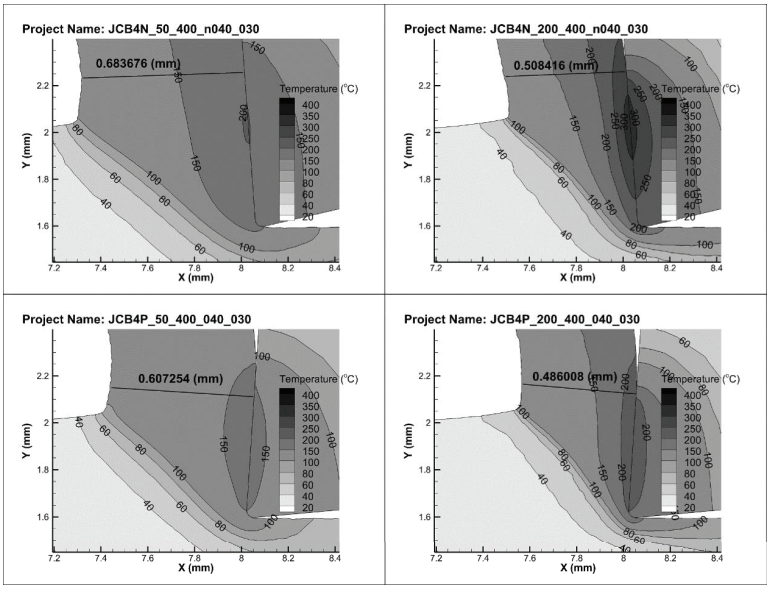

Figure 21 Simulations with the original Johnson-Cook Model with strain cutoff with cutting speeds 50 m/min and 200 m/min and α=-4 and 4°, feed = 0.4 mm/r

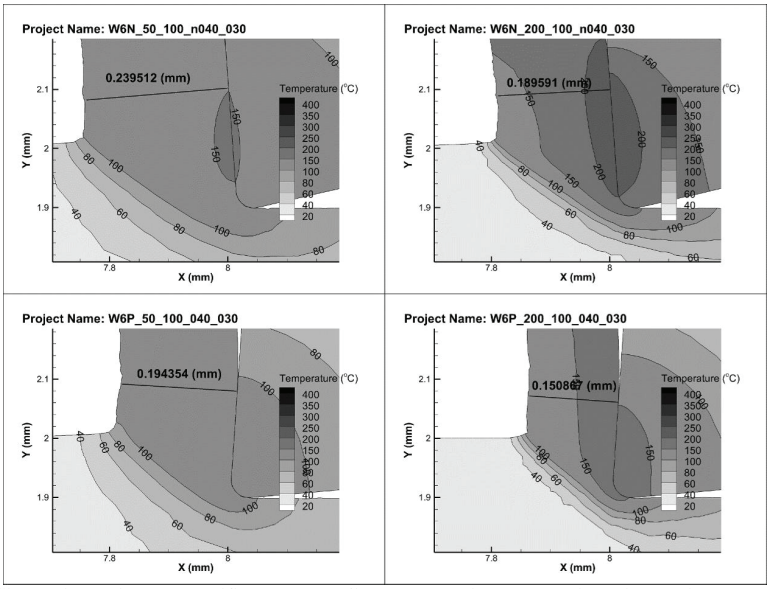

Figure 22 Simulations with the Modified Johnson-Cook Model without damping with cutting speeds 50 m/min and 200 m/min and α=-4 and 4°, f = 0.1 mm/r

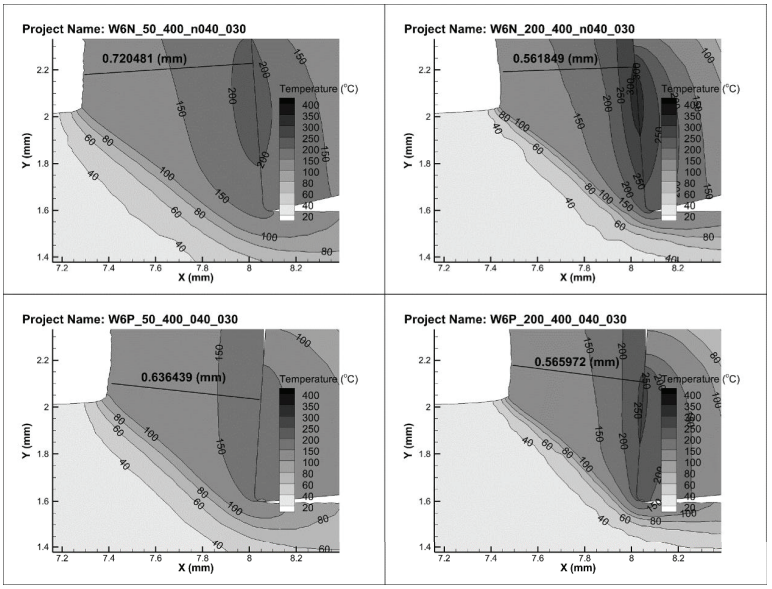

Figure 23 Simulations with the modified Johnson-Cook Model without damping with cutting speeds 50 m/min and 200 m/min and α=-4 and 4°, f = 0.4 mm/r

This dissertation investigates the material model parameter acquisition for finite element simulations of cutting. The model parameters are traditionally determined from tensile testing and SHPB testing, but the shortcoming of this method is that the testing conditions are not the same as in the cutting process. The theory of metal cutting, materials testing, the finite element method and cutting experiments are introduced as the theoretical foundation to this dissertation. Using cutting experiments as a materials testing method is proposed in order to test the material properties in cutting conditions. This requires an analytical model for determining the relationship between cutting experiment outputs, cutting force, temperature and chip morphology to material model inputs that are strain, strain rate and temperature. The model parameters acquired with this method are in good agreement with the experimental results.

Aalto-DD 190/2015

ISBN 978-952-60-6523-6 (printed)
ISBN 978-952-60-6524-3 (pdf)
ISSN-L 1799-4934
ISSN 1799-4934 (printed)
ISSN 1799-4942 (pdf)

Aalto University
School of Engineering
Department of Engineering Design and Production
www.aalto.fi

BUSINESS + ECONOMY

ART + DESIGN + ARCHITECTURE

SCIENCE + TECHNOLOGY

CROSSOVER

DOCTORAL DISSERTATIONS